UNIVERSITY OF
LIVERPOOL

Conceptual design of the PERLE injector

Thesis submitted in accordance with the requirements of the University of Liverpool for the degree of Doctor in Philosophy by

Benjamin Rhys Hounsell

March 2022

Contents

Abstract

Energy recovery linacs (ERLs) are a type of accelerator that works by decelerating the initially accelerated beam once it has been used to recover its energy back into the radio frequency (RF) cavities. They offer access to a unique region of parameter space in terms of average current and beam quality. One proposed application for an ERL is the Large Hadron Electron Collider (LHeC). The LHeC would be an upgrade to the Large Hadron Collider (LHC) that would add a 50 GeV three turn ERL to accelerate an electron beam that would then be collided with the 7 TeV LHC proton beam. This 50 GeV ERL would be a significant step beyond the state of the art for ERLs so an intermediate test facility called PERLE (Powerful Energy Recovery Linac for Experiments) has been proposed. PERLE will be a three turn common transport ERL operating with a bunch charge of 500 pC, an average current of 20 mA, a bunch length of 3 mm and transverse emittances of < 6 mm mrad. In addition to its role as a test facility for the LHeC PERLE will also function generally as a test bed for ERL technology as well as having its own scientific program.

The injector is one of the key components in an ERL as ERL beam quality is source limited. ERL injectors must be capable of delivering high average current beams while mitigating the emittance growth due to effects such as space charge. In this thesis the conceptual design of the PERLE injector is investigated. The injector consists of a 350 kV direct current (DC) photoelectron gun, a low energy section containing two solenoids and a buncher cavity, an superconducting radio frequency (SRF) booster linac and a merger to transport the beam into the main ERL loop. The electrode geometry of the electron gun was optimised for performance at both 350 kV and 220 kV. Then the beam dynamics from the cathode to the exit of the booster linac were optimised and it was shown that it was possible to achieve the specification at that point. However at booster exit an "M" shaped longitudinal phase space developed. Variant injectors with the addition of higher harmonic cavities were explored to see if it was possible to linearise the longitudinal phase space. It was shown that it is possible while still achieving the required transverse emittances. Finally the design of the merger was investigated. Four merger schemes were optimised and compared and two of them were capable of meeting the specification. Once all of the subsections of the injector had been optimised a baseline design without higher harmonic cavities and using a U-bend merger was selected. This design met the

Acknowledgements

Firstly I would like to thank my supervisors Max Klein, Boris Militsyn, Walid Kaabi and Carsten Welsch for all their guidance and support over the years of my PhD.

I would also like to thank Peter Williams, Julian McKenzie, Alex Bogacz, Öznur Apsimon and Christelle Bruni for all of the useful discussions, suggestions and insight they offered into the various beam dynamics problems I faced.

I have had the fortune of being based at two different labs during my PhD and I would like to thank all of the members of the communities of PhD students at those labs for conversations and times we spent together.

Finally I would like to thank my family. My parents Alan and Kathryn and my sister Caitlin for all the support and encouragement over the years.

Chapter 1

Introduction

1.1 High energy physics and particles accelerators

High energy particles have been used in experimental high energy and nuclear physics for over a century to probe the structure of matter. Natural sources of high energy particles such as radioactive sources and cosmic rays were used first. However the desire for sources of particles with higher energy and intensity than could be achieved naturally rapidly drove the development of machines for accelerating particles. These particle accelerators were pivotal in the development of high energy and nuclear physics during the 20th century and into the 21st century. Particle accelerator technology also found application in medicine, industry and security as well as tools as for investigation in other areas of science including structural biology and materials science.

Particle accelerators have been developed to accelerate a range of charged particles including electrons, protons and ions. The energy of the particles is increased using electric fields. These fields can be produced in a number of different ways including electrostatic fields, radio frequency (RF) cavities, terahertz, lasers and plasma. The most widely used acceleration technology for scientific is RF. RF accelerators can roughly be divided into two main types, straight machines and circular machines [1]. Straight machines in which the beam only passes through the accelerating RF cavities once are known as linear accelerators or linacs. The advantages of linacs are that they can provide very good beam quality with very short bunches. An important feature of linacs is that they are source-limited. This means that the beam doesn't come to equilibrium and hence the best possible beam quality is the beam quality at

the start of the machine. This incentivises developing injectors that are capable of delivering high quality beams. In circular machines the beam passes through the same accelerating RF multiple times. Circular machines include types such as cyclotrons, betatrons and synchrotrons. The advantage of circular machines is that higher energies can be reached at lower cost as the same RF structures can be reused. In circular machines the limits on the beam quality are different than in linacs. Circular machines are lattice-limited which means that the design of the magnetic lattice of the ring is what determines the quality of the beam. This is because the beam comes to an equilibrium in the ring between effects that reduce the beam quality and those that increase it and the extent of these effects is determined by the lattice design.

A wide range of particle accelerators of different types have been built for doing high energy physics experiments including cylotrons such as the Berkeley cylotrons, synchrotrons such as LEP (Large Electron Positron Collider) and the LHC and linacs like the SLAC (Stanford Linear Accelerator Center) linac and the LAL (Laboratoire de l'accélérateur linéaire) linac. Early experiments using particle accelerators used a single beam fired into a fixed target, such as the experiments done using the SLAC linac [2]. However it was realised that by colliding two beams moving in opposite directions together the center of mass energy of the collision could be significantly increased. There have been a significant number of colliders constructed including the the Super Proton Synchrotron (SPS), the Stanford Linear Collider and the LHC. Electrons, protons, ions and muons have all been be used particle accelerators intended for use in high energy physics.

1.2 Recirculating and Energy Recovery Linacs

The concept of a linac in which the beam only passes through the accelerating RF once can be modified leading to the machines known as recirculating linacs and energy recovery linacs [1]. These accelerator types require the beams be ultra-relativistic in the main loop so the particles of different energies are all approximately moving at the same speed. This means they are normally only viable for accelerating electrons due to their small rest mass compared to heavier particles such as protons. The first of these is the recirculating linac where once the beam leaves the RF cavities it is recirculated and reintroduced back into the RF cavities to be accelerated further. The distinction between a recirculating linac and a true circular machine is that the number of passes

through the RF cavities is small. This means that the beam still behaves like a linac beam and is source limited. The main advantage of recirculating linacs is that they save cost on RF. An example of a recirculating linac would be CEBAF [3].

The other type of accelerator is a further modification to the concept of a recirculating linac and is known as an Energy Recovery Linac (ERL). In ERLs after the beam has reached its maximum energy and been used the path length of the return beamline is used to adjust when the beam arrives back at the linacs so that it arrives at a decelerating RF phase. As a result now instead of being accelerated the beam is decelerated and the energy in the spent beam is recovered back into the RF cavities where it is used to accelerate fresh beam. This reduces the RF power that needs to be provided to the cavities and hence allows higher average current beams to be accelerated in an economical and energy efficient way. Additionally multi-turn ERLs with multiple accelerating and deccelerating passes also have the advantage of saving cost on RF cavities in the same way as recirculating linacs. This allows the acceleration of high average current beams with economical power consumption. The concept of an ERL was first proposed by Maury Tigner in 1965 [4]. The first machine built which could operate in an energy recovery mode was constructed at Chalk River in 1977 [5]. In terms of its layout this machine was quite different than most modern ERLs as its accelerating and decelerating beams propagate in opposite directions through the linac rather than in the same direction.

ERLs offer access to a unique area of parameter space in terms of the beams they can provide. They are of interest when an application requires linac type beams, meaning low emittance and controllable bunch length, at higher average currents than could be economically provided by a conventional single pass or recirculating linac. In high energy physics this is useful for achieving high luminosity in colliders with reduced electrical power consumption [6]. It is also of interest for high energy electron coolers for cooling ion beams [7]. Outside of high energy physics they have potential applications for high average power or high repetition rate free electron lasers [8] and inverse Compton sources [9]. ERLs have recently been identified as one of the five areas of accelerator technology development that are of interest in the current European strategy for particle physics [10] and a roadmap for ERL development has been published [11].

1.3 The Large Hadron-Electron Collider (LHeC)

The LHeC is a proposed upgrade to the LHC which would add an electron accelerator [6] [12]. The beam from this electron accelerator would be collided with the intense hadron beams from the LHC. This would provide a unique opportunity to explore TeV scale electron-hadron scattering and would have synergy with the hadron-hadron LHC physics program. The LHeC would be a successor to HERA [13] the only previous electron-proton collider and the earlier electron-proton fixed target experiments at SLAC [2]. Early in the development of the LHeC there were two main possible designs. The first of these two options was a ring-ring based design where an electron synchrotron would be built in the same tunnel as the LHC to provide the electron beam. The second was a ring-linac design where the electron beam would be provided by an ERL. Eventually the ERL based design was chosen as the baseline. This was due to the higher luminosity it offered. As well as the fact that as it wouldn't share a tunnel with the LHC meaning that its construction would be less disruptive to normal LHC operations.

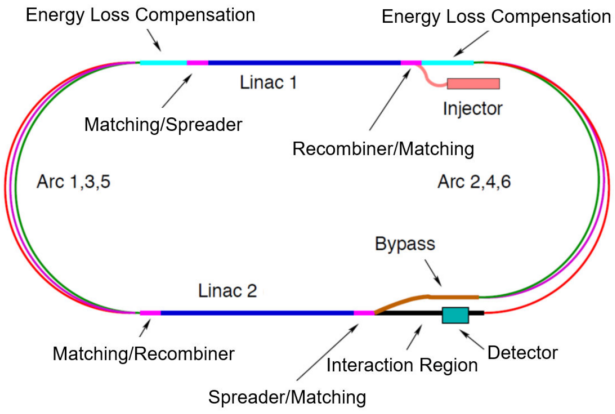

Figure 1.1: The layout of the LHeC ERL [12].[1]

The current LHeC ERL design is a 50 GeV three turn common transport ERL with two linacs in a race track configuration. A diagram of the layout can be seen in figure 1.1. It will operate with an RF frequency of 801.58 MHz which is the twentieth harmonic of the LHC bunch frequency. This was chosen

[1]Figure from P. Agostini et al. "The Large Hadron–Electron Collider at the HL- LHC". In: Journal of Physics G: Nuclear and Particle Physics 48.11 (2021). doi: 10.1088/1361-6471/abf3ba. used under CC-BY 4.0

so that the bunch patterns in the electron and proton accelerators will line up for collisions in the interaction region. The specification for the LHeC can be seen in table 1.1 [12].

Table 1.1: LHeC ERL specification

Parameter	**Values**
Maximum energy	49.19 GeV
Injection energy	0.5 GeV
Bunch charge	499 pC
Bunch repetition rate	40.1 MHz
Current	20 mA
Transverse normalised emittance at the IP	30 mm·mrad
RF frequency	801.58 MHz

1.4 PERLE

As the LHeC ERL is a significant step beyond the state of the art an intermediate test facility called PERLE has been proposed [14] [15]. PERLE will share a number of design features with the LHeC ERL in terms of its layout, RF frequency and some of its beam parameters. However, it will be a much smaller scale machine. This will allow the validation of the design decisions made for the LHeC. PERLE will also allow for general R&D into multi-turn SRF ERLs and have its own scientific program. A preliminary specification for PERLE can be seen in table 1.2.

Table 1.2: Preliminary PERLE specification

Parameter	**Values**
Total maximum energy	500 MeV
Total injection energy	7 MeV/c
Bunch charge	500 pC
Current	20 mA
Emittance	$<$ 6 mm·mrad
RMS bunch length	3 mm

The current layout of PERLE can be seen in figure 1.2. PERLE is a three turn ERL in a racetrack configuration with two linacs providing equal acceleration. Each linac has four 5 cell 801.58 MHz SRF cavities in it. In the first of these linacs will use a Superconducting Proton Linac (SPL) cryomodule

adapted to PERLE [16]. PERLE is a common transport machine which means that the accelerating and decelerating beams pass through the same arcs. The arcs are a 6 dipole design with flexible momentum compaction factor [17]. The beam is injected into the main ERL loop from the injector at an energy of 7 MeV. The injector will be a DC gun based injector reusing, but upgrading, the 350 kV DC electron gun used for the ALICE (Accelerators and Lasers in Combined Experiments) ERL [18] and the Thomas Jefferson National Accelerator Facility (TJNAF)/Advanced Energy Systems (AES) booster cryomodule [19].

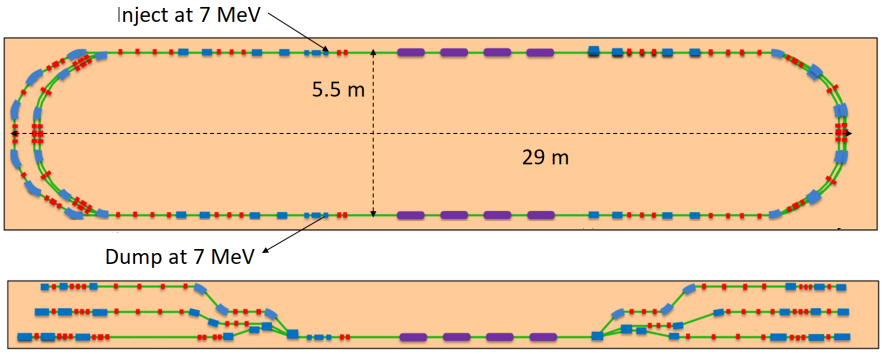

Figure 1.2: The layout of PERLE [20] with the sizes and injection and dump energies labelled. A top down view is shown above and a side on view below.[2]

It is planned that PERLE will be constructed in phases [21]. The first phase will only have a single linac but will still be a three turn machine. It will also use the original ALICE gun without performing an upgrade. Which means that it will use non-interchangeable GaAs photocathode. This phase 1 machine will be limited to a maximum beam energy of 250 MeV and a maximum beam current of 5 mA. The beam current limit is due to the high voltage power supply of the gun and the photocathode material used. The second phase of the machine will add the second linac and upgrade the electron gun. Allowing for the full 500 MeV, 20 mA design performance.

As mentioned above the primary purpose of PERLE is to be a test facility for the LHeC. However, it will also function as a general facility for the development of multi-turn SRF ERL technology. Which will be of benefit to other future ERL projects and applications. PERLE will also have its own

[2]Figure adapted from K. D. J. Andre et al "Studies of the Energy Recovery Performance of the PERLE Project". In Proc. IPAC21. Campinas. Brazil, 2021, pp 2744-2747, DOI:10.18429/JACoW-IPAC2021-WEPAB065 used under CC-BY 3.0

experimental program outside of ERL technology development. Some possible experimental applications include scattering the electron beam off radioactive ion beams for nuclear physics experiments and using PERLE to drive an inverse Compton source.

1.5 Goals and structure of the thesis

The goal of this thesis is to carry out the conceptual design of the PERLE injector. This injector needs to be capable of delivering a high average current beam with good beam quality. In the thesis simulations are performed to design and optimise the beam dynamics of the injector. In this chapter, chapter 1, what energy recovery linacs are, what the LHeC is and then what PERLE is and what the objectives of the machine are are discussed. In chapter 2 previous ERL injector designs will be reviewed. In chapter 3 there will be a discussion of how the properties of a bunch can be quantified, the types of simulation codes used in the optimisation of ERL injectors and a discussion of the optimisation algorithms used later in the thesis to perform the optimisation of the different sections of the PERLE injector. In chapter 4 the optimisation of the electron gun electrode geometry is discussed. Then in chapter 5 an optimisation of the beam dynamics is performed from the cathode to the exit of the booster linac using the electron gun design from chapter 4. In the analysis of the injector optimisation performed in chapter 5 it is identified that a significant "M" shaped non-linearity develops in the longitudinal phase space in the injector before the booster exit. So in chapter 6 a number of variant injectors which have higher harmonic cavities are explored to see if it is possible to to linearise the longitudinal phase space and avoid the appearance of this non-linearity. In chapter 7 the design of the merger, which is the beamline that transports the beam into the main ERL loop, is investigated. Four designs are compared, two of which are shown to meet the requirements. In chapter 8 a start to end simulation of the selected design from the cathode to the exit of the first main linac pass is presented. Then what future work is required and possible directions for development are identified.

Chapter 2

ERL injectors

2.1 Energy recovery linac injectors

The main advantage of ERLs is that they are capable of delivering high brightness, high average current beams. The injector is the component of the machine where the electron bunches are produced and the initial acceleration and beam manipulation is done. As the beam quality in an ERL is limited by the quality of the beam produced at the cathode the design of the injector is important to achieve the required beam performance. A range of different injector designs have been used in previous ERLs and proposed for future ERLs. The typical structure of an injector is in order electron gun, low energy section, booster linac and merger. A sketch of this can be seen in fig 2.1.

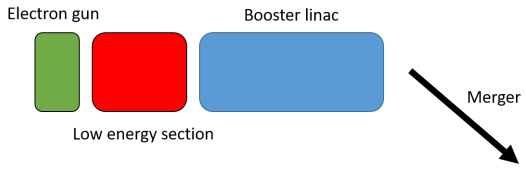

Figure 2.1: The order of the subsections in an ERL injector.

The electron gun is the electron source where the electrons are first produced from a cathode and then the initial acceleration is done. The choice of electron gun technology has a significant effect on the overall injector design. Once the beam has exited the electron gun it passes through a low energy beamline section at the exit energy of the electron gun. This beamline section may be used for beam manipulations which are more easily performed at low energy.

After this low energy section the beam is accelerated up to the injection energy by a booster linac. Finally, the beam is transported from the exit of the booster linac into the main ERL by a special beamline called the merger.

There are a number of factors that influence the designs used for ERL injectors. The most significant of these is the space charge forces. At low energies the repulsive forces between the like-charged electron are significant and can lead to a degradation in the beam quality. This can be mitigated by the design of the injector. The requirements of the main ERL loop also impose constraints on the injector. An example of this is the injection energy of the ERL. There are competing demands between the desire to inject at as high an energy as possible and as low an energy as possible. The desire to inject at high energy is due to the fact that that will minimise the influence of space charge forces in the merger and hence the degradation to the beam quality due to those forces. There are two factors that incentivise lower injection energies. Firstly, the fact that in most ERLs the injected energy is not recovered and is instead just dumped and lost. Therefore a lower injection energy means a higher energy recovery efficiency for the whole machine. Secondly, if the dumped beam energy is below around 10 MeV which is the neutron production threshold of the dump the radiation protection requirements for the dump are a lot simpler [22]. As the injection and dump energies of a typical ERL are the same this requirement can potentially set an upper limit on the injection energy. Considering these factors a typical compromise injection energy is in the range of 5-10 MeV.

2.2 Cathodes

The cathode is the component of the injector which produces the electrons. It is located within the electron gun. There are three mechanism of electron production that can be used. These are photoemission, thermionic emission and field emission [23]. Of these only photoemission and thermionic emission have been used or proposed for ERLs. For ERL applications photocathodes are the more commonly used approach [24] as they can provide both low beam emittance and the bunched time structure required of the beam. Thermionic cathodes are generally not as good at offering low emittance bunched beams but may still be used for applications with less demanding requirements on the beam brightness such as IR FELs (Infrared Free Electron Lasers).

Thermionic cathodes are cathodes which are heated and consequently emit

electrons. They can produce low emittance continuous beams, have longer lifetimes than photocathodes, good vacuum conditions are less important and they don't require complex laser systems. The main issue with thermionic cathodes is obtaining a bunched rather than continuous beam. This can be done in the gun with a grid or RF gating or with RF choppers and collimators later in the injector. This process generally degrades the beam quality so thermionic injector don't offer the same beam quality as photoinjectors. The JAERI (Japanese Atomic Energy Research Institute) ERL [25] and the Novosibirsk ERL [26] both used a grid modulated thermionic DC gun. A thermionic grid modulated RF gun has been designed as an upgrade for the Novosibirsk ERL [27].

In the case of photocathodes the electrons are produced by a laser pulse incident on the photocathode via the photoelectric effect. There are a number of characteristics that are desirable in a photocathode which will be used in an ERL. These include high quantum efficiency to achieve high average current without needing an unreasonable amount of laser power incident on the cathode, producing electrons with a convenient laser wavelength, long lifetime and being as robust as possible to vacuum conditions. Not all of these requirements may be achievable simultaneously in practice. Photocathodes can broadly be divided into two groups of materials metals and semiconductors. The choice of photocathode can be heavily influenced by the electron gun technology used in the injector.

Metals have significantly lower quantum efficiencies than semiconductor based cathodes and are consequently rarely used for the high average current requirements of ERLs. Although they are often used in pulsed NC linacs. One place metals may be of interest for CW (Continuous Wave) injectors is for SRF gun based injectors as it may be desirable to have a superconducting cathode. This could mean either the niobium of the back wall of the electron gun cavity [28] or a specific cathode material such as lead [29].

Semi-conductor photocathodes are more commonly used in the case of ERLs as they have significantly higher quantum efficiencies than metal photocathodes. Meaning they are capable of providing the high average current beams required by ERLs. Three broad categories of materials are used: alkali tellurides, alkali antimonides and gallium arsenide.

Alkali tellurides offer the best resistance against poor vacuum conditions at high quantum efficiency [23]. However they require the use of a UV laser which is a more complex laser system than the green lasers used by the other semi-conductor photocathode options.

Alkali antimonides offer high quantum efficiency, the ability to use green lasers and greater robustness to vacuum conditions than gallium arsenide [23]. Some examples of alkali antimonides include Cs_3Sb and CsK_2Sb. The later of which has been used on the gun designed by Cornell [30]. Alkali antimonides photocathodes were also used on the Brookhaven 113 MHz SRF gun [31]. Alkali antimonides can be used with DC, VHF and SRF electron guns.

Galium arsenide is the final photocathode option. It offers high quantum efficiency, the ability to use green lasers and can potentially be used to produce polarised electrons [23]. However it is extremely sensitive to vacuum conditions requiring very good vacuum in the gun itself. This requirement means that gallium arsenide can only be used in DC electron guns. It also requires reactivation with caesium which can be challenging in a high voltage DC gun. For application as a source of unpolarised electrons gallium arsenide was used in the JLab FEL DC gun [32], the ALICE DC gun [33] and KEK DC gun [34].

For the specific applications which require polarised electrons negative electron affinity activated galium arsinide photocathodes (NEA GaAs) are required. For high polarisation strained superlattice lattice GaAs is used [35]. The current record for the maximum polarised current obtained from GaAs is 10 mA achieved at Mainz [36]. This is less than required by some proposed applications. So further development in polarised photocathode technology is required. The lifetime of these photocathodes is also potentially limited when operated at high current which would mean that regular photocathode replacement would be required.

2.3 Electron guns

DC electron guns

DC electron guns use a fixed electric potential between two electrodes to accelerate the particles. They are the most mature of the electron gun technologies which could be used for ERLs and have historically been the most widely used [24]. In addition to the technological maturity they also have the advantage of being able to achieve the best vacuum condition of all three technologies which makes them the only viable option at present for the GaAs cathodes needed for polarised beams. They can broadly be divided into two types low voltage guns intended as polarised sources and high voltage guns for unpolarised application.

The reason for using lower voltage guns for polarised beams is twofold. Firstly the cathodes are very sensitive to damage due to field emission and lowering the voltage reduces the field emission allowing for longer cathode lifetimes. Secondly spin manipulation is easier with lower energy beams. An example of a polarised gun is the electron gun used for MESA [37].

Unpolarised electron guns tend to be higher voltage as this improves the beam quality out of the injector. This is due to the fact that higher voltage electron guns have higher cathode fields which allows for higher energy beams at the exit of the gun which reduces the space charge forces later in the injector. Additionally higher voltage electron guns tend to have higher cathode electric fields which allows for smaller laser spot sizes to extract the same bunch charge which means smaller initial thermal emittances [23]. The highest achieved voltage in practice was 500 kV at designed at JAERI for KEK [38].

Achieving high voltages is however difficult in practice. The main limit on high voltage performance is the insulators. Field emitted electrons from the metal strike the insulator causing it to charge up and leading to insulator punch throughs. The first way of dealing with this is by modifications to the insulator some examples of these modifications are resistive coatings [39], conductive doping in the insulator [40] or segmented insulators [41]. Alternatively changing the electron gun geometry to an inverted insulator design reduces the number of field emitted electrons incident on the insulator [42]. The limiting factor then becomes the availability of high voltage cables.

SRF guns

Superconducting radiofrequency guns use niobium cavities cooled down to the superconducting temperature of niobium. As they are RF guns they allow for significantly higher cathode electric fields, more rapid acceleration and higher gun exit energies than DC electron guns. All of these factors can lead to improved beam quality. The higher cathode electric fields lead to smaller initial thermal emittances as the initial laser spot sizes can be smaller. While the more rapid acceleration and high energy at the exit of the gun reduces the negative effects of space charge. As they are superconducting they can be run CW unlike most normal conducting RF guns. Which means that they can operate in CW mode rather than needing to be pulsed and can provide the kind of high average current beams used in the ERL. SRF guns can be divided into two types elliptical cavity guns operating at around 1.3 GHz such the BerlinPro

gun [43] and quarter wave resonator guns operating at VHF frequencies such as the BNL gun [44].

VHF guns

VHF guns are normal conducting RF guns which operate at VHF frequencies of typically around 160 - 200 MHz [45]. The cavities are quarter wave resonators (QWR) and are very large which means that it is possible to cool them sufficiently to operate them in CW mode. Compared to DC guns VHF guns have two to four times higher cathode fields and higher beam exit energies. The beam energies are still fairly low compared to higher frequency NC RF guns. This means that the beam dynamics in a VHF gun based injector is similar to that in a DC gun based injector. A proposed improvement to VHF guns is to instead of having a single cell like the first designs is to add an additional cell and have a double cell gun [46]. This would significantly increase the output energy of the gun which will reduce the space charge forces later in the injector. Up to this point no ERL project has yet used a VHF gun.

2.4 Low energy section

After exiting the electron gun the beam passes through a section of beamline before it reaches the booster linac. This is a low energy section of the beamline and hence has significant space charge forces which may degrade the beam performance. However it also presents the opportunity for beam manipulations that may either be easier or potentially only possible at the low beam energy present.

The simplest low energy section is found in the case of the berlinPro SRF gun injector [47] and the JLAB/AES injector [48]. This consists of a single solenoid for emittance compensation between the electron gun and the booster. This design does not allow for significant manipulation of the bunch length in the low energy section as there is no element in the low energy section to control the bunch length. This means that any bunching required in the injector will need to primarily be done elsewhere generally either in the booster or in the merger. If the electron gun used is an RF gun bunching may be possible in the gun and it may be possible to introduce a chirp on the bunch which causes some bunching in this type of low energy section. This won't provide the

same flexibility or amount of bunching as low energy sections which contain components which are specifically for bunching.

The most widely used low energy section consists of a solenoid followed by a buncher and then another solenoid. The solenoids are there to provide transverse focusing to constrain the transverse beam size and for emittance compensation. The buncher cavity is a normal conducting RF cavity that decelerates the head of the bunch and accelerates the tail leading to the bunch length being reduced via ballistic bunching. This is a well established design that has been used on a variety of injectors. It is commonly used for DC gun based injectors but it has also been proposed for some VHF gun based injectors in a non-ERL context [49]. Some DC gun based injectors of this type that have been constructed and operated include the ALICE injector [50], the Cornell injector [51], the cERL injector [52] and the JLAB FEL injector [53]. The JAERI injector also had buncher cavity however the buncher operated at a sub-harmonic of the main RF due to the fact that the electron gun used a thermionic cathode that produced long bunches [25].

A possible variation of this that was proposed for a VHF gun based injector for the European XFEL (X-ray Free Electron Laser) CW upgrade. The European XFEL CW upgrade is not an ERL but shares the requirements of needing high average current beams. The variation involves the addition of a third harmonic cavity between the second solenoid and the booster. This cavity was added to aid with the symmetrisation of the longitudinal bunch distribution [54].

The most complex low energy sections are found in the case of polarised injectors as the spin manipulation is done in this sections. The beam energies in low energy sections intended for spin manipulation tend to be lower as the lower voltages in the electron gun reduces the field emission which increases the cathode lifetimes and the lower beam energy aids with spin manipulation. The MESA low energy transport section has an alpha magnet for bending followed by a spin manipulation section consisting of two Wien filters and a solenoid, then another alpha magnet, a chopper system to bunch the beam, as the beam is continuous until this point, and then a two cavity buncher system with one of the cavities being a second harmonic cavity [55].

2.5 Booster linac

The booster linac is a linac that accelerates the beam from the energy at the gun exit up to the injection energy. A variety of booster linac designs have been used and proposed for ERLs. They are normally superconducting linacs operating at the main frequency of the ERL although there are exceptions to both of those design choices.

The majority of booster uses SRF cavities however the number of cells per cavity and the total number of cavities varies. Some earlier designs used SRF cavities with a relatively large number of cells such the ALICE injector which used two 1.3 GHz nine cell Tesla style cavities [50] and the JLAB FEL booster which used two 5 cell 1.5 GHz CEBAF cavities [53]. However there has been a tendency towards injectors with smaller numbers of cells in each cavity. For example the JLAB/AES injector which uses single cell cavities [48] and Cornell [51], KEK [52] and BerlinPro [47] injectors which use double cell cavities. In combination with a tendency towards a smaller number of cells per cavity there has been a tendency towards a larger number of total cavities with individually controllable amplitudes and phases. The advantage of this is that it allows for finer control of the acceleration and emittance compensation process. The cERL and BerlinPro boosters have three cavities, the JLAB/AES booster has three main harmonic cavities and the Cornell injector has five cavities.

The use of RF frequencies other than the main harmonic of the ERL has also been proposed. The JLAB/AES booster is an example of this in two ways. Firstly its main operating RF frequency was 750 MHz the first subharmonic of the main JLAB FEL ERL RF frequency [56]. Secondly it had a third harmonic cavity in the second position intended for linearization of the longitudinal phase space [57]. Although optimisation of this injector design found that the use of the cavity as a lineariser was not favoured by the optimizer [48].

Normal conducting booster linacs have also been used and proposed. The Novosibirsk ERL which is a normal conducting ERL operating with 180.4 MHz RF cavities as its main linac also has a normal conducting booster operating at the same RF frequency. The low frequency allows the cavities to be operated CW. The booster consists of two single cell cavities with a permanent magnet solenoid between them [26]. The proposed injector for MESA also uses a normal conducting booster. This booster is at the 1.3 GHz operating frequency of the main ERL and is operated at low gradient to allow for CW operation. This means that it is longer than a comparable SRF booster [58].

2.6 Mergers

The merger is the beamline in an ERL that transports the beam, at the injection energy, from the booster exit into the main ERL loop. At typical ERL injection energies the beam dynamics are still space charge dominated and this has a significant influence on merger designs. Mergers need to physical transport the beam into the main ERL loop, mitigate the degradation in beam quality due to the space charge forces and match the beam to the main ERL loop. They also need to physically fit into the available space.

Typical mergers uses dipoles to bend the beam and transverse focusing elements to match and keep the beam controlled transversely. Mergers generally operate in the energy range where both quadrupoles and solenoids are viable focusing elements. All of the elements are typically fixed magnetic elements rather kickers as the repetition rates are too high for kickers to be a workable solution.

A range of merger designs have been used historically. One of the most commonly used merger designs is a three dipole beamline. Variants of this merger have been used for the JLab FELs [59], are used on CBeta [60] and the cERL [61] and are planned for BerlinPro [62]. The JLAB FEL and cERL both use edge focusing to cancel out the dispersion while CBeta and BerlinPro both use quadrupoles. MESA uses a triple bend achromat for its merger bending a full 180° [63]. The Novosibrisk ERL uses a chicane [26].

A few ERL projects have have their merger designs influenced by physical space constraints. The ALICE ERL is an example of this as it was located in a hall that had previously been used for the target station of NSF. This mean to fit the injector into the hall ALICE used a long 4 dipole merger consisting of a U-bend followed by a S-bend [64]. Another example of a ERL that had a merger that was chosen due to space constraints is the JAERI ERL which due to the narrow hall in which it was located used a 4 dipole staircase merger rather than 3 dipole merger [65].

The zig-zag is a proposed merger that uses four dipole magnets bending in alternating directions in a zig-zag shape [66] [22]. It was proposed to mitigate the effects of the space charge induced modification to the dispersion. This leads to growth in the emittance due to residual dispersion. The zig-zag is designed to be capable of achieving achromaticity in the presence of space charge while avoiding crossovers which might negatively effect the emittance compensation process.

A merger that was proposed for BerlinPro but did not end up being the final design consisted of a chicane with the final magnet being a lambertson septum magnet [67]. This helps with reducing the length of the merger. However it would have required one of the injected or recirculated beam to pass through the main linac off axis. That could potentially have driven higher order modes (HOMs) which could lead to beam break up instability (BBU).

An example of a proposed merger which uses solenoids instead of quadrupoles as its transverse focusing elements is the merger proposed for the EIC electron cooler [68]. This merger is a two dipole dogleg with a pair of solenoids between the dipoles to make the dogleg achromatic. The two solenoids have equal strength but opposite field direction so that there is no horizontal dispersion rotated into the vertical plane by the solenoids.

A straight merger design using an RF dipole has been proposed [69]. In this merger design the injected and recirculated beams both pass through a septum magnet the recirclated beams being bent and the injected beam passing through the field free region. They both then pass through a common dipole which is placed overlapping with an RF dipole. When the injected beam passes through these overlapping elements the RF dipole is at such a phase that its transverse kick cancels out the bending of the magnetic dipole so the beam passes straight through without being deflected. When the recirculated beams pass through the RF dipole and magnetic dipoles both bend the beam in the same direction providing appropriate bending to bring the beam onto axis through the main linac.

It has also been proposed that dual axis SRF cavities could be used [70]. One way of doing this would be using them in the booster with one axis for accelerating the injected beam and one decelerating the spent beam. This would allow merging at a much higher energy. Alternatively the merger could be eliminated entirely by using a dual axis cavity in the main linac. One axis would be for the injected beam the other for the other passes.

2.7 Conclusion

The particular beam dynamics found in ERL injectors is a consequence of the significant space charge forces found at the low energies in the injector and the requirement for high average current beams. A wide range of different technical solutions have been proposed and used for ERL. In terms of the electron guns there are three technologies which have the potential to be used. These are high

voltage DC guns, VHF guns and SRF guns. Of these three technologies the most mature and widely used is the DC electron gun. In terms of the structure of the rest of the injector the most common layout is a low energy section consisting of a solenoid, followed by a NC buncher then another solenoid. This low energy section is then typically followed by superconducting booster linac capable of operating in CW mode to accelerate the high average current beam. The final section of the injector is the merger. This is the area with the most diversity in the proposed solutions. However four recent ERL projects have all converged on the same solution of a three dipole merger. Despite the fact that there are a number of common trends in ERL injector design there is plenty of diversity in the possible designs as well as room for novel concepts.

Chapter 3

Beam description, simulations and optimisation

3.1 Coordinate systems and bunch parameters

Coordinate systems

In a particle accelerator there is a design trajectory which is the trajectory a perfectly ideal particle would follow. This can be used to define a co-moving coordinate system relative to this design trajectory which can then be used to describe the motion of non-ideal particles. This coordinate system has two transverse axis perpendicular to the motion of the particles which are called x and y and one along the direction of motion called s. It is common in accelerator physics to use position along s as the independent variable rather than time.

To describe the motion of a particle six coordinates are required. Two different conventions can be used for the coordinates of the particle bunch. The first of these is x, p_x where the transverse coordinates are in terms of the position and the particle momentum. The advantage of this convention is that x, p_x are the canonical coordinates for Hamiltonian mechanics which means that theorems which depend on Hamiltonian mechanics such as Louville's theorem are valid. One issue with this convention is that x, p_x can be difficult to measure experimentally so another convention is sometimes used which is x, x' where the coordinates are the transverse position and the divergence of the particle. Hamiltonian mechanics cannot be applied in this case so theorems derived via Hamiltonian mechanics are technically not valid. However it is much easier to measure trace space than phase space and they generally behave in similar

ways. In this thesis the convention used is x, p_x unless stated otherwise.

Quantifying bunch description

Particle accelerators generally don't accelerate single particles they accelerate beams consisting of many particles. This means that parameters must be found to describe the distribution as whole. The obvious approach is to use the average beam parameters such as the bunch position and energy as well as the RMS parameters such as the bunch size and energy or momentum spreads. This approach doesn't have a single number which is usable as a figure of merit for the quality of the beam.

One more sophisticated approach to describing a bunch is to use the emittance and Twiss parameters. In the ideal case when all of the particles in a bunch are plotted in transverse phase space they occupy an elliptical area in phase space. Assuming only linear forces and no coupling between the planes as the particles move through the accelerator the size and shape of the ellipse will change but the area will remain constant. The area and shape of this ellipse can be used to describe the beam. The equation of the ellipse can be seen in equation 3.1

$$\pi\epsilon = \gamma(s)x^2(s) + 2\alpha x(s)p_x(s) + \beta(s)p_x^2(s) \tag{3.1}$$

where ϵ is a parameter known as the emittance, α, β and γ are the Twiss parameters, x is position in real space, p_x is momentum and s is the position along the reference orbit of the accelerator. As can be seen in equation 3.1 the area of the ellipse in phase space is π times the emittance. The emittance is commonly used as a figure of merit for the quality of a particle beam as it is a conserved in many cases in an accelerator and describes how the transverse size and transverse momentum can be traded off against each. Beams with smaller emittances are considered to be of higher quality as they can be focused smaller with less transverse divergence.

The other coefficients of the equation of the ellipse can be used to describe the size and transverse divergence of the particle bunch. These parameters are called either the Twiss parameters or the Courant-Synder parameters. From looking at the ellipse relationships between the Twiss parameters, the RMS emittance and the RMS beam sizes and momentum spreads can be derived. These relationships can be seen in equation 3.2, equation 3.3 and equation 3.4.

$$\beta_x = \frac{\sigma_x^2}{\epsilon_x} \tag{3.2}$$

$$\alpha_x = -\sigma_x \sigma_{px} \beta_x \tag{3.3}$$

$$\gamma_x = \frac{\sigma_{px}^2}{\epsilon_x} \tag{3.4}$$

The relationship between the three Twiss parameters can be seen in equation 3.5 and equation 3.6.

$$\alpha(s) = -\frac{1}{2}\beta'(s) \tag{3.5}$$

$$\gamma(s) = \frac{1 + \alpha(s)^2}{\beta(s)} \tag{3.6}$$

When there are non-linear forces present the shape of the phase space will be distorted. The area of the distorted phase space may remain constant but the size of the ellipse required to enclose the bunch will be larger leading to a growth in the emittance value.

Another analogous approach to describing a beam is one that uses the moments of the bunch distribution. This is particularly useful for particle tracking simulations as it allows the parameters of the bunch to be calculated off the bunch distribution. The first order moments are the average beam parameters such as the beam position and energy. They however do not describe the extent of the bunch. So bunches with very different sizes or energy spreads may still have the same first order moments. To differentiate between these bunches the second order moments of the distribution are used. The second order moment in space is the RMS beam size and the second order moments of the momentum or energy distribution are the momentum or energy spreads respectively. The second order moment using both the position and the momentum distribution at the same time can be used to obtain the emittance of the beam. The RMS normalised emittance is calculated as shown in equation 3.7 [71]

$$\epsilon_n = \frac{1}{m_0 c}\sqrt{\langle x^2 \rangle \langle p_x \rangle^2 - \langle x p_x \rangle^2} \tag{3.7}$$

where m_0 is the rest mass of the particles in the bunch, c is the speed of light in a vacuum, x is the particles position and p_x is the particle momentum. Using the RMS parameters and emittance obtained this way the Twiss parameters

of the distribution can then be calculated using equation 3.2, equation 3.3 and equation 3.4.

Higher than second order moments can also be used to describe the distribution in more detail but that is less common. The third order moments represent the skewness of the bunch distribution and would quantify the asymmetry of the bunch. The fourth order moments would correspond to the kurtosis of the bunch distribution and would measure how tailed the bunch distribution is. The fourth order moments are used in the definition of the Halo parameter [72] which is a parameter used to quantify the extent and number of the diffuse particles around the bunch core. The Halo parameter is defined in equation 3.8

$$H = \frac{3I_4}{2I_2} - \frac{15}{7} \tag{3.8}$$

where I_4 is

$$I_4 = \langle q^4 \rangle \langle p^4 \rangle + 3\langle q^2 p^2 \rangle^2 - 4\langle qp^3 \rangle \langle q^3 p \rangle \tag{3.9}$$

and I_2 is

$$I_2 = \langle q^2 \rangle \langle p^2 \rangle - 4\langle qp \rangle^2 \tag{3.10}$$

and p is the position and q is the momentum.

It is useful to be able to describe a bunch as a whole using parameters such as the emittance however substructure of the bunch can also be important to describe. In terms of the variation in the bunch parameters along the length of the bunch slice parameters are often used. These are found by dividing the bunch up longitudinally into a number of slices and then calculating the beam parameter of interest for a single longitudinal slice only. The most commonly used slice parameter is the slice emittance but other slice parameters could also be calculated such as the slice halo parameter.

3.2 Simulation codes

Particle accelerators are expensive complicated machines. As a result it is important to understand how the machine will behave before the mechanical design and construction begins. This means that extensive calculations must be done during the conceptual and technical design phase. As the behaviour of real accelerator systems is too complicated to be calculated using purely

analytical approaches numerical simulations need to be performed. Although analytical calculations do provide important conceptual understanding of the behaviour of the system. There are many simulation codes for modelling the different sub-components of the accelerator such as the magnets and RF cavities as well as codes for modelling the beam dynamics in the accelerator.

Beam dynamics simulation codes

The behaviour of particle beams in accelerators can be complicated particularly when lattices are large or collective effects such as space charge are relevant. There are a range of different approaches to simulating beam dynamics which have different ranges of applicability, specific effects they are capable of modelling and computational cost. It is important to ensure that an appropriate code is used when modelling a particular section of an accelerator.

Matrix formulation based codes

One of the most commonly used descriptions of the beam dynamics in a particle accelerator is the matrix formalism. In this formalism elements in the accelerator are represented by matrices. The matrices for series of elements can be found by multiplying the matrices for each of the elements together. The transfer matrices can be used to calculate the motion of a particle through the lattice or to calculate how the Twiss and dispersion functions change through the lattice. This matrix description of beam dynamics can be used to develop codes that calculate how the Twiss parameters and dispersion propagate through an accelerator lattice. These codes can be capable of accounting for coupling between the different planes in the phase space of the beam. They can also be extended to calculate higher order dispersions. Matrix codes are very fast but are not capable of modelling all phenomena that occur in accelerators in particular they are not capable of modelling collective effects accurately. A prime example of this would be space charge in low energy beams. Examples of codes that have the ability to make matrix calculations are MADX [73] and OptiM [74].

Simulation codes for space charge dominated beams

To simulate the effect of space charge on the beam dynamics in injectors specialised simulations codes must be used. These generally work by tracking

macroparticles. In this approach the large number of particles in the bunch are approximated by a significantly smaller number of macroparticles with the same mass to charge ratio as the particles in the real bunch. The self fields due to the space charge is calculated by dividing space up into a grid or mesh and calculating the fields generated by the macroparticles in each of the mesh cells. The motion of the macroparticles when acted upon by the external fields of the accelerator lattice elements and the space charge fields is calculated. An example of a commonly used integrator for calculating the motions is fourth order Runge-Kutta.

There are a number of codes of this type. Some examples include ASTRA [75], OPAL [76] and GPT [77]. In this thesis ASTRA and OPAL are used for the space charge simulations. These codes have a number of simulation parameters which can be adjusted. These include the number of macroparticles, the number of grid cells and the length of the time steps. To ensure that the simulations are accurate the appropriate settings for these parameters should be investigated. Some space charge codes allow for the values of some of these parameters to be adaptive. The version of OPAL used in this thesis does not have that functionality.

Electrostatics codes

The calculation of the electromagnetic fields produced by specific accelerator components can be done using a number of codes. In this work some calculations of electrostatic fields are needed, for this the code POISSON was used [78]. POISSON is a 2D finite element code and calculates the fields either in 2D cartesian coordinates or for axially symmetric fields. In the case of the electron gun electrostatics in chapter 4 the electron gun is axially symmetric. It uses a triangular mesh. The size of this mesh is an adjustable parameter which may affect the simulation run time and accuracy.

3.3 Genetic algorithms

Introduction

Genetic algorithms are a form of optimisation algorithm that work in manner analogous to evolution in nature [79]. They have been used for accelerator optimisation in wide range of situations for example the optimisation of the Cornell DC gun based injector [80]. Genetic algorithms are useful as they can

be effective for optimisation problems which may not be tractable with other optimisation techniques. They are also conveniently parallelisable as they are population based optimisation algorithms and the different solutions in the population can be evaluated in parallel. However despite ease of parallelisation they are often very computationally intensive. In addition they rarely have theoretical guarantees of convergence at the true local minima. Another consideration is that they are stochastic optimisation algorithms so will never give the same results twice.

They work by optimising a population of individuals over a number of generations. An initial population is created and evaluated. Then a selection operator is used to select good solutions, then these solution are used to produce the next generation of solutions. This is done using a crossover operator to combine two parent solutions and a mutation operator to randomly vary the offspring solutions. These offspring solutions are then evaluated. The process then repeats from the selection of new parents for the next generation until some termination criteria is met. A flowchart of this process can be seen in figure 3.1.

The different part of the genetic algorithm have different functions in the optimisation. The selection process is what guides the search. The crossover and mutation operators both generate new solutions but they affect the search in different ways. The crossover operator combines the good solutions in various ways with the hope of finding better solutions. While the mutation operator changes solutions in a random way to find new areas in the solution space to explore which may potentially lead to an improvement in the quality of the solutions. Generally crossovers cause the optimisation to tend towards convergence and mutation will cause it to tend towards exploration. An effective genetic algorithm needs a balance between convergence and exploration. The termination condition determines when the optimisation process ends. There are a number of different termination conditions which could be used for example a maximum number of evaluations of the solutions being carried out or it could be based on the amount of improvement in the population generation by generation. So the optimisation would finish after no further significant improvement is seen.

The genetic algorithm described above is a generic one with no specific description of how the different components work or what the parameters are. However there are a wide range of possible selection methods, crossover and mutation operators, and termination criteria as well as algorithm parameters

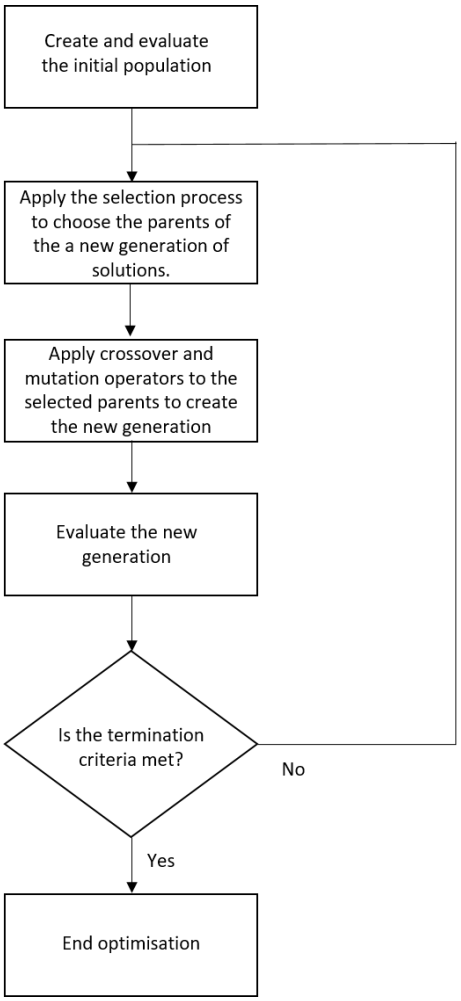

Figure 3.1: A flowchart of the process of a genetic algorithm.

which need to be set. These parameter can include the population size, mutation rate, crossover rate and any parameters which specific operators used might have. The choice of operators and the settings of the parameters can have a significant effect on the convergence speed and quality of the solutions found.

Optimising multiple objectives

Often it is desirable to optimise more than one aspect of the solution at the same time. This would mean that optimisation has more than one objective. The simplest way to achieve this is to combine the objectives into one objective and then to optimise this objective. This can be done by weighting the objectives and then summing them. However the chosen weighting can have a significant effect on the solution which is found and it isn't obvious prior to completing the optimisation how a given weighting will effect the search.

It is also possible to do true multiobjective optimisation where multiple objectives are optimised without needing to reduce them to one objective [81]. This requires finding a way to rank solutions based on how good they are. This is not as easy as it is for single objective optimisation as there is no single measure of solution quality. There are a number of ways to do this. One commonly used approach is the concept of Pareto dominance. Assuming minimisation a solution is said to Pareto dominate another solution if all of its objective values are equal to or smaller than those of the dominated solution and at least one of the objective values is smaller. Any solutions which don't Pareto dominate each other can be considered to be equivalently optimal. If the objectives are competing with each other there is not a single best solution there is instead a set of equivalently optimal solutions which do not dominate each other. These can be referred to as non-dominated solutions. The line or surface on which all of the non-dominated solutions lie is called the Pareto front. One advantage of multi-objective optimisation algorithms is that they give a set of non-dominated solutions rather a single solution at the end. This allows the choice about how to trade off between the objectives to be made after the optimisation once how the objectives trade off is understood.

The concept of Pareto dominance can be further extended to allow for constraint handling. This is done by assigning every solution a constraint violation value in addition to their objective values that is determined by how much it violates the constraints. Then when the ranking of solutions is done when two solutions with constraint violation values are compared the one with the lower constraint violation dominates the other. When a solution with a constraint violation value is compared with with a solution that satisfies all the constraints then the solution that satisfies the constraints always dominates. When solutions with no constraint violations are compared the usual Pareto ranking approach is used. This approach does lead to the loss of information

about the solution space contained in the solutions with constraint violation.

As the number of objectives increases the algorithms typically used for two and three objectives become less successful. One reasons for this is that Pareto dominance as a concept to distinguish between different solutions becomes less effective. As larger and larger proportions of the population are in first Pareto front. So there is less selection pressure towards better solutions. This means that specialised many objective algorithms are needed for problems with four or more objectives.

Algorithms

NSGAII

NSGAII is a widely used multiobjective genetic algorithm [82]. The main defining feature of NSGAII is its selection mechanism. It uses an elitist Pareto dominance based selected mechanism with a mechanism to help maintain diversity in the population. When a selection mechanism is described as elitist it means the best individuals are selected from both the parent and offspring populations. The advantage of using an elitist selection method is that it guarantees that the best solutions will not be lost and the newly selected population will not be worse than the previous generation's population.

NSGAII's selection mechanism works as follows. Firstly the parent and offspring populations are combined into one population. Then this population is ranked based on Pareto dominance. Initially individuals are selected exclusively based on Pareto dominance. The Pareto fronts are added in order (first, second, third and so on) until adding a front to the next generations population would cause that population to be larger than the population size used in the optimisation. Only a portion of this final front can be selected. The individuals are selected from the last front in a manner which helps maintain diversity in the population. This is done by calculating the crowding distance for all of the individuals. The crowding distance is found by finding the normalised distance between the two neighbouring points for all of the objective values. Then averaging the distances from the different objectives to give a single crowding distance value. The individuals with the highest crowded distance are selected first as they are in less occupied areas of the solution space. Individuals are selected until the selected population size is the population size set for the optimisation. Then the selection process ends.

This selection mechanism can in theory be combined with any crossover and mutation operators. However in the original NSGAII paper the simulated binary crossover [83] and polynomial mutation are used for real coded optimisation problems. These operators will also be used for the optimisations done in this thesis. They both have a free parameter that determines how far from the parent solution or solutions that the probability distribution that the new individual is sampled from extends.

NSGAIII

NSGAIII is a many objective optimisation algorithm based on NSGAII [84] [85]. The difference between the algorithms is in the selection mechanism. The selection mechanism is the same except instead of the crowding distance it uses a set of reference points to help with maintaining diversity. The arrangement of the reference points is an additional input to the algorithm compared to NSGAII. Essentially any arbitrary arrangement of points can be supplied. However there are two main reasonable types of arrangements. Firstly those that ensure a good spread over a hyperplane such as the approach of Das and Dennis [86] and secondly those that articulate preferences about which areas of the solution space should be explored.

As mentioned above the selection method is the same as in NSGAII until the diversity maintaining partial selection of the last selected front. The way that the reference point based approach works is as follows. Once all of the individuals which are selected based on Pareto dominance have been selected and there is a front that needs some but not all of the individuals selected from it. The individuals already selected based on Pareto dominance are associated with the reference points. A count of how many individuals are associated with each point is calculated. The individuals in the final front that is only going to have some of the individuals selected from it are associated with the reference points as well. The references points with the smallest number of already selected individuals are found. The points within this group with no individuals in the final selected front associated with them are discarded for this generation as there are no individuals which could be selected associated with them. The remaining points that do still have individual associated with them which could be selected are found. If there is more than one point remaining a point is selected at random. Then if there is a single individual associated with the point from the last selected front the individual is selected. Otherwise

if there is more than one individual associated with the reference point one is selected at random. The selected individual is added to the parents of the next generation and is removed from consideration so it isn't selected twice. Then the counter of how many selected individuals are associated with the reference point increases.This procedure is then repeated until the selected population size is equal to the population size parameter used in the optimisation. Just like with NSGAII this selection mechanism can be combined with any crossover and mutation operators but in the original paper simulated binary crossover and polynomial mutation are again used.

Chapter 4

Electron gun optimisation

4.1 The PERLE injector and electron gun requirements

The PERLE injector must be capable of delivering high average current beams at the required beam quality. The specification for the PERLE injector can be seen in table 4.1. To be capable of meeting this specification PERLE will need to use an electron gun capable of delivering a bunches at MHz repetition rates. This means either a DC, VHF or SRF gun.

Table 4.1: The specification of the PERLE injector [15].

Parameter	**Values**
Emittance	< 6 mm·mrad
Bunch charge	500 pC
Repetition rate	40.1 MHz
Current	20 mA
RMS bunch length	3 mm
Total injection energy	7 MeV

Of these three options PERLE will use a DC gun. This is for two reasons. Firstly, of three technologies DC is the one with the most proven record having been used successful on several previously operational ERLs. Secondly, the 350 kV DC electron gun previously used on the ALICE ERL is available after the decommissioning of that machine. The gun will need to be upgraded to meet PERLE's requirements but being able to reuse it will still save costs.

4.2 Electron gun upgrade

An upgrade was designed for the electron gun when it was being used for the ALICE ERL [87]. However this upgrade was never carried out. A version of the upgrade, modified for the needs of PERLE, will be carried out. Some of the components needed for the original upgrade were manufactured and will be used for PERLE others will need to be manufactured specifically. The upgrade broadly consists of four improved capabilities: allowing photocathode exchange without breaking the gun vacuum, allowing the photocathode material to be changed to an alkali antimonide, reducing the back ion bombardment which should help extend the photocathode lifetime and replacing the electrodes which should have positive effects on the beam dynamics.

Cathode exchange without breaking the gun vacuum will be added through the addition of a load lock system. As the cathode electrode has a back mounted geometry the cathodes need to be inserted and removed via the side of the cathode electrode rather than through the back of the electrode as would be done for a top mounted electrode. The benefit of the load lock system is that it significantly reduces the time required to replace the photocathodes. Previously as the vacuum needed to be broken the process of ventilating the gun, replacing the cathode, pumping down to the required vacuum, activating the photocathode and doing high voltage conditioning meant that replacing the photocathode could take up to four to six weeks [88]. The load lock system allows for photocathode exchange in a few hours. This will lead to a reduction in the machine downtime. The load lock systems also allows photocathodes of different materials to be used. In the case of PERLE for unpolarised operation instead of GaAs an alkali antimonide such as CsK_2Sb will be used. The addition of the load lock system would allow for different photocathode material options to be explored in the real machine. If an upgrade to allow for a polarised operation mode was performed this would also allow for switching between polarised and unpolarised operation by switching the photocathode.

Another part of the upgrade is that the anode in the gun will be biased to +5 kV. The reason for this is to mitigate the back ion bombardment [89]. Back ion bombardment is the process by which positively charged ions produced when the electron beam ionises the residual gas are accelerated by the DC electric field of the gun towards the photocathode [90] [91] [92]. These ions strike the photocathode and damage it causing a degradation in the quantum efficiency. Once the quantum efficiency has degraded past a certain point

the photocathode is no longer usable. So this mechanism causes a reduction in the photocathode lifetime. The ions can either be produced in the gun where they are immediately accelerated towards the photocathode by the gun electric field or outside the gun where they drift towards the gun due to pressure differences in the vacuum system. Then once they arrive in the gun they are accelerated towards the photocathode. The biased anode is to prevent the ions produced in the injector after the gun from entering the gun where they would be accelerated towards the photocathode.

Another possible way of mitigating the effect of back ion bombardment is to illuminate the photocathode off center as the ions mostly strike the center of the photocathode. So if the emission area isn't in the center of the photocathode the damage to the emission area will be less. This is however unfortunately not an option for PERLE as the combination of high bunch charge and the low photocathode electric fields of DC electron guns mean that the spot size of the photoinjector laser pulse will be large enough that it is impossible to avoid it covering the center of the photocathode. A final possible way to mitigate the back ion bombardment which was explored during the design of the original upgrade is to offset the cathodes from the center of the gun [93]. This unlike the biased anode would help with the ions produced inside the gun. However this approach was not modelled or simulated in these investigations for PERLE. It is a potential area for future investigation.

The cathode electrode also needs to be replaced. The current electrode is a flat faced electrode. However this could be replaced with a focusing electrode. An example of this would be a Pierce electrode which has a focusing angle of 22.5°. For a continuous beam this electrode geometry theoretically leads to a balance between the space charge defocusing and the cathode electrode's focusing [94]. The beam in PERLE is not continuous it is instead bunched. So this focusing angle may not be optimal for the high charge bunches required by PERLE. The use of a focusing electrode could help with the emittance compensation and controlling the transverse beam size. This does however come at the expense of reduced surface electric field on the photocathode. Which means that larger laser spot sizes would be needed to extract the same charge leading to larger thermal emittances. Finding an appropriate balance between the focusing and the photocathode surface field is something which requires optimisation.

4.3 Electron gun optimisation process

Overview

The electrode geometry was optimised on the basis of beam dynamics performance with the objectives of minimising the beam sizes and slice emittance. This required simulation of the electrostatics fields in the electron gun and the beam dynamics to obtain the required beam parameters. The electrostatics of the gun were simulated using the code POISSON [78] and the beam dynamics were be simulated using the accelerator code OPAL [76]. The optimisation itself was done using the multiobjective evolutionary algorithm NSGAIII [84] [85] implemented using the python library DEAP [95].

The beam dynamics simulations start at the cathode in the gun and then continue through the first solenoid up to the approximate position of the second solenoid. The second solenoid and buncher cavity were not included in the simulation. The layout of the beamline simulated can be seen in figure 4.1.

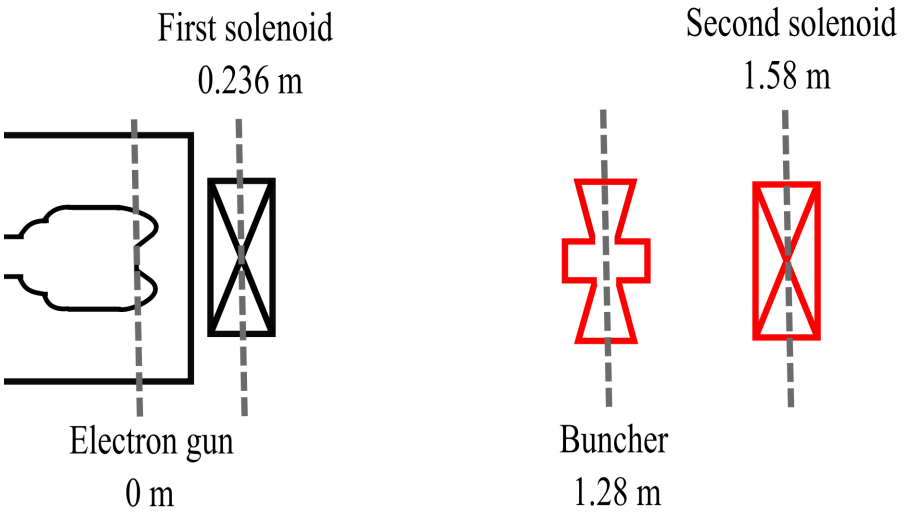

Figure 4.1: The layout of the section of the beamline simulated in the electron gun optimisation. The elements marked in black are included in the simulation while the second solenoid marked in red is not.

Initially PERLE will operate with an unpolarised 20 mA beam, however having the potential to carry out an upgrade to allow operation with polarised electron beams is something that may be of interest. This would require lowering the operational voltage of the electron gun to 220 kV. The motivation

for lowering the voltage is to reduce the field emission in the gun which might lead to damage to the sensitive GaAs polarised photocathode. As well as to reduce the energy of the beam at the exit of the gun as a lower energy beam will be easier to perform spin manipulations on. At the current level of technology polarised cathodes are not capable of delivering the same average currents as unpolarised cathodes. The current record for polarised average current is 10 mA [36]. This limit on achievable average current and the lower quality polarised beams due to both the lower gun voltage and the effect of the spin manipulation system mean that it will remain desirable to have a higher current lower emittance unpolarised operation mode. So an electrode optimised purely for 220 kV operation would not be ideal. As a result a hybrid unpolarised-polarised electrode which is designed to be effective at both 350 kV and at 220 kV would be preferred as it would leave the possibility of a later polarised upgrade open. This hybrid electrode is what will be optimised in this chapter.

Objectives, constraints and variables

The optimisation had four objectives, two for each voltage. For both voltages the two objectives were to minimise the maximum RMS beam size which occurs at any point along the simulated beamline and the average slice emittance value at the end of the simulated beamline. The transverse beam size was minimised as it should be kept as small as possible to ensure that the beam will fit through all the apertures of the beamline. Slice emittance was chosen over projected emittance as an objective in this optimisation as the value of the projected emittance at the position of the second solenoid is not particularly important as the it isn't compensated at that point. Instead what matters is the final value that the transverse emittance can be compensated down to at the point of the transition out of the space charge dominated regime. Slice emittance is a better measure of the compensatibility of the emittance value than the projected emittance. To ensure better statistics for all slices the slice emittance was calculated using 10 slices of equal particle count. As there were more than three objectives the many objective optimisation algorithm NSGAIII was chosen [84] [85].

In addition to these four objectives the optimisation also has four constraints, again two for each voltage. The two constraints for each voltage were that there should be no particle losses and that the maximum surface electric field should be less than 10.0 MV/m. The no particle losses constraint is to

prevent the optimisation from finding solutions with settings that are not capable of extracting the full bunch charge from the cathode. As one way the optimisation could reduce the effects of the space charge on the beam quality would be to optimise to intentionally loose particles and hence have lower bunch charge. These solutions do not meet the specification and hence should be avoided. The goal of the surface electric field constraint is to prevent breakdowns and field emission. A value of 10 MV/m for the maximum surface field was chosen as a technically achievable value.

The optimisation has 14 variables to describe the electron gun, the photoinjector laser pulse and the modelled section of the following injector beamline. There are 8 variables to describe the electron gun geometry. The cathode is described by 5 of these, the anode by 2 and then the final geometry variable is to describe the cathode-anode gap. In addition to 8 variables to describe the electron gun geometry which is fixed for both voltages there are six variables to describe the laser pulse and first solenoid. These are in two groups of three one for each voltage as the lasers for the unpolarised and polarised operation will be different and the solenoid field strength is an adjustable parameter. The two parameters that describe the photoinjector laser pulses are the transverse spot size and the laser pulse length.

Electrode geometry description

As mentioned in the section above there are 8 variables which describe the geometry of the electron gun. A diagram of the electron gun with different regions and control points marked can be seen in figure 4.2. Certain aspects of the geometry are fixed by the pre-existing upgrade design. In particular by the design of the load lock system. The position of the photocathode cannot be changed. So to change the cathode anode gap the anode must be moved closer to the cathode. Additionally the slot in the side of the cathode electrode for the photocathode to be inserted has a fixed position and must be on the side of the cathode electrode before the curvature at the front begins so how far down the side of the cathode electrode the electrode can continue to be curved is limited.

The cathode electrode is described by five variables. It is divided into two regions. The first region A is the flat focusing section of the electrode. It consists of a straight line described by two variables. The end of the line closest to the photocathode is fixed due to the fixed location and size of the

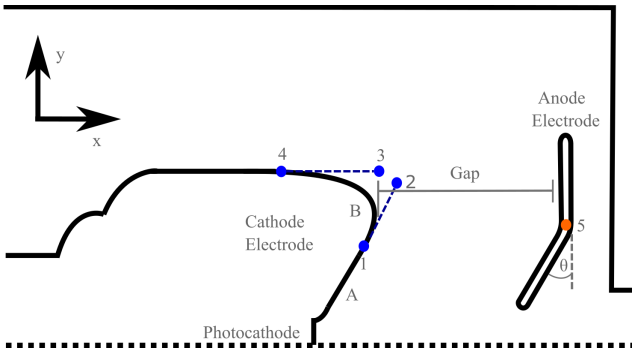

Figure 4.2: A sketch of the electrode geometry with the regions, distances and control points are marked. In the coordinate system marked on the axis x indicated the longitudinal direction of the axis the beam moves along while y indicates the radial distance transversely to the beam axis.

photocathode. The other end of the line can move freely and is described by two variables that are the radial and longitudinal positions of the end of the line. The second region B is the curve of the electrode ball. It is represented by a third order Bézier curve [96] [97] with four control points and is described by three variables. The first of the control points, point 1, is the end of the straight focusing section of the electrode (section A) and is described by the same two variables. Point 2 is enforced to be in line with point 1 to ensure smooth continuity between sections A and B. It is described by one variable that determines how far it is from point 1. Point 4 is the end of curved section of the electrode and determines where the cylindrical side of the cathode electrode ball begins. It is described by one variable that specifies its longitudinal position as its radial position is fixed. Point 3 is enforced to be in line with point 4 to ensure smooth continuity between the curved section B of the electrode and the flat side. This is done by fixing its radial position to the same value as point 4. So point 3 is described by one variable that determines its longitudinal position. Bézier curves are not a type of curve that POISSON supports in its input files. As a result the Bézier curve is approximated by a series of circle sections using the method described in this paper [97] so that the curve of section B can be represented in the input file.

The anode consists of a flat section and an angled section and is described by two variables. One which is the angle between the angled and flat sections and one which represents the position on the anode the angled section begins.

The distance between the cathode and anode electrodes is described by one variable. As indicated in figure 4.2 the distance is between the closest point on the cathode to the anode and the flat unbent section of the anode.

This geometry is translated into two POISSON input files, one for each voltage, which are then run with a mesh size of 1 mm. From each electrostatic simulation three things are obtained. Firstly the electron gun fieldmaps. These are are used in the beam dynamics simulations. Secondly the photocathode surface field which is used when calculating the Shottky modification to the initial momentum distribution. Finally the maximum surface electric field in the gun which is used as a constraint in the optimisation.

Beam dynamics simulation

The fieldmaps for both the 220 kV and 350 kV versions of the gun are then used in a beam dynamics simulations done using ASTRA [75]. The simulations are done with a particle count of 4096 and space charge grid of 16x16x16. From the simulations the beam sizes and max slice emittance values which are used as objectives are obtained. The beamline simulated in both cases can be seen in figure 4.1. For both voltages the initial energy distribution of the bunch which leads to the initial emittance is modelled taking account of the the cathode material, laser wavelength. For the 350 kV the cathode assumed is Cs_3Sb with a 532 nm green laser while for the 220 kV the cathode assumed is negative electron affinity activated (NEA) GaAs. Additionally for the 350 kV case the modification to the initial emittance due to Schottky effect as a result of the electric field on the photocathode surface is taken into account.

4.4 Results of the optimisation

The optimisation produces a 4D Pareto front of equivalently optimal electron gun designs. Visualisation of a 4D front is challenging. In this case as the optimisation is for two different voltages it makes sense to present them separately so two different 2D projections of the 4D front were plotted. The Pareto front projections can be seen in figure 4.3.

From looking at the Pareto fronts it can be seen that the slice emittances at a gun voltage of 220 kV are larger than at 350 kV and to get lower slice emittances the beam needs to be larger. To get the best values the transverse beam size needs to be > 7.5 mm. However in practice the beam size needs

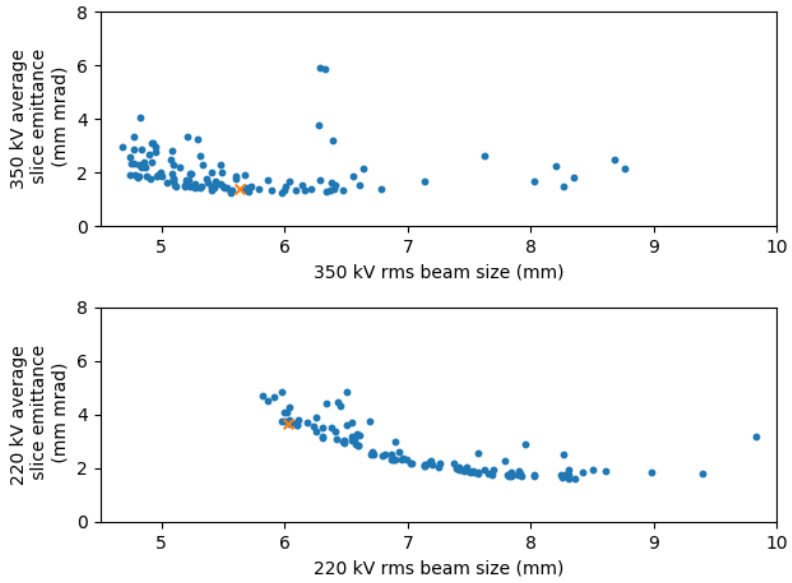

Figure 4.3: Two 2D projections of the 4D Pareto front showing the trade off between transverse beam size and average slice emittance for the two voltage separately. The chosen solution is plotted as an orange ×.

to be kept small enough to pass through all of the apertures of the beamline. A maximum transverse beam size of 6 mm was chosen as a reasonable upper limit to ensure that the beam will be small enough to fit. Considering this a preferred solution was selected from the Pareto front which is marked with an orange × in figure 4.3. In the polarised operation mode this selected point makes a significant trade off of average slice emittance against beam size to get the beam size within the acceptable range. An image of the geometry of the chosen solution can be seen in figure 4.4

The chosen electron gun geometry has a relatively small focusing angle of 7.3°. This is significantly less than the 22.5° angle of a Pierce electrode [94]. Having a smaller focusing angle means that the transverse focusing will be less but the photocathode surface field will be higher. It is likely that the 220 kV operation mode is more significant than the 350 kV for determining what the optimal electrode geometry is. As the need to extract the relatively large bunch charge of 500 pC at the lower voltage of 220 kV with a laser spot size small enough to fit on the 10 mm diameter photocathode puck will set a limit on how low the photocathode surface electric field can be. It may be the case

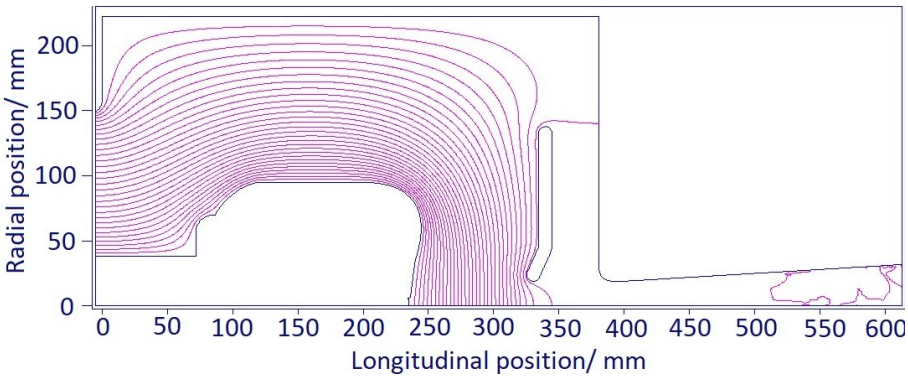

Figure 4.4: The geometry and field lines of the chosen hybrid electron gun solution.

that a gun optimised to exclusively operate at 350 kV would have a larger focusing angle without the constraint of the 220 kV operation mode. Although to confirm that an optimisation would need to be done for that single voltage.

4.5 Conclusion

A hybrid 350 kV - 220 kV electrode geometry has been optimised. The motivation for optimising for two voltages is to allow for the possibility of a later upgrade to polarised operation for PERLE. The later injector optimisations in this thesis will be using the electron gun fieldmap from the chosen solution here.

As part of future work it should be evaluated if the hybrid electrode is the best option. This decision should be based on whether the experiments that are going to be done with PERLE will need polarised electrons. If they don't there is no need for an electrode that can function at two voltages and an electrode optimised exclusively for 350 kV should be used. If polarised electrons will be required but as an upgrade rather than as a baseline feature an electrode optimised exclusively for 350 kV should be used initially and then replaced with a hybrid electrode or an electrode specifically optimised for 220 kV as part of the upgrade. If the hybrid electrode is not initially the best option an optimisation for a 350 kV electrode geometry should be performed. If that optimisation is carried out it will also allow it to be determined if it was the low voltage requirements that led to the smaller focusing angle in the electrode geometry discussed early in this chapter as speculated above.

It should also be decided whether the use of an offset cathode to minimise the back ion bombardment is an approach which is going to be used for PERLE. This decision will depend on how significant an effect the back ion bombardment will have on the cathode lifetime and the operational effectiveness of PERLE as well as whether the required beam quality can be achieved using an offset cathode. Further investigation is required in both of these areas.

Once a final decision has been made about the required operational voltages and whether or not to use an offset cathode a more realistic electron gun model should be created in a code capable of doing 3D electrostatic simulations such as CST. The surface electric fields and beam dynamics performance of the more realistic 3D design should then be investigated and if necessary further optimisation should be done. After the 3D electrostatics simulations have been carried out and it has been confirmed that the surface fields are acceptable and that the beam quality can be achieved the mechanical design of the electrodes can be carried out.

Chapter 5

PERLE injector

5.1 Injector overview

The PERLE injector will be based on a DC photocathode gun with a SRF booster linac. The specification of the injector is reproduced in table 5.1 for reference. As discussed in the previous chapter the DC electron gun will be a reused and upgraded ALICE electron gun. For the details of the upgrade see the previous chapter. In addition to the gun another reused component will be used. The booster will use a pre-existing cryomodule. This cryomodule housed a 750 MHz SRF booster with four single cell cavities the second of which is a third harmonic cavity [56]. For PERLE the booster will need to be modified to operate at 801.58 MHz. This will require the replacement of all of the SRF cavities so there is the potential to change the types of cavities. This could involve either using all main harmonic cavities or having one of the cavities be a higher harmonic as in the original booster linac design.

Table 5.1: The specification of the PERLE injector.

Parameter	**Values**
Emittance	< 6 mm·mrad
Bunch charge	500 pC
Repetition rate	40.1 MHz
Current	20 mA
RMS bunch length	3 mm
Total injection energy	7 MeV

The first injector layout to be investigated is the one that can be considered

as the baseline design. It uses two solenoids and a buncher cavity in the low energy section and does not use any higher harmonic cavities. The layout of this design can be seen in figure 5.1.

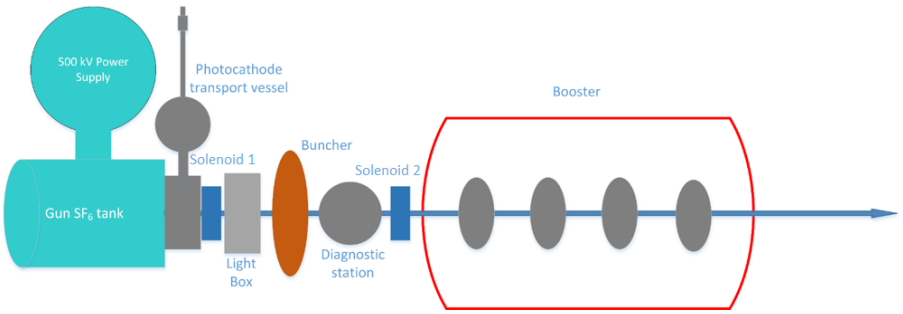

Figure 5.1: The baseline layout of the PERLE injector [88].

The positions of the magnets and RF cavities in the injector is important and there are a number of factors that need to be considered. In injector design, from a beam dynamics perspective, it is generally preferable to keep the beamline as short as possible. However there are competing technical requirements as elements must be separated enough that their fringe fields don't overlap. Additionally other important components such as diagnostics, vacuum pumps and the lightbox for the laser need to be included in the beamline.

The position of the first solenoid is fixed by the design of the ALICE electron gun. It is placed against the outer wall of the gun vacuum chamber as close as is physically possible to the photocathode. The ALICE gun has a nose cone shaped beam pipe at its exit around which the solenoid is placed. As a result the solenoid position cannot be changed to be further away from photocathode as it will not fit around the enlarged beam pipe. For the positions of the buncher cavity, the second solenoid and the entrance of the booster the distances in the ALICE injector were used as guidelines to estimate the minimum distances between each element required to accommodate the necessary non-beam dynamics relevant components. Although some of the distances were shortened as there was some beampipe without any other components on it in the ALICE injector that could be removed and it was assumed that due to the higher bunch charge in PERLE it would be possible to use shorter BPMs. The booster linac is a pre-existing component and as a result the distances between the RF cavities and the distance between the entrance and exit flanges is fixed.

The injector needs diagnostics so that the behaviour of the beam can be

observed as an understanding of the beam dynamics is important for tuning the machine. However the fact that a longer injector will have more opportunity for space charge to degrade the beam quality means that the number of diagnostics that can be included before the booster is limited. Two BPMs (Beam Position Monitors) and a YAG (Yttrium Aluminium Garnet) screen is a common set of diagnostics [98] [99]. These diagnostics are only able to measure a small number of the beam parameters and are thus insufficient for fully tuning the beam. For example with these diagnostics there is no way of measuring the bunch length. For obtaining a more comprehensive set of beam parameters a diagnostic line after the booster needs to be used which should be capable of measuring the transverse and longitudinal beam sizes and emittances as well as the beam energy.

The specifics of the cavities in the booster also need to be considered. An important factor is that the particles entering the first cavity of the booster are not yet ultrarelativistic. They are moving at approximately 80% of the speed of light. This means that they take longer than ultrarelativistic particles to pass through the RF cavity. RF cavities are designed for particles with a specific velocities. The cavity length is what determines what particle velocity a specific cavity is designed for. The ratio of particle velocity to the speed of light that a specific cavity is designed for is referred to as the cavity beta. Higher beta cavities are longer than lower beta cavities. To reduce manufacturing costs it was decided that the booster linac should have a single type of accelerating cavity rather than manufacturing multiple cavities. Therefore a decision needed to be made about whether to use $\beta = 0.8$ cavities or $\beta = 1.0$ cavities. Both of these choices have pros and cons. The lower beta cavities will have less deceleration of the bunch in the first cell and hence the initial brief increase in the space charge force which could cause degradation of the beam will be smaller. However they will be less efficient for acceleration of the ultrarelativistic beams later in the booster. The $\beta = 1.0$ cavities will be more efficient at accelerating the ultrarelatistic beams in the booster. However they will have more decceleration in the first cavity which will lead to a larger momentary increase in the space charge forces. To favour better beam quality it has been decided that $\beta = 0.8$ cavities will be used.

5.2 Injector design theoretical considerations

The goals of the injector design are to have as small a transverse emittance as possible while maintaining as linear a longitudinal phase space distribution as possible and also meeting the other requirements such as achieving the desired final bunch length and energy. In photoinjectors the beam quality is never better than it is at moment of emission at the photocathode so the objective is minimise the degradation in the beam quality that occurs in the injector.

Particle emission and thermal emittance

The thermal emittance in an injector depends on the photocathode material, the photoinjector laser wavelength, the electric field on the photocathode and the transverse spot size of the laser on the photocathode. A comparison of the thermal emittance against the final emittance will show how effective an injector is at preserving the beam quality.

Spicer's three step rule

In photoinjectors the electrons are produced by the photoelectric effect from a photocathode. A pulsed laser shines on the photocathode stimulating the emission of the electrons. To be emitted the electrons must be given sufficient by the laser photons to escape the photocathode's potential barrier. This photoemission process can be thought of as taking place in three distinct steps. This is know as Spicer's three step model [100]. The three steps are:

1. Absorption of the photon
2. Transport to the surface
3. Escape from the potential barrier

Using this model an expression for the thermal emittance of the electron beam at the point of emission can be derived [23]. This is given by equation 5.5.

$$\epsilon_{thermal} = \sigma_x \sqrt{\frac{\hbar\omega - \phi_{eff}}{3mc^2}} \tag{5.1}$$

Where $\epsilon_{thermal}$ is the thermal emittance, σ_x is the rms beam size, $\hbar$ is the reduced Planks's constant, ω is the wavelength of the incident light, ϕ_{eff} is the effective work function of the photocathode, m is the mass of the electron and c is the speed of light in a vacuum.

The effective work function is used because the work function of the phot-cathode may be changed by the applied electric field via the Schottky effect.The equation for the effective work function taking account of this effect is given by equation 5.2.

$$\phi_{eff} = \phi - \sqrt{\frac{e^2 E_{applied}}{4\pi\epsilon_0}} \tag{5.2}$$

Where ϕ is the work function of the photocathode material and e is the charge of the electron

Space charge limited emission

The electric field of the emitted particles can limit the amount of extracted charge from the photocathode leading to saturation of the emission. The electrons in the bunch produce an image charge on the cathode which acts to counteract the extracting electric field. In photoinjectors where the laser pulses are short an expression for the the space charge limit can be found by assuming that the emitted bunch is an infinitesimally thin sheet of charge close to the cathode [23]. The electric field due to the space charge can then be modelled as the electric field between the plates of a capacitor. The space charge limit on emission is when the electric field from the space charge is equal to the electric field on the cathode. Following this reasoning we get equation 5.3.

$$E_{SC} = \frac{q}{A\epsilon_0} = \frac{\sigma}{\epsilon_0} = E_{applied} \tag{5.3}$$

Where E_{SC} is the space charge field, q is the bunch charge, A the area that the electrons are being emitted from, ϵ_0 is the permittivity of free space, σ is charge density and $E_{applied}$ is the electric field on the cathode.

Assuming a uniformly circular bunch is emitted an expression for the radius of the space charge limited emission spot in terms of the bunch charge and electric field on the cathode can be derived. It is given by equation 5.4.

$$r = \sqrt{\frac{q}{\pi\epsilon_0 E_A}} \tag{5.4}$$

Combining this with the expression for thermal emittance given in equation 5.5 we can get an expression for the minimum thermal emittance of a given combination of applied electric field, bunch charge, photocathode work function and laser energy. This expression is given in equation 5.5 [101].

$$\epsilon_{thermal} = \sigma_x \sqrt{\frac{\hbar\omega - \phi_{eff}}{3mc^2}} \tag{5.5}$$

Ballistic bunching

At low energies where the beam is not yet relativistic differences in particle energy can produce significant differences in particle speed. This fact can be exploited to bunch the electron beam. This done by imposing a linear energy chirp on the beam using an RF cavity with the tail of the bunch having more energy than the head. This causes the tail of the bunch where the particles are moving faster than the head of the bunch to catch up with the head compressing the bunch.

Assuming no space charge there are two sources of non-linearity during this bunching process. Firstly a second order non-linearity due to relativistic effects. This occurs because a linear energy chirp does not correspond to a linear velocity chirp at energies where relatively is relevant. Secondly a third order RF non-linearity. The RF non-linearity is third order rather than second order as the RF cavity is set to the zero cross rather than on crest. The non-linearities are the limiting factor on how short the bunch can be compressed to. An expression for the final bunch length can be derived [102]. This expression is given in equation 5.6.

$$\sigma_{zf} = \sqrt{\left(\frac{f}{\beta^2\gamma^2}\sigma_\delta\right)^2 + \left(\frac{3\sqrt{2}\gamma^2}{2}\frac{\sigma_{z0}^2}{f}\right)^2 + \left(\frac{1}{\sqrt{6}}k^2\sigma_{z0}^3\right)^2} \tag{5.6}$$

Where σ_{zf} is the final bunch length, f is the focal length of the buncher cavity, β is the relativistic beta, γ is the relativistic gamma, σ_δ the uncorrelated relative energy spread of the electron bunch, σ_{z0} is the initial bunch length and k is the angular wave number of the RF buncher cavity divided by the relativistic beta.

The three terms correspond to three potential limiting factors on the final bunch length. The first term corresponds to the minimum bunch length in the absence of nonlinearities. To minimise the contribution from this term shorter focal length RF cavities can be used which means imposing larger chirps on the bunch. Additionally bunches with smaller initial relative spreads will lead to smaller final bunch lengths. This can be achieved with either higher beam energies or smaller absolute energy spreads. Higher beam energies however work against the bunching process due to the $\frac{1}{\beta^2\gamma^2}$ terms. As once the energy

becomes too high the difference in velocity between the particles becomes too small for there to be bunching via this approach.

The second term corresponds to the second order nonlinearity due to the nonlinearity in the relationship between the particle energy and particle velocity due to relativity. This term is minimised by reducing the relativistic gamma as the effect is less significant when relativity is less a significant factor. Increasing the focal length of the buncher cavity can also help with minimising this term. This runs counter to trying to minimise the first term so the optimal focal length will depend on which of the terms is most significant. Minimising the initial bunch length can also help with minimising this term.

The third term corresponds to the third order nonlinearity due to the imprint of the RF of the buncher cavity. This term can be minimised by increasing the wavelength of the RF cavity which means using a lower RF frequency. It can also be minimised by minimising the initial bunch length. As minimising the bunch length in the buncher minimises the amount of the non-linear component of the RF wave seen by the bunch.

The addition of space charge reduces the effectiveness of the bunching and leads to a longer minimum bunch length. The linear component of the space charge causes a change in the chirp of the bunch. The space charge accelerates the head of the bunch and decelerates the tail. This reverses the chirp induced by the RF buncher cavity and hence acts against the bunching. The non-linear space charge is also a source of non-linearities in the longitudinal phase space and hence a limiting factor on the compression. To accurately model the complete and complex behaviour of the bunch with space charge analytical approaches can no longer be used and simulations are required.

Emittance growth

In a photoinjector there are two main mechanisms which cause transverse projected emittance growth. These are space charge and aberrations. The transverse emittance growth caused by these mechanisms can be divided into two categories. The first of these emittance growth categories is due to the phase space distributions of different slices of the bunch being misaligned or mismatched with each other while the second is growth in the emittance of the slices themselves due to distortions in the shape of the slice's phase space distributions. In most injectors the first of these emittance growth mechanisms can be reversed while the second, slice emittance growth, is irreversible. As a result

the slice emittance sets a floor for how low the emittance can be compensated down to. The slice emittance can be compared to the projected emittance to see how much of the total emittance comes from the the contribution of slice misalignments and mismatches.

The space charge forces cause emittance growth in two ways. The first of these mechanisms causes projected emittance growth but not slice emittance growth. This mechanism can be reversed to significantly reduced the emittance growth that occurs in the injector. The origin of this mechanism is that as the space charge field along a bunched beam is not uniform the space charge forces are different at different positions along the length of the bunch. This means that the bunch has different transverse phase space distribution evolution at different longitudinal positions leading to an increase in the total transverse phase space area occupied by the bunch. One approach to conceptualising this is to think of the bunch as being divided along its length into different slices with constant emittances. These slices will experience different space charge forces which will cause them to evolve differently. These different evolutions cause the slice to rotate out of alignment in transverse phase space leading to growth in the projected emittance despite the fact that emittances of the individual slices remains constant [103].

This effect can potentially lead to substantial emittance growth but there is a commonly used technique for mitigating and reversing this emittance growth. The technique is called emittance compensation and was first described in 1989 [103]. This technique requires transverse focusing of some form and an accelerating structure. A simple conceptual description of the way this technique works is as follows. The space charge forces in the bunch cause the constant emittance slices to rotate out of alignment. This occurs in a correlated fashion so there is a correlation between the angle of the slice in transverse phase space and its longitudinal position. The application of transverse focusing can reverse the development of this correlation causing the slices to realign in phase space restoring the emittance back to the original slice emittance value. The beam should be matched into the accelerating structure such that it is accelerated as the emittance value compensates and the bunch transitions into the emittance dominated regime at the point where the slices realign freezing the emittance at its minimum value. This is a simplified description and the true behaviour is more complex as perfect slice realignment is not achievable in reality.

Secondly the non-linear space charge forces cause distortion to the transverse phase space distribution and consequent slice emittance growth. This

slice emittance growth is in practice irreversible and hence the focus in injector design is on minimising it [103]. This mechanism depends on the non-linear space charge forces present in the bunch which are dependent on the charge distribution of the bunch. This means that different bunch charge distributions will lead to different amounts of slice emittance growth. The bunch distribution can be shaped using the laser pulse distribution on the cathode as the initial bunch distribution will correspond to the laser pulse distribution. The optimal bunch distribution is a uniformly filled ellipsoid as it has linear space charge forces in all directions [104]. Achieving this bunch distribution is challenging in practice although it can be done. The space charge forces of the bunch itself can be used to produce an ellipsoid bunch in an RF gun [104]. Alternatively the photoinjector laser pulse can be shaped to be ellipsoid so an equivalently shaped electron bunch will produced [105]. Both of these approaches are challenging in practice and in the case of PERLE for technical reason a cylindrical laser pulse and hence a cylindrical initial bunch distribution will be used. This bunch distribution will have non-linear space charge forces but they are smaller than found in many other distributions such as gaussian distributions [23]. In addition to shaping the bunch distribution the slice emittance growth can be minimised by minimising the length of the injector, particularly the lowest energy section before the booster. This works simply by minimising the amount of time that non-linear space charge forces have to cause degradation of the slice emittance. Finally avoiding strong focuses where the bunch is very small and the space charge forces are high can help with avoiding space charge related emittance growth.

The other main transverse emittance growth mechanism in the injector is aberrations in the transverse focusing of the beamline elements [23]. There are two main types of aberration that need to be considered. Firstly the third order spherical aberration which depends on the transverse beam size in the focusing elements. This aberration causes slice emittance growth. The impact of the aberration is dependent on the focusing element itself and the transverse size of the beam. The elements cannot be changed in this design so this aberration can only be mitigated by making the beam smaller as it passes through the elements. Secondly the other aberration of significance is the chromatic aberration. This is caused by energy dependent focusing in the elements of the injector and as a result depends on the energy spread of the beam. Beams in photoinjectors tend to have small slice energy spreads but may have significantly larger correlated energy spreads over the length of the

whole bunch. This means the chromatic aberration may only cause small slice emittance growth while still causing a larger projected emittance growth [23]. Minimising the energy spread of the beam as it passes through focusing elements of the injector will reduce the contribution of the chromatic aberration to the final emittance. Although this may run counter to other requirements in the injector. For example the energy spread that is needed in the bunch for ballistic bunching.

The transverse emittance is not the only important factor in the injector. The linearity of the longitudinal phase space distribution is also important as a non-linear longitudinal phase space distribution will lead to a larger energy spread at the interaction point. As with the transverse emittance the longitudinal phase space distribution degrades along the length of the injector and this degradation needs to be minimised. The ideal longitudinal phase space distribution produced at the cathode would be linear with some small uncorrelated energy spread due to the initial energy spread of the electrons emitted from the photocathode which leads to the thermal longitudinal emittance. There are a number of mechanisms in the injector that lead to longitudinal phase space distribution non-linearities.

Firstly the space charge will have an effect on the longitudinal phase space distribution. It will lead to a linear chirping of the bunch accelerating the head and deccelerating the tail. This aspect of the longitudinal space charge forces will not lead to a distortion of the longitudinal phase space distribution. However in a bunch with a non-ideal charge distribution there is also a non-linear component of the space charge forces that will distort the longitudinal phase space distribution. Additionally, near longitudinal focuses where the space charge forces are strong, more complicated longitudinal dynamics can occur introducing additional non-linearities to the longitudinal phase space distribution.

Secondly, as previously discussed, in a drift where the bunch is still low enough energy that the difference in the speed of the particles is significant but high enough energy that relativity is important and the relationship between kinetic energy and speed is no longer linear a second order non-linearity is introduced to the longitudinal phase space distribution.

Thirdly the RF cavities will impose non-linearities on the longitudinal phase space distribution as the RF amplitude with time is sinusoidal not linear. Near the crest, as would be the case in an accelerating cavity, the non-linearity will be approximately second order while near the zero cross, as is the case in the

buncher cavity, the non-linearity will be approximately third order. These RF non-linearities will be smaller if the bunch is shorter particularly the non-linearity near the zero cross where the RF is approximately linear for a short enough bunch.

5.3 Injector optimisation

The space charge dominated dynamics of the low energy beams found in photoinjectors are not analytically tractable. Instead to model the physics particle tracking simulations are required. Additionally the requirements for the properties of the beam are often competing. Injectors also have a large number of variables in their design and how these variables affect the final result is not necessarily immediately obvious. This combination of complicated physics and competing objectives means that injectors are typically optimised using multi and many objective optimisation algorithms and 3D space charge tracking codes such as OPAL [76]. The first application of a multi-objective genetic algorithm to optimise a high voltage DC gun based ERL injector was published by Cornell in 2005 [80].

Injector optimisation procedure

The injector was optimised using the many objective optimisation algorithm NSGAIII [84] [85]. This algorithm was chosen as it is capable of effectively optimising more than three objectives. For the case of the PERLE injector five objectives were used in optimisation procedure. These were: the transverse emittance, the longitudinal emittance, the RMS energy spread, the transverse halo parameter and the longitudinal halo parameter. The specification requires that the transverse emittances should be less than 6 mm mrad. The RMS energy spread should be as small as possible both in terms of the correlated and uncorrelated energy spreads so minimising it was an objective. The halo parameters [72] were used to control the shape of the bunch distributions they are defined as shown in equation 5.7.

$$H = \frac{3I_4}{2I_2} - \frac{15}{7} \tag{5.7}$$

I_4 and I_2 are the fourth and second order moments of the bunch distribution in phase space. The fourth order moment I_4 is essentially the kurtosis of the

bunch and is a measure of how tailed the distribution is. Additionally like the emittance it is a conserved quantity under symplectic forces. I_4 is

$$I_4 =< q^4 >< p^4 > +3 < q^2p^2 >^2 -4 < qp^3 >< q^3p > \tag{5.8}$$

and I_2 is

$$I_2 =< q^2 >< p^2 > -4 < qp >^2 \tag{5.9}$$

where p is the position and q is the momentum.

The optimisation had two constraints. First an inequality constraint that the transverse beam size should be smaller than 6 mm. This is to ensure that the beam will fit through the apertures of the beamline. Secondly the final bunch length was constrained to be equal to 3 mm $\pm$ 0.5 mm. In addition to the constraints in the optimisation the final output energy of the booster is set to be 7 MeV within a certain tolerance. However this was not done using a constraint in the optimisation and is instead done using the definition of the optimisation problem.

The optimisation had 15 variables representing the spot size and pulse length of the laser pulse, element positions, magnet settings and cavity settings. The laser pulse is modelled in an idealised fashion as a perfect cylinder with a small rise and fall time of 3.5 ps. It is described by two variables: the spot size and the pulse length. All of the elements have minimum distances between them which were determined by using the mechanical size of the ALICE injector as a guideline of reasonable values. However three variables describe possible additional distance between the first solenoid and buncher, the buncher and the second solenoid and the second solenoid and the booster. Two variables describe the magnetic field strength of the two solenoids. The buncher cavity is describe by one variable which describes its RF amplitude. Its phase is not specified by a variable as it is always set to the zero cross. The cavities in the booster are each described by two variable. One for the phase and one for the amplitude. The exception to this is the final cavity which is only described by a single variable which describes the phase. The amplitude is set so that the final beam energy is 7 MeV with a certain tolerance.

The appropriate amplitude for the final RF cavity is found by initially finding the energy of the beam after the first three cavities of the booster by running a simulation of the injector with no space charge and only a 100 particles. In this simulation the buncher is set to an amplitude of 0 MV/m as

without the repulsive longitudinal space charge forces the buncher will cause significant overbunching of the bunch. This is acceptable as the buncher is set to exactly the zero cross so it should have no effect on the final beam energy. The simulation continues through the first three cavities where it then stops and the average beam energy is read in. If the total energy is higher than 7 MeV the solution is rejected and given a very large constraint violation value. If it is smaller than the target energy the difference between the energy after 3 cavities and the target energy is found. Then an estimated value for the required cavity amplitude to achieve the target energy is calculated using equation 5.10

$$A_4 = \frac{\pi \Delta E}{\lambda cos(\theta_4)} \tag{5.10}$$

where A_4 is the cavity field amplitude in MV/m, ΔE is the energy difference, λ is the cavity wavelength and θ_4 is the cavity phase. This amplitude estimate will not be exactly correct due to the fact that this equation assumes an ultrarelativistic beam which is not a valid assumption in the energy range of the injector. So the low particle space charge free injector simulation is run again but this time all the way through the four cavities of the booster. The final energy of the booster in the simulation is found and the energy gain in the fourth cavity calculated. If this energy gain is not correct it is used to determine a new guess for the amplitude using equation 5.11

$$A_f = A_0 \frac{\Delta E_R}{\Delta E_S - \Delta E_R} \tag{5.11}$$

where A_f is the new amplitude guess, A_0 is the old amplitude guess, ΔE_R is the required energy gain and E_S is the simulated energy gain. The new amplitude guess is then used in a simulation. This process is repeated iterative until the simulation gives an energy at the booster exit which is within a certain tolerance of the target energy. The amplitude found using this approach is then used in the main simulation of the injector. The objective values are found using this final simulation with space charge.

The optimisation using NSGAIII was done with a population size of 120 and was run for 300 generations. The NSGAIII implementation used was from the python library JMetalPy [106]. The parameters of the mutation and crossover operators were set using the values from the NSGAIII paper [84] [85]. A mutation rate of 1/L where L is the number of variables, in this case 15. A mutation eta of 20 and a crossover eta of 30, where the eta parameters are

a measure of how far from the parent solutions that the offspring solutions produced by the mutation and crossover are.

Pareto front

The optimisation produces a 5D Pareto front of equivalently optimal solutions. The visualisation of this Pareto front is challenging as it exists in an objective space with more dimensions than physical space. One way to visualise it is to plot projections of the Pareto front into two dimensional space to show the trade off between two of objectives. These plots are however often difficult to interpret. Four Pareto front projections were plotted showing the trade offs of longitudinal emittance, RMS energy spread, transverse halo parameter and longitudinal parameter against the transverse emittance. A chosen solution is marked on the plots which can be found in figure 5.2.

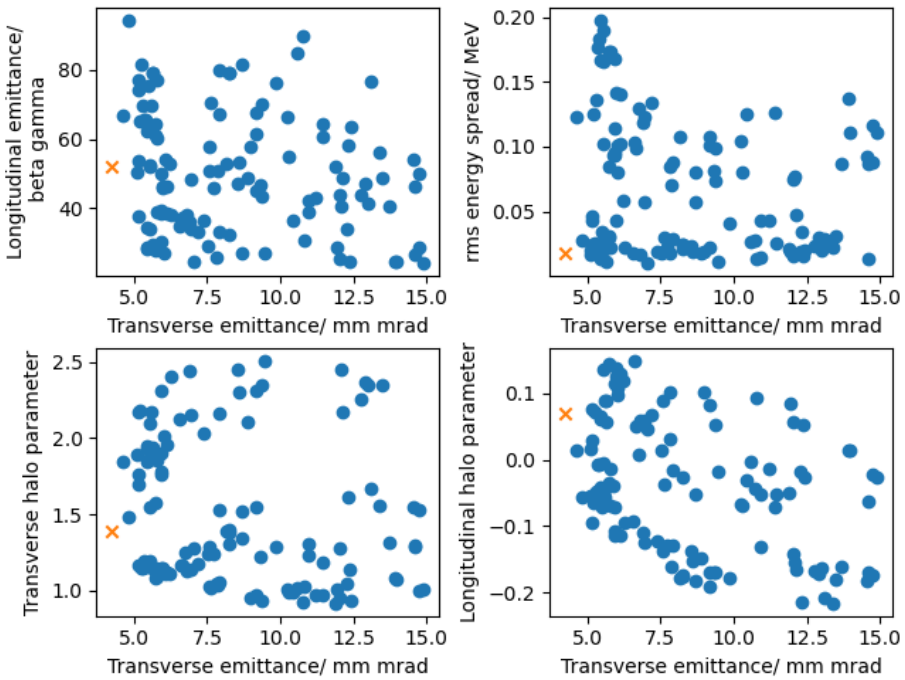

Figure 5.2: Four Pareto front projections showing how the objectives trade off against the transverse emittance. The chosen injector solution is plotted as an orange ×.

These Pareto front projections have significant numbers of points behind

the front edge of the curve on the lower left. They do however give an idea of the bounds of the obtained solutions. The chosen solution was selected primarily due to its low transverse emittance and RMS energy spread. Trade offs were made with regards to the longitudinal emittance and the longitudinal halo parameter. The beamline parameters of the chosen solution can be seen in table 5.2.

Table 5.2: The parameters of the chosen injector solution. The element positions indicate the location of the center of the element.

Parameter	**Value**
Laser spot diameter/ mm	4.44
Laser pulse length/ ps	117.5
Solenoid 1 position/ m	0.23
Solenoid 1 max field/ T	0.0323
Buncher position/ m	0.993
Buncher amplitude/ MV/m	1.3
Buncher phase/ degrees	-90
Solenoid 2 position/ m	1.50
Solenoid 2 max field/ T	0.0238
Booster cavity 1 position/ m	2.40
Booster cavity 1 amplitude/ MV/m	20.8
Booster cavity 1 phase/ degrees	-0.08
Booster cavity 2 position/ m	3.11
Booster cavity 2 amplitude/ MV/m	24.0
Booster cavity 2 phase/ degrees	0.2
Booster cavity 3 position/ m	3.84
Booster cavity 3 amplitude/ MV/m	14.4
Booster cavity 3 phase/ degrees	-13.2
Booster cavity 4 position/ m	4.58
Booster cavity 4 amplitude/ MV/m	11.7
Booster cavity 4 phase/ degrees	-10.4

Chosen solution

RMS parameters

The RMS parameters of the chosen baseline injector solution are examined below. The beam sizes of the solution can be seen in figure 5.3. The transverse beam size rapidly grows from the cathode. It is desirable to have a small transverse beam size on the cathode to minimise the thermal emittance however the space charge forces are strong in the electron gun and low energy section

of the injector so they cause the beam size to grow rapidly. The two solenoids keep the beam size controlled below 6 mm the maximum acceptable value as set in the constraints of the optimisation. The initial bunch length at the cathode is long as this will reduce the strength of the space charge forces without increasing the thermal emittance of the beam. The space charge forces cause debunching up to the point of the buncher cavity where the bunch is compressed. The majority of the bunching is done via the ballistic bunching induced by the buncher cavity but there is also some velocity bunching in the first cavity of the booster as well.

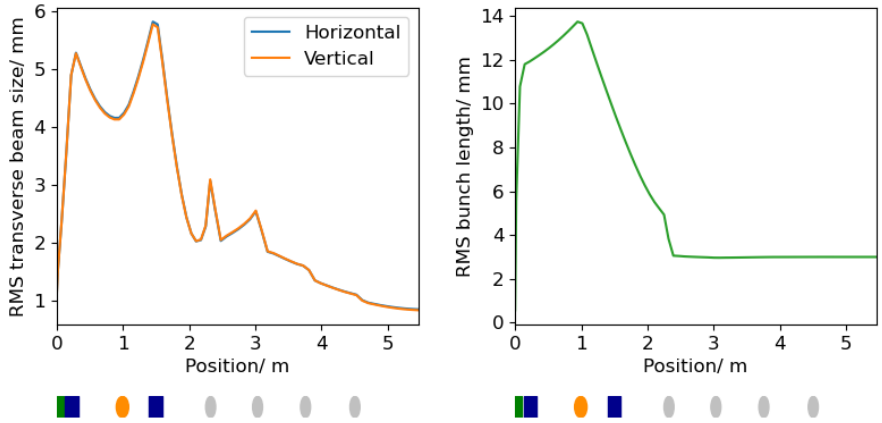

Figure 5.3: The RMS beam sizes of the chosen baseline injector. The transverse beam sizes are on the left and the bunch length is on the right. The positions of the beamline elements are indicated below the plots. The electron gun is indicated by a green box, the solenoids by dark blue boxes, the buncher cavity by the orange ellipse and the accelerating cavities by the grey ellipses.

The transverse and longitudinal emittances can be seen in figure 5.4. The transverse projected emittance starts low and grows over the course of the injector. The spikes of the emittance value at the positions of the solenoids and buncher cavities are artifacts of the emittance calculation process and are not physical. A first emittance minimum can be seen at approximately 2 m then the emittance rises to its maximum physical value before compensating back down. This behaviour of a double emittance minimum on either side of a transverse waist matches with what would be theoretically expected [107]. This emittance compensation process is not complete at the position of the end flange of the booster linac and the emittance will continue to decrease past this

point. The longitudinal emittance starts small then grows up to the point of the buncher then decreases until the booster linac where it then grows through the booster due to RF non-linearities introduced by the booster cavities.

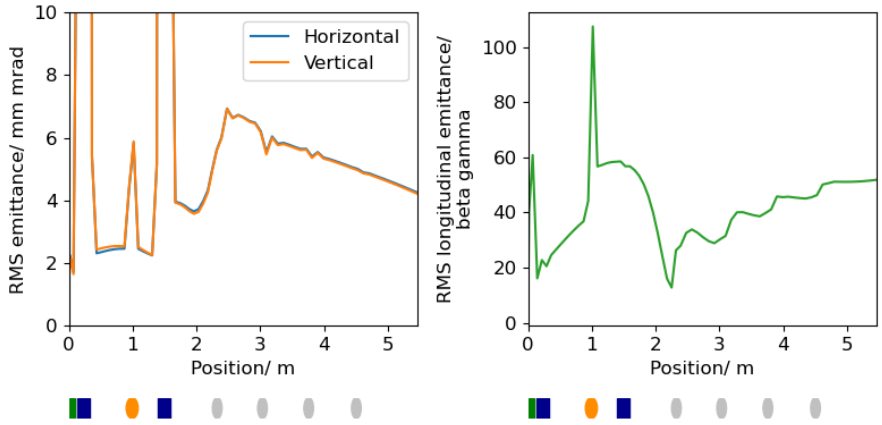

Figure 5.4: The RMS emittances of the chosen baseline injector solution. The transverse emittances are on the left and the longitudinal emittance on the right. The positions of the beamline elements are indicated below the plots. The electron gun is indicated by a green box, the solenoids by dark blue boxes, the buncher cavity by the orange ellipse and the accelerating cavities by the grey ellipses.

The average kinetic energy of the bunch and energy spread of the bunch can be seen in figure 5.5. The energy plot shows that the first two cavities cause the largest energy gain. This would have the advantage that the space charge forces are reduced more rapidly due to the rapid energy increase. Some momentary deceleration of the beam can be seen at the start of the cavities. This will lead to a brief increase in the space charge forces which can lead to a degradation in the beam quality. Cavities with $\beta = 0.8$ were used to minimise this deceleration. The energy spread is very high at the start of the beamline as the long bunch is still in the process of being accelerated by the electron gun so parts of it have been accelerated while others haven't. Once the bunch has been fully accelerated it then has a lower energy spread which grows as the longitudinal space forces chirp the electron bunch. The buncher then introduces a large energy spread which decreases along the beamline towards the booster as the longitudinal space charge forces act against the buncher introduced chirp. Then once the beam enters the booster the energy spread

changes up and down as the cavities introduce and remove chirp. In the end the energy spread is 8.9 keV.

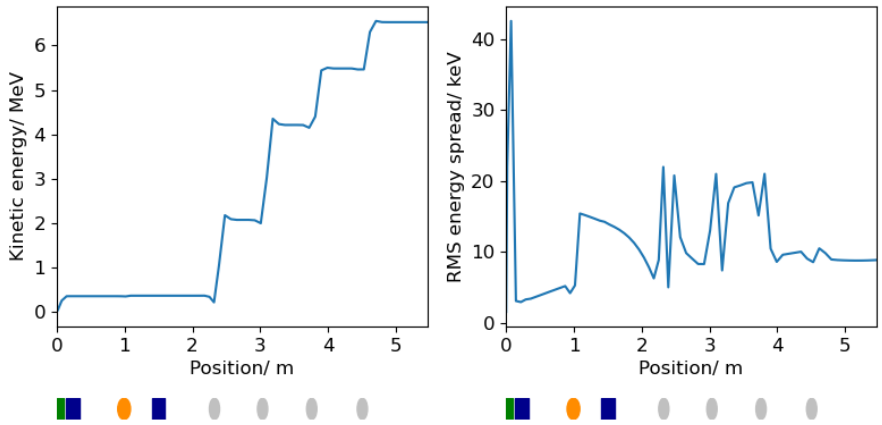

Figure 5.5: The average kinetic energy of the bunch on the left and the RMS energy spread of the bunch for the chosen baseline injector solution. The positions of the beamline elements are indicated below the plots. The electron gun is indicated by a green box, the solenoids by dark blue boxes, the buncher cavity by the orange ellipse and the accelerating cavities by the grey ellipses.

Phase space and bunch distribution evolutions

Single parameter quantifications of a bunch such as average and RMS parameters are important and can be illuminating with regards to bunch behaviour. They also make optimisation possible as the optimisation algorithms require numerical values as objective values. However single numbers don't necessarily capture the entirety of the complexity of the bunch behaviour. To fully understand the bunch behaviour the evolution of the bunch in both real and phase space should be examined. The plots in this section show the bunch at five different positions along the injector: just after the emission still partially in the electron gun, just before the buncher, just after the buncher, in the booster and at the exit flange of the booster. In the phase space distribution plots there are two rows both of which show the same distributions. The top row has fixed axes to show the relative sizes of the distributions while the bottom row has re-scaling axes to zoom in and see the details of the distributions. Additionally in all the plots in this section the bunch is divided up into longitudinal slices

at the first distribution and then the particles are plotted in different colours based on their initial longitudinal slice.

The transverse phase space evolution is shown in figure 5.6. If non-linearities can be seen in the slices this indicates slice emittance growth. It can be seen in the phase space distributions at the final two positions that the tail is misaligned with the rest of the bunch in phase space as it is diverging while the rest of the bunch is converging. This is an example of poor slice alignment and imperfect emittance compensation. The tail slice will contribute to the projected emittance growth.

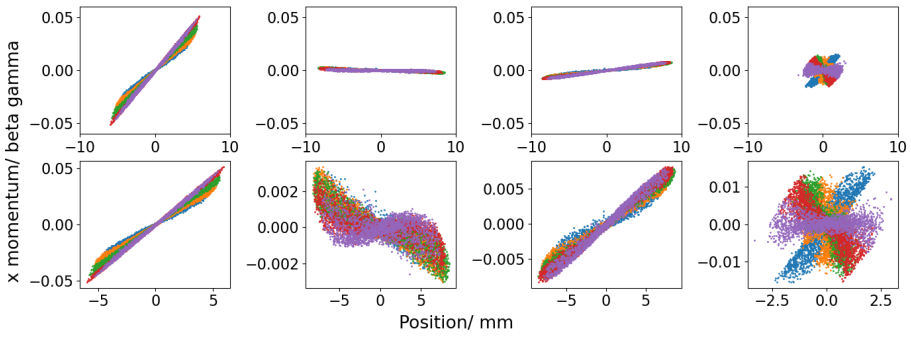

Figure 5.6: The transverse phase space distribution of the bunch at different points along the injector. The initial longitudinal slice that a particle belongs to is indicated by the particle colour. With purple being the front of the bunch and blue the back.

The longitudinal phase space distribution evolution can be seen in figure 5.7. In the phase space plot at the first beam position the electron bunch has not yet left the electron gun so the difference in acceleration along the bunch can be seen. In the second plot, the linear chirp caused by the longitudinal space charge forces as well as the third order non-linearity introduced by the non-linear component of the longitudinal space charge forces can be seen. In the third plot, the reversal of the linear chirp due to the buncher cavity can be seen. In the fourth plot, the central dip which forms close to the the longitudinal waist, due to the interaction between the space charge forces and the ballistic bunching process, can been seen. The central dip occurs because the non-linear relationship between particle energy and velocity during the ballistic bunching causes the bunch to develop an asymmetric charge distribution with more charge, and stronger space charge forces, at the head. This means that the particles at the head of the bunch gain energy faster than the particles at the tail

lose energy leading to a "V" shape in the longitudinal phase space distribution seen as the central dip. Additionally in the fourth plot, a second order RF distortion, introduced by the sinusoidal time dependence of the booster SRF cavities electric fields, and a linear chirp with the head of the bunch having higher energy can be seen. In the final plot the linear chirp has been removed, using the final SRF cavity operated at an appropriate off crest phase of -10.4°, leaving an "M" shaped longitudinal phase space distribution.

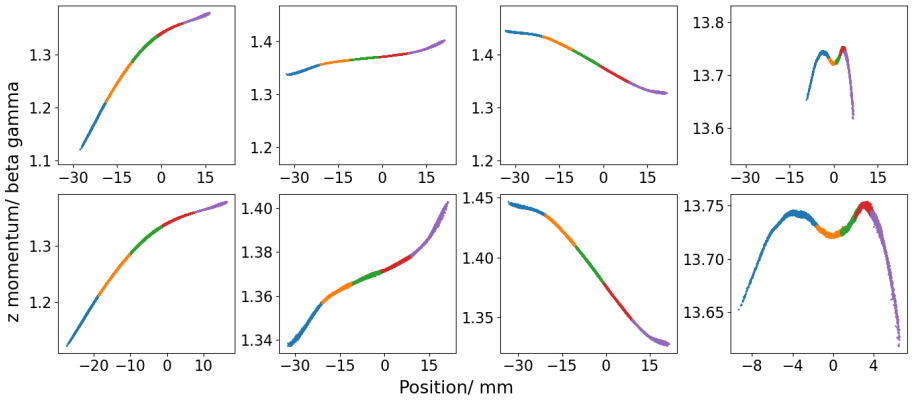

Figure 5.7: The longitudinal phase space distribution of the bunch at five different positions along the bunch. In this plot the length of the top row y axis is constant but the central value is changed as the average momentum of the bunch changes significantly as it is accelerated.

The z-x distribution of the particles in the physical space can be seen in figure 5.8. This distribution is useful for determining where particles start and where they end up and what effects that might have on the beam properties. The top row of the figure with the same axis for all five plots makes the longitudinal compression and transverse focusing of the bunch clearly visible. Looking at the different slices which had equal length initially it can be seen that there is minimuml longitudinal slice mixing. This is a desirable behaviour as one of the assumptions required for emittance compensation is that there should be no longitudinal slice mixing [108]. If slice mixing occurs the emittance growth will be irreversible due to the loss of the correlation between the longitudinal position of the particles and their phase space evolution.

in the differences in the slice behaviour along the bunch. Additionally from looking at the slices it can be seen that the longitudinal compression is not uniform along the bunch. The tail in particular is only composed of the last of

the initial slices.

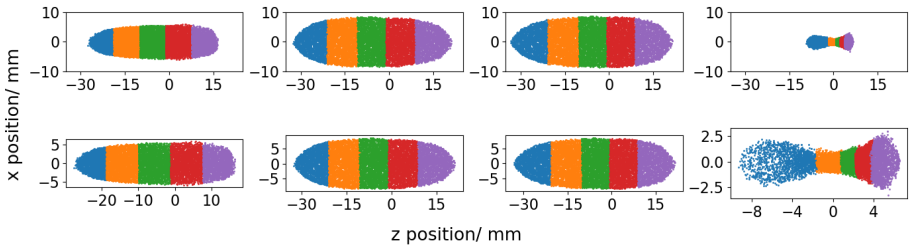

Figure 5.8: The z-x bunch distributions of the bunch in physical space. The colour that particles are plotted indicates which longitudinal slice they initially belonged to.

A more detailed examination of z-x distribution at the exit of the booster can be seen in figure 5.9. The first plot shows which longitudinal slice of the bunch particles initially occupied. The bunch was sliced into 10 slices of equal length at the approximately 9 cm from the cathode. The different colours indicate different slices at the initial output distribution. Again, as in figure 5.8, the fact that there is minimuml longitudinal slice mixing (overbunching) can be seen which is desirable. The non-uniform compression along the bunch can also be seen.

The second plot shows if and where in the bunch particles cross from one transverse side of the bunch to the other in real space. The particles were divided into two groups just after the second solenoid based on which side of the horizontal plane they were on. The different colours in the plot indicate which side of the axis the particles started on. The division was done after the solenoids as the solenoid rotates the bunch as well focusing it so will lead to particles crossing the central axis of the beam without being focused across. This means that plots showing a division made before the solenoids will show particles on the other side of the axis without there having been a crossover and crossovers are what is of interest in this plot. In this plot we can see that in the core the two sides are fairly well separated but in the tail there is a full crossover. Which lines up with what is seen in figure 5.6 where the tail slice is diverging while the intermediate slices are converging. There is also an incomplete crossover at the head of the bunch where some but not all of the particles have crossed over.

The final plot shows the density of particles from this it can be seen that

there is a dense core with a diffuse head and even lower density tail. This corresponds to what is seen in the first plot where there is a region in the center of the bunch where a significant number of the central slices are compressed with short slice lengths. A "V" shape in the charge density at this point can also be seen.

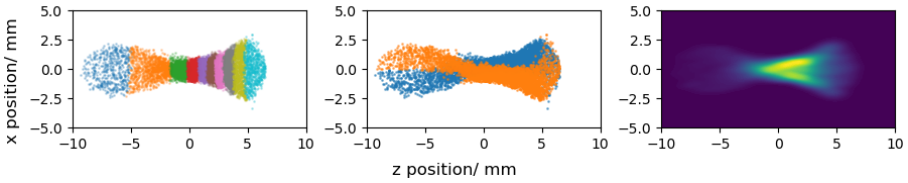

Figure 5.9: The z-x distribution at the exit of the booster plotted in three different ways. Firstly sliced longitudinally, secondly divided into two based on which side of the x axis the particles were on shortly after the second solenoid and thirdly showing particle density in the bunch.

The final bunch particle distributions in z and x can be seen in figure 5.10. From the z plot it can be seen that the bunch distribution is asymmetric with a diffuse tail which is what is shown in previous plots. The x distribution is relatively symmetric and as the simulated beamline is axially symmetric any asymmetry is a statistical artifact. The bunch distribution exhibits transverse tails.

Emittance growth

As mentioned previously the minimum achievable projected emittance in an injector is the thermal emittance which can be calculated using equation 5.5. Using the parameters for this solution, a laser spot radius of 2.2 mm and a mean transverse energy of 0.292 eV, an estimate of the thermal emittance can be obtained of 0.96 mm mrad. This is the absolute minimum value that could be achieved at the booster exit for this design. The average slice emittance at approximately 9 cm after the cathode is 1.49 mm mrad which is noticeably larger than the estimated value potentially indicating slice emittance growth in the electron gun when the particle energy is still very low near the cathode.

The emittance growth as previously mentioned is divided into two types slice emittance growth due to distortions in the transverse phase space distribution due to non-linear space charge forces and aberrations and growth in the projected emittance due to misalignments and mismatches between the

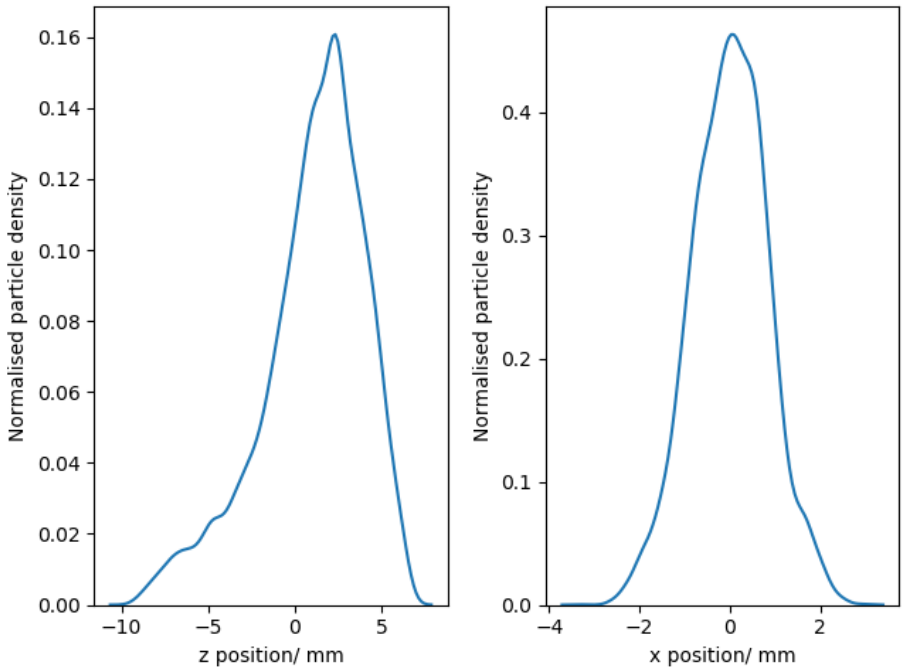

Figure 5.10: The particle distributions at the exit of the booster. On the left is the longitudinal z distribution and on the right is the transverse x distribution.

longitudinal slices of the bunch in phase space as a result of emittance decompensation and chromatic aberration. The emittance compensation process is incomplete at the booster exit so to investigate the limits of the compensation for this design the simulation was run out to 6.7 m the approximate location of the emittance minimum. This is is just under 1.25 m after the exit flange of the booster.

To investigate the contribution of the slice emittance growth versus the slice misalignments and mismatches the projected emittance, average slice emittance weighted by number of particles in the slice and maximum slice emittance were all plotted. This can be seen in figure 5.11. When doing the calculations in this plot the bunch was divided into 25 slices of equal length.

From the graph of projected and slice emittances the characteristic behaviour of emittance compensation can be seen with the projected emittance rising and then decreasing through the booster down to a minimum while the slice emittance values remain largely constant. The biggest slice emittance growth is from the first outputted distribution still inside the electron gun to

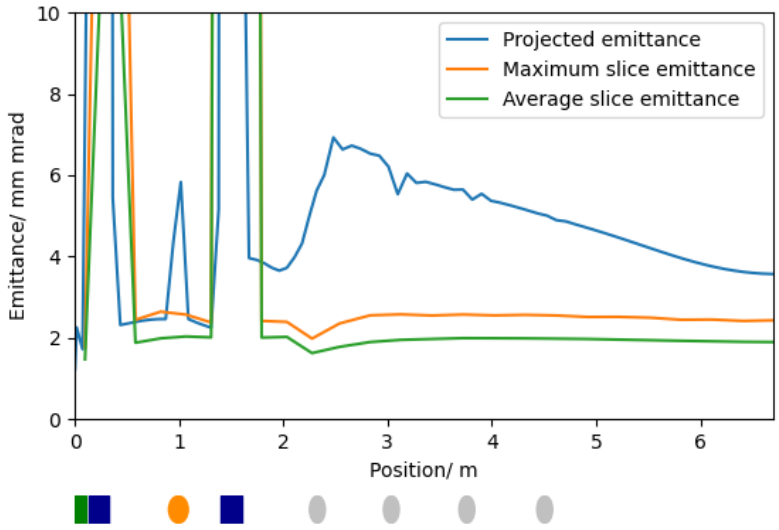

Figure 5.11: The projected emittance, average slice emittance and maximum slice emittance along the injector out to the position of the projected emittance minimum. The positions of the beamline elements are indicated below the plots. The electron gun is indicated by a green box, the solenoids by dark blue boxes, the buncher cavity by the orange ellipse and the accelerating cavities by the grey ellipses.

the distribution after the first solenoid where it goes from 1.48 mm mrad to 1.92 mm mrad. The initial distribution is still however partially in the gun with a significant energy spread so the effect of that on the normalisation of the emittance with respect to the average energy of the bunch needs to be borne in mind. After this point in the rest of the beamline up to the booster exit there is some variation in the slice emittance visible in the graph but any difference between the final value and the value at this point is very small. The location of the largest and most visible increase in the maximum slice emittance is in the first cavity of the booster linac. The maximum slice emittance does then compensate back down to the value after the first solenoid. The slice emittance can change in this way because the simulated slices are not ideal and have finite length so some rotation in transverse phase space within the slices is possible. Due to this compensation there is not much significant slice

emittance growth after the first solenoid. However there there is some growth in the gun and through the first solenoid.

The projected emittance compensates down to a minimum value of 3.58 mm mrad at the emittance minimum after the booster. At this point the weighted average slice emittance is 1.91 mm mrad and the maximum slice emittance is 2.44 mm mrad. The projected emittance is 1.67 mm mrad larger than the average slice emittance which corresponds to an 87.4% increase and 1.14 mm mrad larger than the maximum slice emittance which is an increase of 46.7%. This shows that the projected emittance has a significant contribution from the misalignments and mismatches.

The slice emittances at approximately 9 cm from the cathode and the slice emittance at the projected emittance minimum can be seen in figure 5.12. Also plotted in the graph is the line charge density.

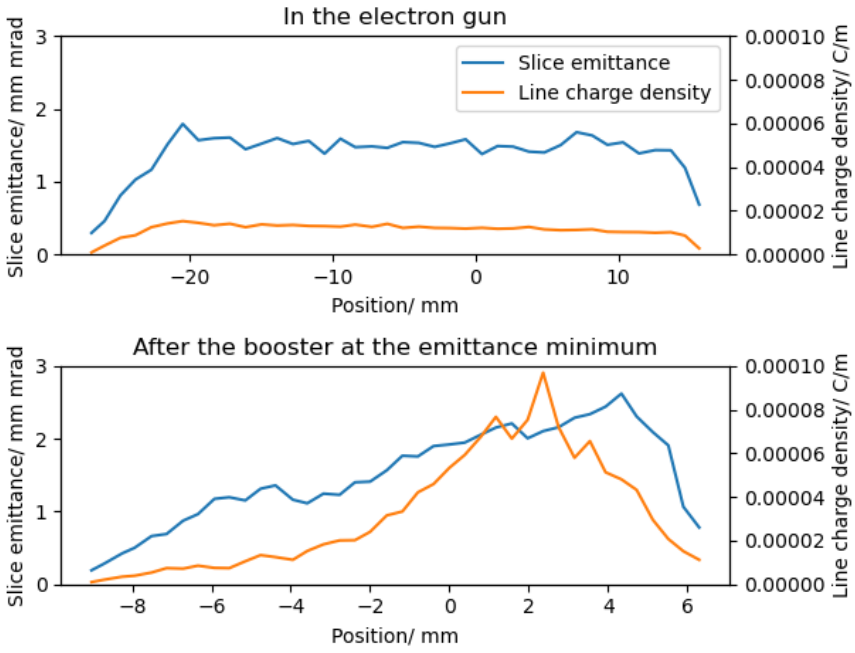

Figure 5.12: The slice emittance and line charge density at two points in the beamline. On the left hand side the values in the electron gun are shown and on the right hand side the values at the emittance minimum after the booster are shown. The slice emittance is marked in blue and the line charge density in orange.

Figure 5.12 shows that both the slice emittance and the line charge density are fairly uniform along the whole length of the bunch at the start of the injector. By the end there has been slice emittance growth predominately at the front of the electron bunch. The line charge density distribution along the bunch is also no longer uniform and the peak line charge density is significantly larger as the bunch has been compressed. The diffuse tail of the bunch can be seen in the line charge density distribution.

The transverse phase space distribution at the emittance minimum can be seen in figure 5.13.

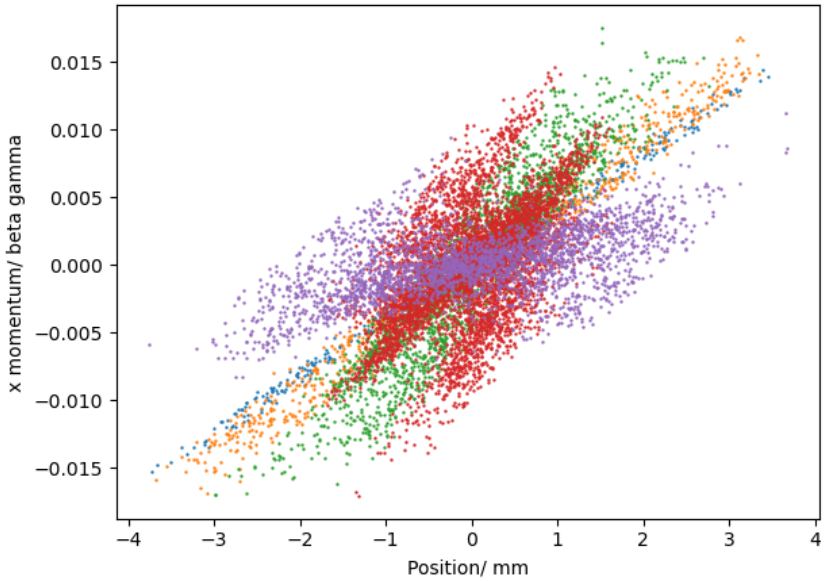

Figure 5.13: The transverse phase space distribution at the emittance minimum after the booster. The bunch has been divided into five slices plotted in different colours to illustrate which features correspond to each slice.

Compared to the phase space distribution at the booster exit which can be seen in figure 5.6 it can be seen that the tail of the bunch is now in better alignment with the rest of the bunch which is now predominantly diverging as well. This improvement in alignment is probably a contributing factor in the reduction of the emittance down to the minimum. The five individual slices were also plotted separately this can be seen in figure 5.14

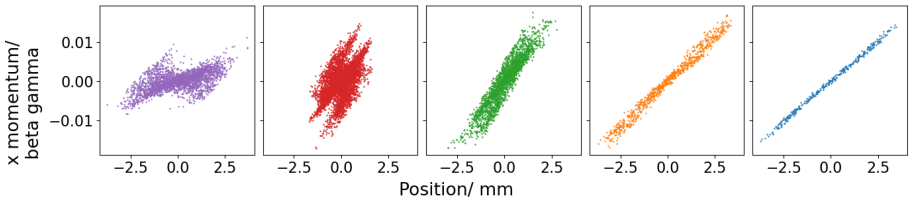

Figure 5.14: The transverse phase space distribution at the emittance minimum after the booster. The bunch has been divided into five slices which have been plotted separately.

As a final investigation into the emittance growth the emittance of different longitudinal sections of the bunch will be calculated to investigate where in the bunch contributes most significantly to the total emittance. To do this the bunch was divided into the 5 longitudinal slices of equal length at the initial distribution used in previous analysis. These slices were then used when slicing the distribution at the emittance minimum. In the following calculations the front slice is called the head, the central three slices the core and the back slice the tail. The emittance was calculated for different combinations of these three sections of the bunch. The results of those calculations are summarised in table 5.3.

Table 5.3: The emittance of different combinations of bunch sections at the emittance minimium after the booster.

Bunch sections	**Emittance/ mm mrad**
Whole bunch	3.57
Core	2.55
Core + head	3.10
Core + tail	3.20
Head	2.26
Tail	2.61

From this it can be seen that the emittance of the core is 2.55 mm mrad which is larger than the maximum slice emittance calculated earlier with 25 slices as but not significantly larger indicating that the compensation of the bunch core is good and the slices are well aligned. The core has an emittance 1.02 mm mrad less than the bunch as a whole. From looking at the core + tail and the core + head it can been seen that both the tail and head make a significant contribution to the projected emittance. Although the tail makes a

larger contribution.

5.4 Conclusion

The results of this optimisation show that it is possible to meet the specification for PERLE at the booster exit using the baseline injector design. The transverse emittance does grow from the thermal emittance value initial at the cathode but is comfortably within the specification. Despite the fact that the transverse emittance and bunch length specification have been met there are two non-ideal features of the bunch at the booster exit which have been identified. Firstly there is a clear "M" shaped non-linearity which has developed in the longitudinal phase space distribution. Secondly the longitudinal profile of the bunch is asymmetric with a long diffuse tail. Full start to end simulations of PERLE will be needed to identify if these two issues are acceptable or if they will need to be corrected in some way. In the next chapter the use of higher harmonic cavities to correct both of these problems will be explored.

Chapter 6

Variant PERLE injectors

6.1 Alternate injector layout optimisations

The baseline injector variant shows acceptable performance in terms of its beam sizes and transverse phase spaces however the "M" shaped longitudinal phase space is not ideal. In cases where low energy spread is required at the IP it will lead to an increase in the energy spread of the beam and in cases where short bunches are required it will limit the how effectively the bunch can be compressed. The "M" shape comes from a combination of two main sources of non-linearities. Firstly the ballistic bunching process from the normal conducting buncher cavity introduces a "V" shape near the longitudinal waist which is the source of the central dip of the "M". This is because at the longitudinal waist the space charge forces cause the reversal of the bunch from bunching to debunching and the head of the bunch transitions before the tail as it has higher charge density and stronger space charge forces. The bunch is accelerated by the booster in this intermediate state between bunching and debunching leaving the "V" shape in the longitudinal phase space distribution. Secondly the booster linac introduces a 2nd order distortion which is the outer quadratic shape. In addition to the phase space distortion the ballistic bunching process causes a change to the longitudinal bunch profile leading to the formation of a tail on the bunch. This is due to the relativistic effects meaning that a linear energy chirp is not a linear velocity chirp.

There are two potential solutions for minimizing non-linearities in the longitudinal phase space at the interaction point. Firstly the injector layout could be modified to eliminate the longitudinal phase space distortions prior to the

bunch reaching the main ERL loop. This could be done in two ways. Firstly using higher harmonic cavities before the merger or secondly using higher order multipoles in the dispersive region of the merger to manipulate the second and third order longitudinal dispersion of the merger to do optical linearization. In this thesis the use of multipoles in the merger will not be considered only the use of higher harmonic RF. Alternatively instead of modifying the injector linearization could be done later in the arcs. This would be done optically using the second and third order longitudinal dispersion of the arcs of the ERL loop [109]. As this is outside of the injector it is out of the scope of this thesis.

There are two locations where higher harmonic RF cavities could be added to the injector. The first is in the low energy section prior to the booster. The function of this cavity would be to correct the third order non-linearity from the longitudinal space charge and the third order non-linearity from the RF distortion of the buncher. Both of these third order non-linearities have the same sign. To correct them a higher harmonic cavity which is operated at the opposite zero crossing phase to the buncher can be used as it will have a third order non-linearity of the opposite sign. This cavity before the booster will need to be normal conducting as adding a cryomodule for an SRF cavity would increase the length of the low energy section of the injector which is undesirable and would add significantly to the cost of the injector. The second location where a higher harmonic cavity could be added is in booster in place of either the second or third accelerating cavity. This cavity would be an SRF cavity and its function would be to remove the 2nd order non-linearity introduced by the RF distortion in the booster. To do this it would be operated on the decelerating phase of the RF. In this chapter three variant injector designs with added higher harmonic RF will be investigated. In all cases the use of a 2404.74 MHz third harmonic cavity will be considered. Higher than third harmonics would introduce a larger non-linearity for a smaller linear component. The first of the three injector schemes analysed has the normal conducting higher harmonic in the low energy section, the second has the SRF cavity in the booster and the third has both. A sketch of the baseline and the three variant injectors can be seen in figure 6.1.

6.2 Injector optimisations

The three variant injectors were all optimised using NSGAIII and OPAL following the procedure described in the previous chapter. The difference is ad-

Figure 6.1: The layout of the baseline injector and the three variant injectors. The electron gun is represented by the green square, the solenoids by the blue rectangles. Cavities are represented by ellipses. Normal conducting cavities are orange and superconducting cavities are grey. The larger ellipses are main harmonic cavities and the smaller ellipses are higher harmonic cavities.

ditional variables to represent the amplitudes of the cavities and when the normal conducting third harmonic is added the addition of another variable to represent the additional gap in the low energy section of the injector. From the Pareto fronts produced from the optimisation processes one solution was selected for each variant. The beam dynamics of the selected solutions will be compared with each other and the baseline injector design in this chapter. The beamline parameters of the chosen solutions can be seen in table 6.1.

6.3 RMS parameters

The RMS parameters of the three variants will be examined first.

The transverse beam sizes can be seen in figure 6.2. In all four solutions the largest beam sizes are seen in the low energy section. However in all cases the beam size is kept controlled below 6 mm as required by the constraint. Additionally in all four solutions the beam is brought to a focus just before entering the booster linac. This what would be theoretically expected if the emittance compensation was being done into the second emittance minimum which generally has a lower projected emittance [107]. Looking at the four different injectors shows that there are two sets of solutions for the beam dynamics in the low energy section. One with a weaker focusing at the location of the first solenoid and one with a stronger focusing. The baseline and injector

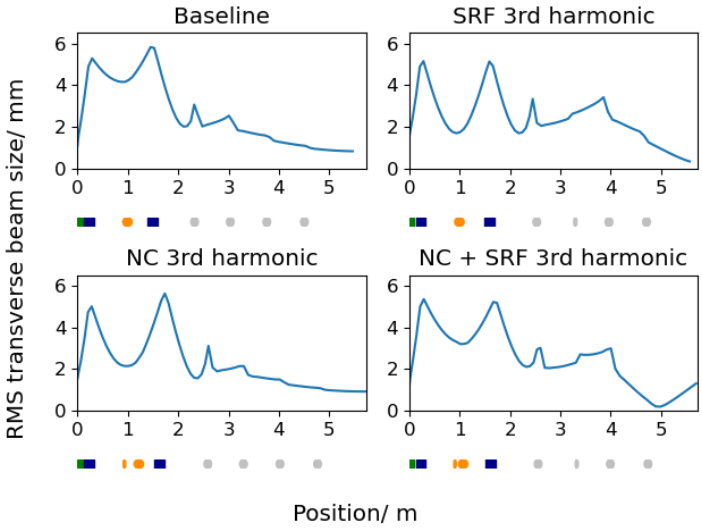

Figure 6.2: A comparison of the beam sizes for all studied injector solutions. The positions of the beamline elements are indicated below the plots. The electron gun is indicated by a green box, the solenoids by dark blue boxes, the NC third harmonic cavity by the shorter orange ellipse, the buncher cavity by the longer orange ellipse, the accelerating cavities by the longer grey ellipses and the SRF third harmonic cavity by the shorter grey ellipse.

Table 6.1: The parameters of the chosen injector solution. The element positions indicate the location of the center of the element.

Parameter	**Baseline**	**SRF 3rd harmonic**	**NC 3rd harmonic**	**NC+SRF 3rd harmonic**
Laser spot diameter/ mm	4.44	5.06	6.16	4.59
Laser pulse length/ ps	117.5	33.3	56.7	101.5
Solenoid 1 position/ m	0.23	0.23	0.23	0.23
Solenoid 1 max field/ T	0.0323	0.0359	0.0352	0.0333
NC 3rd harmonic position/ m	n/a	n/a	0.934	0.908
NC 3rd harmonic amplitude/ MV/m	n/a	n/a	1.45	1.02
NC 3rd harmonic phase/ degrees	n/a	n/a	90	90
Buncher position/ m	0.993	0.996	1.10	1.07
Buncher amplitude/ MV/m	1.31	1.96	2.49	1.91
Buncher phase/ degrees	-90	-90	-90	-90
Solenoid 2 position/ m	1.50	1.50	1.63	1.61
Solenoid 2 max field/ T	0.0238	0.0311	0.0274	0.0246
Booster cavity 1 position/ m	2.40	2.61	2.66	2.64
Booster cavity 1 amplitude/ MV/m	20.8	27.31	20.8	21.5
Booster cavity 1 phase/ degrees	-4.80	-0.338	0.245	8.87
Booster cavity 2 position/ m	3.11	n/a	3.37	n/a
Booster cavity 2 amplitude/ MV/m	24.0	n/a	24.1	n/a
Booster cavity 2 phase/ degrees	0.2	n/a	29.6	n/a
SRF 3rd harmonic position/ m	n/a	3.20	n/a	3.35
SRF 3rd harmonic amplitude/ MV/m	n/a	26.2	n/a	21.9
SRF 3rd harmonic phase/ degrees	n/a	-197.1	n/a	180
Booster cavity 3 position/ m	3.84	4.04	4.10	4.07
Booster cavity 3 amplitude/ MV/m	14.4	24.6	16.0	29.8
Booster cavity 3 phase/ degrees	-13.2	18.9	-14.7	6.78
Booster cavity 4 position/ m	4.58	4.79	4.49	4.82
Booster cavity 4 amplitude/ MV/m	11.7		10.4	26.1
Booster cavity 4 phase/ degrees	-10.4	-10.9	-29.3	-8.05

with both higher harmonics are examples of the weaker focusing solution and the two solutions with just one of the higher harmonic cavities are examples of the stronger focusing solution. There is not obviously a particular reason why an injector layout would favour one of the two solutions over the other and it doesn't appear to depend on which harmonic cavities are added. However both solutions meet the requirements. Different runs of the optimisations might find the other solution. In the booster the two solutions with SRF higher harmonic cavities have strong transverse focusing at the location of the accelerating cavity after the third harmonic cavity. This potentially causes a crossover in the booster which may be problematic for emittance compensation. Of the two solutions with an SRF third harmonic cavity the solution with both higher harmonic cavities has a much stronger transverse focus due to a higher field in the cavity.

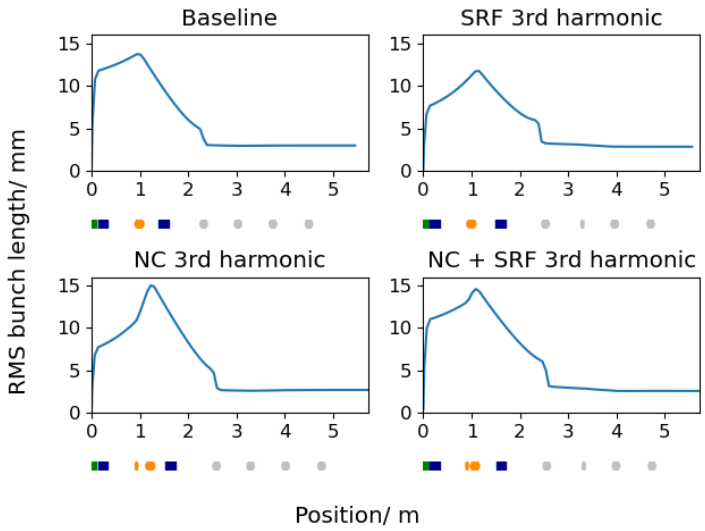

Figure 6.3: A comparison of the bunch length for all chosen injector solutions. The positions of the beamline elements are indicated below the plots. The electron gun is indicated by a green box, the solenoids by dark blue boxes, the NC third harmonic cavity by the shorter orange ellipse, the buncher cavity by the long orange ellipse, the accelerating cavities by the longer grey ellipses and the SRF third harmonic cavity by the short grey ellipse.

The RMS bunch lengths can be seen in figure 6.3. The initial laser pulse length can be seen to vary for all of the solutions. However all exhibit the expected space charge induced increase in bunch length before the buncher.

The two solutions with the NC third harmonic cavity show increased debunching from the position of the higher harmonic cavity. This is what would be expected as the higher harmonic cavity is operated at the zero crossing phase which causes a linear chirp with the head of the bunch having higher energy. So the head will move faster that the tail and the bunch length will increase. In general though all the solutions show roughly the same approach to bunching. With the majority of the bunching done using the buncher cavity and the final bunching done using velocity bunching in the first cavity of the booster.

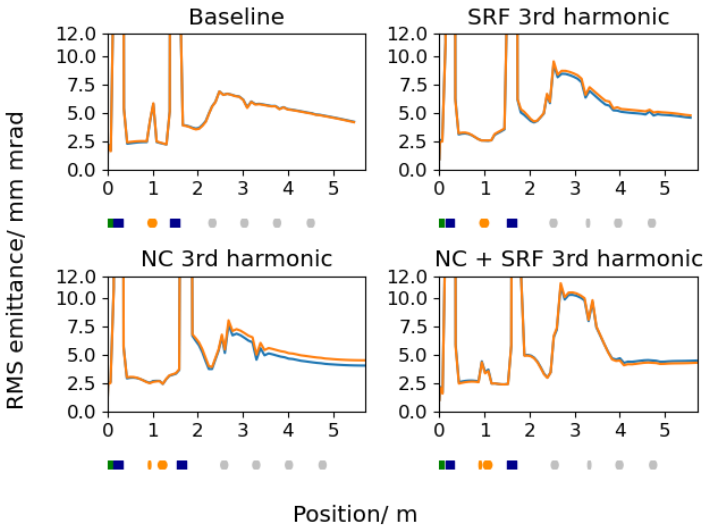

Figure 6.4: A comparison of the transverse emittance for all chosen injector solutions. The horizontal emittance is plotted in blue and the vertical emittance in orange. The positions of the beamline elements are indicated below the plots. The electron gun is indicated by a green box, the solenoids by dark blue boxes, the NC third harmonic cavity by the shorter orange ellipse, the buncher cavity by the long orange ellipse, the accelerating cavities by the longer grey ellipses and the SRF third harmonic cavity by the short grey ellipse.

The transverse emittances can be seen in figure 6.4. All four solutions show an emittance minimum before the booster linac and then a rise towards and in the first cell of the booster before the emittance begins to be compensated down to a second emittance minimum. All the final emittances are within the specification. The two solutions with the SRF third harmonic cavity show a sharp emittance decrease at the point of the third harmonic cavity. The injector with just the SRF third harmonic cavity and the lower amplitude in the higher

harmonic shows some emittance compensation after the third harmonic while the injector with the stronger focusing shows no further significant emittance compensation. One thing to note in these plots is that in the case of the injectors with higher harmonic cavities, particularly the injector with only the NC third harmonic, some divergence in the values of the transverse emittances can be seen. This should not exist because the injector is axially symmetric and any non-ideal aspects of the injector that might lead to legitimate asymmetries are not modelled in these simulations. This means that the asymmetries here are artifacts of the simulations and are indicative of insufficient convergence in some aspect of the modelling of the higher harmonics. The asymmetry originates in the initial bunch generation due unphyscial random variations in the distribution of macroparticles produced. Some level of trading off between the accuracy and computational tractability of the optimisation is necessary with evolutionary algorithm based optimisation due to limited computational resources.

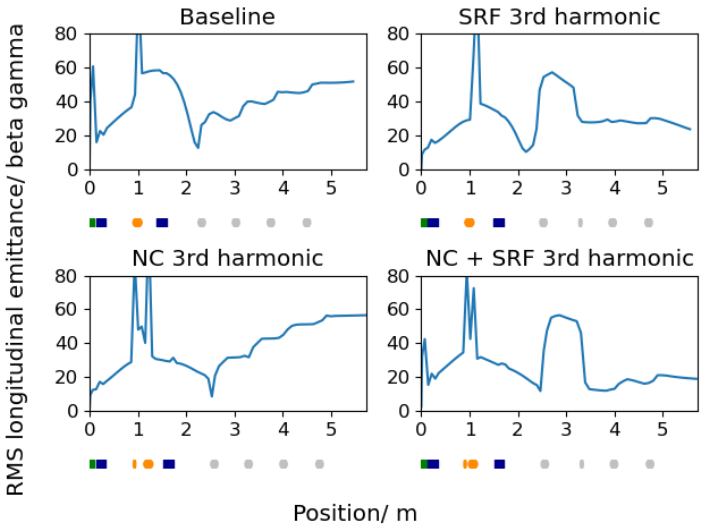

Figure 6.5: A comparison of the longitudinal emittance for all chosen injector solutions. The positions of the beamline elements are indicated below the plots. The electron gun is indicated by a green box, the solenoids by dark blue boxes, the NC third harmonic cavity by the shorter orange ellipse, the buncher cavity by the long orange ellipse, the accelerating cavities by the longer grey ellipses and the SRF third harmonic cavity by the short grey ellipse.

The longitudinal emittances can be seen in figure 6.5. From these plots it

can be seen that the majority of the longitudinal emittance increase occurs in the booster linac due to the RF non-linearity. This means that the NC third harmonic cavity is less effective than the SRF cavity from the perspective of reducing the final emittance. However the NC cavity does have an effect on the evolution of the longitudinal emittance in the low energy section. Firstly it pre-compensates the longitudinal emittance gain after the buncher by imposing an equal but opposite third order non-linearity to the non-linearity introduced by the RF distortion of the buncher. The NC cavity does also reduce the rate at which the longitudinal emittance decreases between the buncher and the booster. The effect of the SRF third harmonic cavity is more significant on the final emittance and can be clearly seen in the form of the significant decrease in the longitudinal emittance at the location of the higher harmonic cavity. The injector with both higher harmonic cavities which has a higher amplitude SRF cavity has greater reduction in the longitudinal emittance. This is because the non-linearity induced by the higher harmonic cavity is larger than in the solution with just the SRF higher harmonic cavity so it has a greater compensating effect on the RF distortion.

The evolution of the average bunch energies can be seen in figure 6.6. In these injector designs significant energy gain in the first cavity of the booster is a common feature. In the injectors without the SRF third harmonic cavity it can be seen that the first two cavities of the injector have the most significant energy gain and then the last two cavities have less of an energy gain. This would lead to a more rapid reduction of the space charge forces. In the injectors with the SRF third harmonic cavity it leads to deceleration of the beam which is to be expected as it is run on a decelerating phase. In the injectors with the SRF third harmonic cavity all three accelerating cavities have significant energy gain and no reduction in energy gain along the booster is visible. The higher amplitude SRF third harmonic cavity in the injector with both cavities leads to more deceleration which is the expected behaviour.

The variation in the RMS energy spread along the injectors can be seen in figure 6.7. These injectors all exhibit the expected behaviour of a larger initial energy spread in the gun when the long initial bunch is still accelerating which significantly decreases once the bunch is fully accelerated. The buncher then increases the energy spread which is required for the ballistic bunching. This energy spread is then reduced by the longitudinal space charge forces of the bunch as it moves towards the booster. In the booster the energy spread depends primarily on the chirps introduced by the booster cavities. The specifics

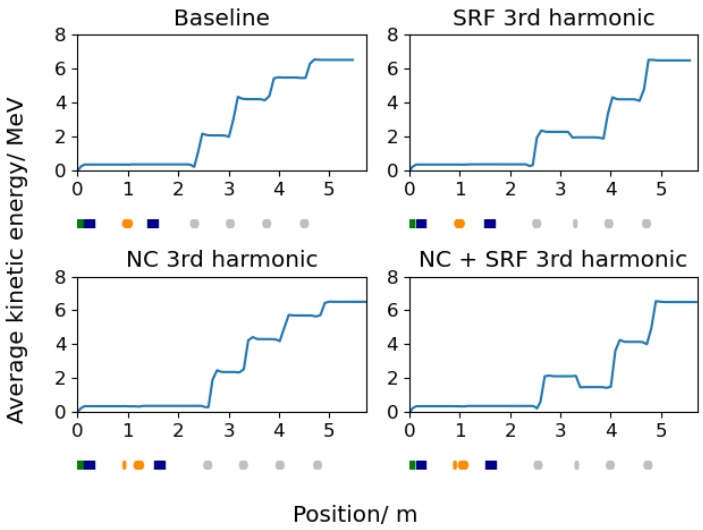

Figure 6.6: A comparison of the average kinetic energy for all chosen injector solutions. The positions of the beamline elements are indicated below the plots. The electron gun is indicated by a green box, the solenoids by dark blue boxes, the NC third harmonic cavity by the shorter orange ellipse, the buncher cavity by the long orange ellipse, the accelerating cavities by the longer grey ellipses and the SRF third harmonic cavity by the short grey ellipse.

of these vary depending on the injector and different variations of the energy spread are seen in the different injector schemes but in all cases the chirp is mostly removed from the bunch at the exit of the booster.

6.4 Slice emittance

All of the four injector schemes are capable of meeting the specification in terms of the projected emittance at the booster exit and none of the solutions are dramatically worse than any other. Looking at the slice emittance evolutions should give an idea if the emittance compensation is limiting factor on the projected emittance or whether the slice emittance is. It should also give an idea of where in the injector the slice emittance growth occurs. With this information it may be possible to determine if the slice emittance growth can be avoided.

The evolution of the projected emittance, average slice emittance and maximum slice emittance for the four injector schemes can be seen in figure 6.8.

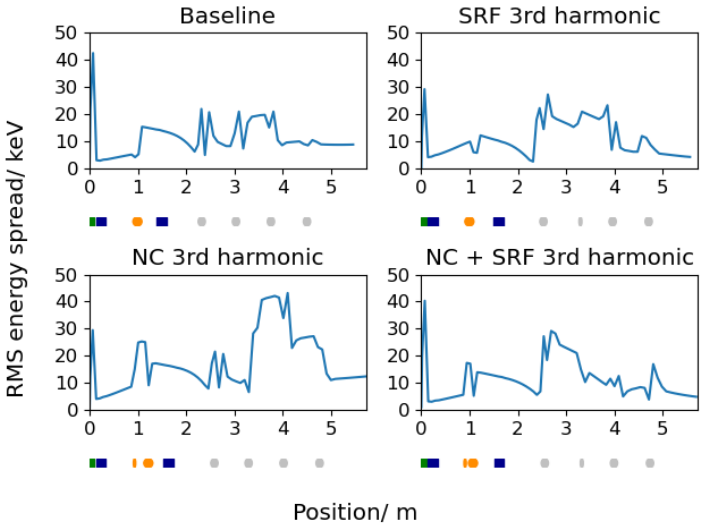

Figure 6.7: A comparison of the energy spread for all chosen injector solutions. The positions of the beamline elements are indicated below the plots. The electron gun is indicated by a green box, the solenoids by dark blue boxes, the NC third harmonic cavity by the shorter orange ellipse, the buncher cavity by the long orange ellipse, the accelerating cavities by the longer grey ellipses and the SRF third harmonic cavity by the short grey ellipse.

From this it can been seen that there is minimal slice emittance growth along the baseline injector and that the limiting factor on the projected emittance is the emittance compensation not the slice emittance. From the plots of the other three schemes it can be seen that there is noticeable slice emittance growth. Significantly however it can be seen that the slice emittance growth does not occur specifically at the locations of the higher harmonic cavities. So the higher harmonic cavities themselves are not the direct source of the slice emittance growth. The slice emittance growth is in the booster but not specifically at the location of the higher harmonic cavity. Looking at the average slice emittance it seems to mostly occur in the first cell of the booster linac. The exception to this is scheme with both cavities where some slight increase of the average slice emittance occurs at the very end. The maximum slice emittance growth is larger but still localised to the booster. In the scheme with just the normal conducting third harmonic cavity the max slice emittance growth is entirely localised to the first booster cavity. In the schemes with the SRF third harmonic cavity the growth of the maximum slice emittance value extends over a

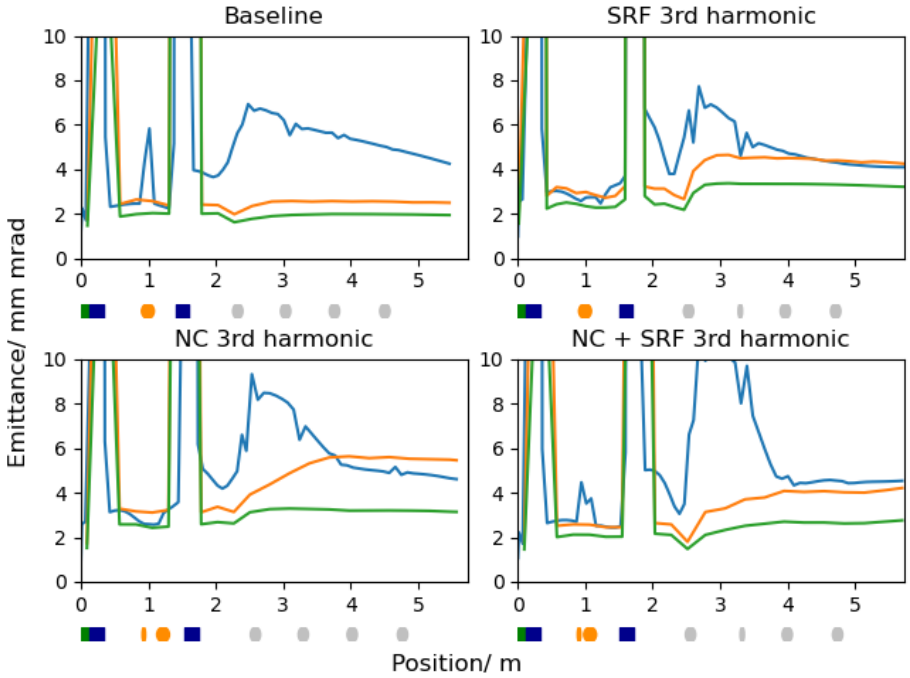

Figure 6.8: A comparison of the projected emittance (plotted in blue), average slice emittance (plotted in green) and maximum slice emittance (plotted in orange) for the four schemes. The positions of the beamline elements are indicated below the plots. The electron gun is indicated by a green box, the solenoids by dark blue boxes, the NC third harmonic cavity by the shorter orange ellipse, the buncher cavity by the long orange ellipse, the accelerating cavities by the longer grey ellipses and the SRF third harmonic cavity by the short grey ellipse.

larger section of the booster. In all three schemes with higher harmonic cavities the projected emittance at the booster exit has been comparable in magnitude to the maximum slice emittance. This suggests that compared to the baseline solution the slice emittance is more of a limiting factor on the projected emittance than the emittance compensation.

The initial and final slice emittances and line charge densities for the four schemes can be seen in figure 6.9. The slice emittances near the start of the injector are similar for all four schemes. As are the line charge densities with the exception of the scheme with just the NC third harmonic which has a shorter initial bunch length and hence higher line charge density at the time the distribution is outputted. For the plots at the exit flange of the booster the line

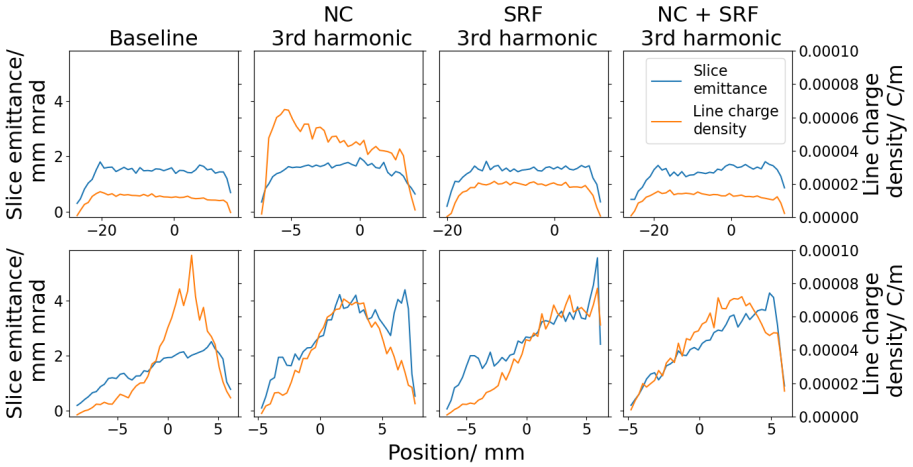

Figure 6.9: A comparison of the initial (on the top row) and final (on the bottom row) slice emittance (in blue) and line charge density (in orange).

charge densities are different for the four schemes. The baseline scheme has the sharpest peak with an diffuse tail. The solution with the normal conducting third harmonic cavity has the most symmetrical line charge density distribution. This is expected as the diffuse tail forms as part of the ballistic bunching process and the purpose of the NC cavity is to correct the non-linearities in that process. The solution with the SRF third harmonic still has the diffuse tail that forms during the ballistic bunching as it has no means of correcting that non-linearity. It does however have a less sharp peak in the particle distribution than the baseline solution as well as sharper boundary at the front of the bunch. The solution with both higher harmonic cavities line charge density distribution is similar in shape to the solution with just the normal conducting third harmonic. However it is less symmetrical and does still have a tail which is probably indicative of less effective compensation of the non-linearity in the bunching. All four of the schemes exhibit slice emittance growth with the most significant growth typically in areas of higher charge density. The three solutions with higher harmonic cavities all exhibit significantly more slice emittance growth than the baseline solution. Compared to the other solutions the solution with just a normal conducing third harmonic cavity exhibits a rise in the slice emittance at the center of the bunch where the line charge density is highest. On the other hand the solution with just the SRF third harmonic cavity exhibits a spike in the slice emittance at the front of the bunch.

6.5 Phase spaces and bunch distributions

The final phase spaces and spatial bunch distributions of the four chosen solutions are examined in this section. The plots in this section are laid out in two rows like the similar figures in chapter 6 with the top row having the same axis for all schemes allowing comparisons between the different phases spaces. While the bottom row has axis scaled differently for each distribution so that the shape of the phase spaces can be compared. Instead of showing the evolution of the phase space along the injectors only the phase space at the booster exit is shown.

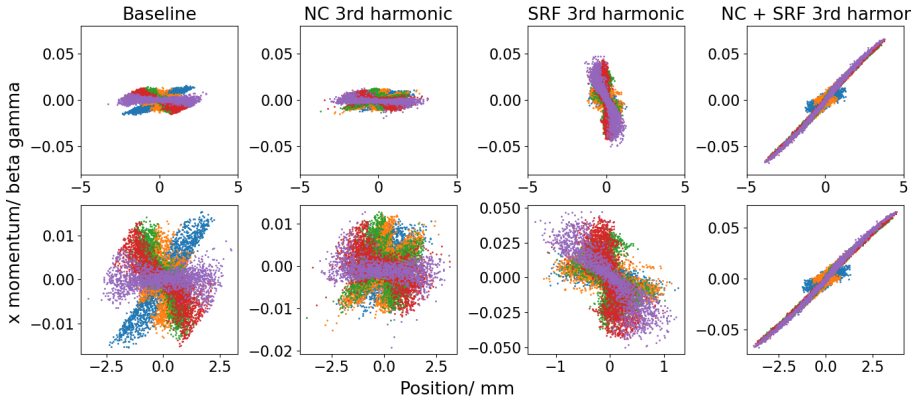

Figure 6.10: A comparison of the transverse phase spaces at the booster exit for all chosen injector solutions. Particle colour indicates the initial longitudinal slice that the particle occupied. The slice colours are from front to back purple, red, green, orange, blue.

The transverse phase spaces of the four different selected solutions can be seen in figure 6.10. From figure 6.8 it was seen that for the baseline solution the projected emittance was significantly larger than the slice emittances indicating that the limiting factor on the projected emittance is the slice alignment and matching not the slice emittance values. While for the three other solutions the projected emittances are much closer to the maximum slice emittance values indicating that the limiting factor is the slice emittance values not the slice alignments. These inferences line up fairly well with what is depicted in figure 6.10. The transverse phase space of the baseline solution clearly shows that the tail slice of the bunch is significantly misaligned with the other slices of the bunch. For both of the schemes with a single higher harmonic cavity the

distortions to the slices occupy a large amount of the area and adjusting the slice alignments will not significantly reduce the area occupied in phase space. For the scheme with both there is a clear non-linearity in the purple head slice and the tail slices are poorly matched with the front of the bunch.

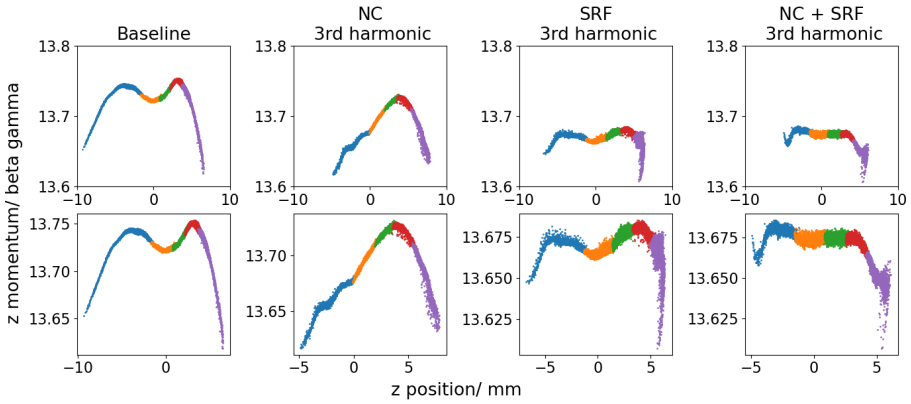

Figure 6.11: A comparison of the longitudinal phase spaces of the different schemes at the booster exit. Particle colour indicates the initial longitudinal slice occupied by a particle. The slices are the same as those in figure 6.10.

The longitudinal phase spaces of the selected solutions for each scheme can be seen in figure 6.11. The analysis of the longitudinal phase spaces is particularly important for the comparison between the schemes as the purpose of the addition of the higher harmonic cavities is to linearise the longitudinal phase space. So being able to visualise how effective this is, is required for selecting an appropriate scheme. The baseline scheme exhibits the characteristic "M" shape seen and discussed in the previous chapter. It can be seen that the normal conducting third harmonic cavity removes the central dip as expected leaving a longitudinal phase space which is closer to a 2nd order RF distortion. Although it is not exactly 2nd order as there is some modulation in the blue tail slice of the bunch that deviates from the 2nd order phase space shape. The maximum to minimum energy spread is however not that much smaller than for the baseline injector and more of the particles in the bunch have energy values which deviate further from the design beam energy. The addition of the SRF third harmonic removes a large amount of the 2nd order distortion as expected. Although there are some low energy particles in the tail and the head of the bunch. This does lead to reduction in the energy spread of the bunch compared to the baseline scheme as the energy tails at either end of the

bunch are smaller than the tails of the "M" shaped bunch. The central dip from the ballistic bunching is still present as would be expected without the NC third harmonic to correct it. The combination of both higher harmonic cavities removes both the central dip and the majority of the 2nd order distortion as expected. Although some low energy particles are still present at the front and back of the bunch.

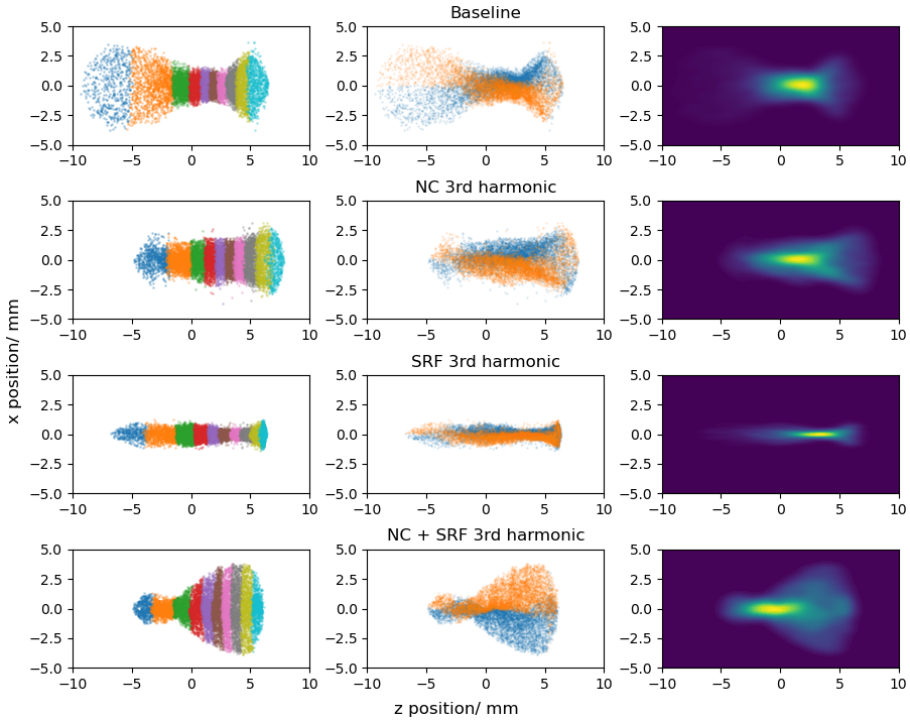

Figure 6.12: A comparison of the Z-X distributions of the bunches for each scheme in real space. For all four options the longitudinal slices, whether particles have crossed over after the second solenoid and the density of particles in the bunch are shown. The axis are the same for the distributions.

The top down view of the bunch distributions in real space can be seen in figure 6.12. This allows the structure of the bunch in space and any crossovers or longitudinal slice mixing to be seen. The baseline scheme has non-uniform longitudinal compression along the bunch but no longitudinal slice mixing. It also has a diffuse tail which has crossed over and some transverse mixing at the head of the bunch.

The addition of the NC third harmonic cavity leads to a more uniform

compression along the length of the bunch as can been seen from the length of the slices. Although the back two slices are slightly longer so it isn't completely uniform and there is a small tail. The more uniform bunching and more uniform charge density also leads to more uniform transverse shape without the pinched central section and the larger crossed over tail. From looking at on which transverse side the particles originate it can be seen that the core of the bunch does not cross over but there is a crossover at both the head and the tail of the bunch. In terms of the density of the bunch there is not a noticeable diffuse tail. Though a "V" shaped structure in the particle density appears to have formed at the head of the bunch.

When a third harmonic SRF cavity is added on its own without the normal conducting cavity the bunching is less uniform along the bunch than with the normal conducting cavity which is the expected behaviour. The beam noticeably has a smaller transverse size at the exit of the booster than the other schemes this is a result of the strong transverse RF focus from the higher harmonic cavity. The bunch has not crossed over except at the very end of the tail where the two initial sides of the bunches are beginning to overlap. From figure 6.2 which shows the RMS transverse beam sizes it can be seen that the beam is transversely focusing and has not yet started diverging at the exit flange of the booster. This indicates that the bunch will potentially crossover after exiting the booster. From the density plot the fact that the bunch is longitudinally asymmetric with a diffuse tail is clear. Although the tail is noticeably smaller than in the baseline solution.

The scheme with both the normal conducting and SRF third harmonic cavities like the scheme with with just the normal conducting cavity has more uniform bunching along its length as can be seen from the slice lengths. It however does not have the more uniform focusing along the bunch. Instead at the exit of the booster the front slices are much larger than the tail slices. From the plot indicating the initial transverse position of particles it can be seen the bunch core has crossed over. In the first part of the tail the two sets of particles are overlapped and at the very end they are on their original side. The strong transverse focus from the higher harmonic cavity that leads to this crossover can be seen in figure 6.2 with the crossover occurring at about the 4 m mark. In terms of the particle density, and hence the strength of the space charge forces, in the bunch the highest density is located towards the tightly focused back of the bunch. It should be noted that the area of highest particle density, and hence strongest space charge forces, is not necessarily the area with the highest

longitudinal line charge density as areas with larger transverse size may have more total particles. From looking at the longitudinal slice visualisation this can be seen as the region with the shortest slices is located in the transversely larger front third of the bunch.

6.6 Conclusion

The addition of higher harmonic cavities allows for correction of the nonlinearities in the longitudinal phase space and the spatial distribution of the particles in the bunch. This is achievable while still meeting the transverse emittance specification of the injector. However the injectors with higher harmonic cavities exhibit greater slice emittance growth than the baseline design. This slice emittance growth does not occur at the higher harmonic cavities so they do not necessarily seem to be directly responsible for it. One potential factor in why lower slice emittance solutions where not found for the injector schemes with higher harmonic cavities is that the projected emittances of the solutions are all comparable and that the optimisation algorithm optimises projected not slice emittance. So even if there are solutions with less slice emittance growth the optimiser may not find them if they have comparable projected emittance values. As they will not appear to be better than solutions with higher slice emittance but equal projected emittance to the optimiser.

In this chapter it has been shown that the addition of higher harmonic cavities to the PERLE injector does allow for the longitudinal phase space to be linearised while still maintaining a transverse emittance low enough to meet the specification. However just because the higher harmonic cavities can fulfil their function does not mean that that should be used for PERLE. The decision about whether or not to use the cavities depends on more than the injector performance and needs to be made in the context of the whole machine. The addition of higher harmonic cavities will increase the cost and complexity of the injector. Therefore it firstly needs to be confirmed whether or not linearisation of the longitudinal phase space is necessary. It may be the case that the current non-linearity from the injector is small enough to be acceptable. This will require start to end simulations of PERLE with realistic bunches from the injector to see what the consequences of the non-linearity are. These simulations have not yet been performed if once these simulations are performed and it is established that linearisation is needed further work will still need to be done to determine if higher harmonic cavities are the correct

approach as the linearisation could also be done optically in the arcs of the ERL. That option will need to be compared to the higher harmonic option to determine which is best. In conclusion the work in this chapter has shown that higher harmonic cavities are a viable approach but not if they are the best approach.

Chapter 7

Merger

7.1 Merger overview

After the beam has been accelerated to the injection energy it must be transported into the main ERL loop. The section of the injector beamline which does this is called the merger. The merger must do at least three different things simultaneously. It needs to transport the beam from the booster exit to the entrance of the main linac in such a way that is compatible with the geometrical constraints of a real beamline in terms of necessary transverse offsets and distances between magnets. It also needs to match the beam to the required Twiss parameters of the main ERL loop and preserve the transverse emittance of the beam. In addition to these three main functions the longitudinal dynamics of the beam in merger need to be considered. Mergers can be used as bunch compressors. However this is not required for PERLE instead a merger with as small a first order longitudinal dispersion (R56) as possible is preferred.

Mergers consist of a matching section, a dispersive region consisting of a number of dipoles where the final dipole is part of the main ERL loop and seen by both the injected and recirculated beams and then an optional matching section between the common dipole and the main linac that will be seen by both the injected beam and the recirculating beam. To prevent the common dipole from bending the reirculated beams off axis a reinjection chicane is used. This consists of a number of dipoles before the injection dipole which bend the recirculated beam off axis so that the injection dipole then bends it back on axis. The MHz to GHz repetition rates of ERLs prevents the use of kickers

for injection hence why this fixed dipole solution is used. A sketch of a merger layout with the merger regions and reinjection chicane marked can be seen in figure 7.1.

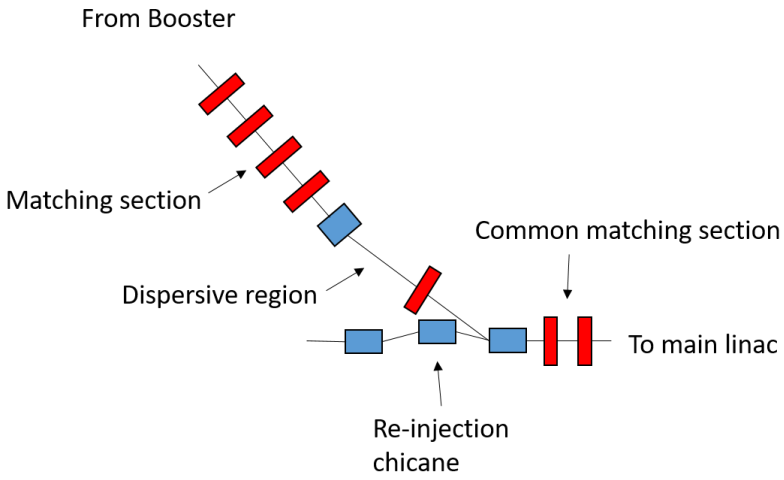

Figure 7.1: A sketch of a possible merger and reinjection chicane with the sections labelled.

The big difference between the earlier stages of the injector and the merger is that in the merger the beam is bent which introduces dispersion and breaks the axial symmetry of the beamline. Space charge forces are also still significant in the merger despite the higher beam energy after the booster. It is the combination of space charge, an axially asymmetric beamline and dispersion that lead to the mechanisms that cause emittance growth in mergers.

7.2 Merger schemes and layouts

Dipole arrangements

There are a significant number of different merger schemes which could be used. In the case of PERLE there are some which can be eliminated based purely off physical layout and geometric considerations. Mergers which have the booster linac in line with the main linac are not an option for PERLE. This is because they would have to be located in the position already occupied by the recirculating arcs. As a result only mergers where the injector is at a transverse offset to the main ERL loop can be considered.

There are a number of other constraints that will be applied to the merger schemes that will be considered for PERLE. Firstly only merger schemes in which all of the dipoles are the same will be considered. This is to reduce the number of different types of magnets needed and hence the cost as developing and manufacturing many types of magnets is expensive. If this constraint was relaxed it would open up new possible layouts with dipoles with different bending or edge focusing angles. In addition to only using one type of dipole magnet, only mergers with symmetric or antisymmetric bending will be considered. Finally only merger schemes with two to four dipoles will be investigated. A single dipole is not enough to cancel the dispersion and have the merger be achromatic. Mergers with more than four dipoles are not examined as it is considered desirable to keep the merger as short and simple as possible. After applying the constraints list there are only a limited number of different layouts. They can all be seen in figure 7.2 with the options that are being considered marked.

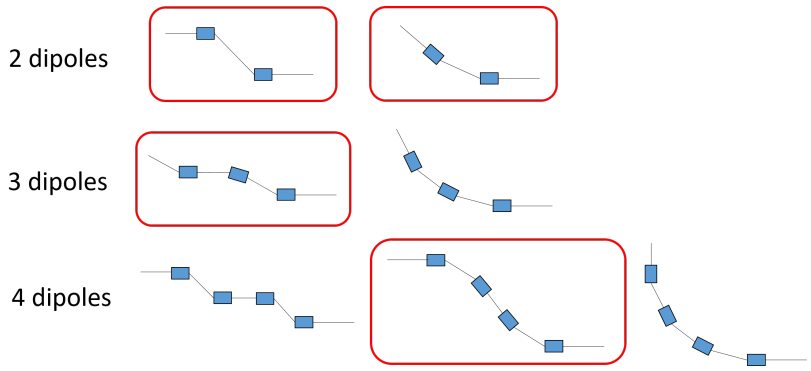

Figure 7.2: All possible merger dipole layouts which meet the described constraints. The layouts which will be examined later in this chapter are marked by a red box.

Transverse focusing

Element type

Mergers require transverse focusing elements for matching the Twiss parameters, performing emittance compensation and cancelling the dispersion. There are three different ways for providing transverse focusing which are quadrupoles, solenoids and dipole edges. Dipole edge angles are capable of cancelling the dis-

persion but for matching and emittance compensation they must be combined with one of the other focusing options.

Quadrupoles and solenoids have different advantages and disadvantages. Quadrupoles are generally used at higher beam energy and the quadrupoles needed in the merger will not be particularly strong. They do however have the downside that they do not have symmetrical focusing in both planes. This breaks the axial symmetry of the beam meaning that beamlines containing quadrupoles don't intrinsically have symmetrical emittance compensation in both transverse planes. Solenoid magnets have the advantage that they have symmetrical focusing in both planes. Which means that they intrinsically have the same emittance decompensation and compensation behaviour in both planes. To retain axis symmetric focusing along the whole merger requires the use of special dipole designs with equal focusing in both transverse planes. Dipoles with equal focusing in both planes can be obtained either using edge focusing or combined function magnets with a quadrupole component. Retaining axial symmetry along the whole merger simplifies the design and tuning of the emittance compensation process as the emittance compensation is the same in both planes. Additionally having axis symmetric focusing halves the number of free parameters needed to match the beam. So half the number of matching magnets are needed which means that a shorter matching section could be used. Solenoids do however have a number of disadvantages. Firstly much more expensive and complicated solenoids are needed to get the same focusing effect as from quadrupoles. Which is why solenoids are generally not used at higher energies. Whether normal conducting solenoids are practically capable of achieving the required field strength for the merger would need to be investigated. Secondly solenoids can only provide focusing not defocusing like quadrupoles. Thirdly solenoids rotate the beam. Earlier in the injector where the beam is completely axially asymmetric this is not important. However in the dispersive region of the merger this would cause a component of the dispersion in the bending plane to be rotated into the non-bending plane where it would cause emittance growth. This issue can be mitigated by using counter-wound pairs of solenoid where each focusing magnet is actually composed of a pair of solenoid with opposite field directions but equal strengths. So the first magnet in the pair rotates the beam and then the second rotates it by an equal amount in the opposite direction leading to no net rotation. How accurately this can be achieved in reality would need to be investigated. In the case of PERLE quadrupole based merger will be preferred due to the simpler focusing

magnets and the fact that quadrupole based mergers are a proven approach which have been used successfully on previous ERLs.

Edge focusing in the dipole magnets is unavoidable. It could be used for balancing the focusing between the two transverse planes. As horizontal focusing quadrupoles are needed to cancel the dispersion so using rectangular magnets which have a horizontal defocus and a vertical focus would reduce the amount of pure horizontal focusing in the merger. Edge focusing could also be used to control the dispersion. Merger designs which have at least three dipoles of which at least one bends in the opposite direction to the others can use edge focusing to cancel the dispersion. This offers some advantages and some disadvantages. In terms of advantages the use of edge focusing can free up space between the dipole as focusing elements don't need to be placed in those gaps. These allows for more space for the other required components of the accelerator such as diagnostics, collimators and vacuum pumps. It could also allow for the distances between the dipoles to be reduced. Shorter mergers, particularly in the dispersive region, being considered preferable as there is less time for the space charge forces to degrade the beam quality. However in terms of disadvantages edge focusing is fixed focusing. The edge angles cannot be changed once the magnet has been manufactured. The space charge forces will have an effect on the dispersion and the edge angle that is optimal for the one space charge case may not be optimal for a case with difference space charge forces. In fact different bunch charge, bunch lengths and beam sizes may lead to different amounts of space charge forces and hence the optimal edge angle will depend on the injector settings as a whole. This means that a decision would need to be made about which settings to set the edge angle for. Finally the edge angles of the dipoles need to be set to a specific value to achieve equal focusing in both transverse planes for solenoid based mergers. In the case of PERLE which will use quadrupoles for its transverse focusing for both matching and dispersion cancellation rectangular magnets will be used to balance the focusing.

Matching

A merger needs to have sufficient transverse focusing elements to match the beam to the requirements of the main ERL loop. The PERLE main linac has matching conditions which are determined by the requirements for the optics in later main linac passes. The requirements are for a round beam with

equal alpha and beta functions in both transverse planes. This requires four independent free parameters to do the matching if the axial symmetry of the beamline is broken or two if the axial symmetry isn't broken. This means four quadrupoles or two solenoids. The PERLE Twiss matching conditions also require a crossover in both planes just prior to entrance of the main linac. This will potentially reduce the effectiveness of the emittance compensation through the main linac.

The matching elements can be placed in three different locations in the merger. Prior to the dispersive section, in the dispersive section and after the dispersive section in the main ERL loop. There is no particular disadvantage to placing matching elements prior to the dispersive section. However if only matching elements before the dispersive region are used it can be challenging to match across the dispersive region. Placing matching elements in the dispersive region lengthens the dispersive region increasing the amount of time that the longitudinal space charge forces can modify the dispersion and potentially cause emittance growth. It also means that the focusing elements in the dispersive region are no longer simply for cancelling the dispersion so there is less separation of the function of different elements in the design. Focusing elements associated with the merger introduced after the dispersive section are in the main ERL loop and are hence seen by the higher energy recirculating beams. These focusing elements will be significantly weaker than the elements that would typically be used to act upon the higher energy beams. Hence the effect of the focusing elements on the recirculated beams will be smaller than their effect on the injected beam. Whether or not their effect is significant is something that needs to be investigated during the design of an ERL. In the following work matching elements will be placed both before the dispersive section and in the main ERL loop for all the schemes. Some of the schemes also have quads in the dispersive region which are not for dispersion cancellation and can be used for matching.

In the case of the PERLE lattice there is not much space between the final merger dipole and the entrance flange of the main linac cryomodule. This limits the number of matching elements that can be located there. In addition to the matching elements there needs to be a way to measure the dispersion and Twiss parameters just before the entrance into the main linac. So that dispersion cancellation and matching at the entrance to the main linac can be performed. This requires a diagnostic station to be located between the final merger dipole and main linac cryomodule entrance. Based on these space

constraints it has been decided that a maximum of two quadrupoles can be fitted into this space. Alternatively a single solenoid could be located in this region.

Merger diagnostics considerations

The requirements of the diagnostics in the merger may influence the layout chosen. It desirable to have a diagnostic line to allow for detailed measurements of the beam. It is not possible to fit enough diagnostic systems to fully characterise the beam as the end of the merger goes directly into the main linac and diagnostics cannot be placed inside the cryomodule. One way of having a diagnostic line is to have a beamline running from one of the dipoles so that if the dipole is turned on the beam continues down the merger while if the dipole is turned off the beam goes down the diagnostic line. This does have the disadvantage that the diagnostic line does not see the final beam that enters the main linac.

Another way of setting up the merger diagnostics which is intended to mitigate this to have a mirror merger. This is an approach that was used for the CBeta injector [60]. In this approach the first dipole in the merger can be set to one polarity to bend the electron beam down the merger and into the main linac but it can also be set to the other polarity to bend the electron beam the other way down another merger line which is the mirror image of the actual merger. This beamline ends with the diagnostic line. If the two mergers are set up to be exact mirror images of each other this should give a better idea of what the beam looks like as it enters the booster.

The mirror merger approach does however constrain the merger design as the first dipole must appear identical to the beam irrespective of which way it is bending. This means that the entrance angle to the dipole must be 0° and the exit angle must be equal for both bending directions. This can easily be achieved with a rectangular magnet however it means that the exit angle must be the same as the bending angle. It could also be achieved for other bending angles including a sector magnet it would just require a specific dipole design. The requirements of a mirror merger also rule out using a pole face shaping to achieve a combined function magnet with equal focusing in both planes. As this will not look identical to the beam in both bending directions.

One potential way to get a combined function magnet that can appear identical to both bending magnets would be to have a magnet with two sets

of independently controllable coils. A dipole pair and a quadrupole pair. A potential way to relax the restrictions on the edge angles or whether the magnet is a combined function magnet would be to reverse the polarity by physically rotating the magnet. Both of these approaches may be challenging to physically implement. In general combining a mirror merger and a solenoid based merger is challenging.

In the case of the PERLE merger which uses quadrupoles for its transverse focusing and rectangular magnets for its dipole the entrance dipole will be set to have 0° entrance angle to allow the use of a mirror merger with the options studied here if that is deemed to be a desirable option. To have symmetry in the merger the entrance angle of the final dipole will be the bend angle. In the case of the three dipole scheme that is examined the central dipole will have half bending angle edges on both sides.

7.3 Merger beam dynamics considerations

Emittance growth mechanisms

The merger presents a significant potential for emittance growth if not designed appropriately. The beam is still space charge dominated and so space charge effects must be mitigated. There are three mechanism by which space charge can cause emittance growth in the merger. The first two of these effects are the same as earlier in injector. Firstly different transverse space charge kicks at different positions along the bunch lead to different longitudinal slices of the bunch moving differently in phase space. This causes the slices to rotate out of alignment leading to a growth in the projected emittance. This can be mitigated using the process of emittance compensation. There are however two challenges when it comes to achieving good emittance compensation which are not seen earlier in the injector. The first of these is that the focusing in the merger is not axially asymmetric so the bending and non-bending plane emittances evolve differently and their emittance minima are not necessarily in the same location. So the merger should be optimised to get the best trade off between the emittance compensation in both planes. The second is that the merger has other requirements than just emittance compensation and meeting those requirements may present challenges for the emittance compensation. For example canceling the dispersion and matching in the merger often necessitate strong focusing which leads to the presence of crossovers in the beam which can

be detrimental to the effectiveness of the emittance compensation technique.

The second source of space charge induced emittance growth is also present earlier in the injector. It is the non-linear space charge forces which can cause a distortion to the transverse phase space distribution leading to a growth in the slice emittance of the beam. This can be mitigated by having as short a merger beamline as possible so that there is less time for the non-linear space charge forces to degrade the beam quality. The non-linear space charge forces are very dependent on the shape of the underlying beam distribution so this source of emittance growth can also be potentially mitigated if the bunch distribution can be tailored towards one with smaller non-linear forces. The bunch distribution can be shaped by shaping the initial laser pulse. One example of this would be shaping the initial laser pulse to have an ellipsoid shape leading to a bunch with the same shape and more linear space charge forces [105].

The final emittance growth mechanism caused by space charge is related to how the space charge affects the dispersion. The introduction of space charge can lead to occurrence of residual dispersion in what should be an achromatic beamline. The process by which this residual dispersion occurs is as follows the longitudinal space charge forces cause the energy of the particles to change as they propagate through the merger increasing the energy of the head of the bunch and decreasing the energy of the tail. This means that the particles towards the head and the tail of the bunch are bent differently by each dipole despite the fact that the dipoles have the same field strength. This leads to a modification of the dispersion of those particles leading to residual dispersion at the exit of the merger. Although the dispersion for the particles at the bunch centroid which do not change energy is the same for both the space charge free case and when there is space charge. The residual dispersion due the particles in the bunch which changed energy leads to associated projected emittance growth in the bending plane. There are a number of different approaches which can be used to try and minimise this emittance growth mechanism.

Firstly the merger can be kept as short as possible with as small bending angles as possible. This approach is the simplest and doesn't make any attempt to cancel the residual dispersion. Instead it just tries to make it as small as possible by keeping the particle energy change between the dipoles and the dispersion in the merger as small as possible.

A second approach works by matching the Twiss at the entrance into the merger so that offset in the bending plane transverse phase space caused by the residual dispersion is along the long axis of the phase space ellipse rather

than the short axis [22]. This minimises the increase in the phase space area due to any slice offset from the residual dispersion. This approach also doesn't attempt to cancel the residual dispersion instead it attempts to reduce the emittance growth caused by it. A similar approach to this has been used to reduce the emittance growth due to CSR (Coherent Synchrotron Radiation) [110].

A third approach involves defining a generalised dispersion for which the particle energies change as they move through the dispersive region [22]. Achromaticity conditions for this generalised dispersion can then be derived by making the assumption that space charge forces are frozen. The generalised dispersion has four achromaticity conditions, double the usual number for a space charge free beamline. If the merger meets these conditions there should be no residual dispersion even in the presence of space charge. The zig-zag merger scheme was designed to meet these achromaticity conditions.

A fourth and final approach is to have a merger consisting of two separate dispersive regions with equal but opposite dispersion and an achromatic region with π phase advance between them. Given that the two dispersive regions have equal but opposite dispersion if the energy change of the particles is the same in both dispersive regions the residual dispersions at the exit of the two dispersive regions should then be equal in magnitude but opposite in sign allowing them to cancel each other out. Like the second approach this is also similar to an approach used to cancel the emittance growth due to CSR in transfer line [111]. This approach depends on the space charge forces being the same in both dispersive regions so the charge density must be the same in both. This is challenging to make compatible with compression or non-symmetric optics. As can be seen from the fact that two of these approaches are similar to those used to cancel CSR there are some similarities between the effects of CSR and the effects of longitudinal space charge in that they are both effects which lead to particles changing energy inside the dispersive region.

In addition to the space charge related emittance growth there are other potential emittance growth mechanisms. Firstly geometric and chromatic aberrations in the magnets may cause emittance growth. Secondly uncancelled higher order transverse dispersion may be a potential source of emittance growth in the merger. The use of higher order multipoles to cancel out the higher order dispersions is potentially possible but in the interest of simplicity of design will not be considered here.

Finally CSR is an effect which could be an issue in bending regions and

can lead to emittance growth. This effect is less significant at lower energies and longer bunch length and may not be an issue for PERLE. Modelling CSR effects at the relatively low energies found in mergers is not trivial as most codes which model CSR make the ultrarelativistic assumption which is not valid in the energy regime of the PERLE injector. For example, OPAL's CSR model makes this assumption. In comparison with a GPT model, which does not make the assumption, the two codes did not agree at 7 MeV [112]. It should be noted that there were significant differences in the parameters used in this comparison compared to those used for the PERLE merger. The bunch length was an order of magnitude smaller and the bunch charge was 1 nC which is twice the 500 pC bunch charge used in PERLE. The bending angle in the comparison was 20° the same as used for all of the PERLE merger schemes investigated apart from the S-bend which has 35°. This means that the CSR effects seen in this comparison will be much larger than those which will be seen in the PERLE merger. However the divergence between the results of the two codes due to the ultrarelativistic assumption should only depend on the particle's relativistic gamma. So the conclusion that OPAL's CSR model isn't valid in the 7 MeV energy range of PERLE is still valid. CSR is not not modelled in the following simulations as the CSR is likely to be a small effect and the code used for the simulations makes an invalid assumption for the mergers energy range in its CSR model.

Longitudinal beam dynamics

In addition to the transverse emittance preservation and matching in the merger the longitudinal dynamics also need to be considered. The merger is a dispersive region and will generally have a non-zero R56, which is the longitudinal dispersion, unless specifically designed to be isochronous. The booster linac could be used to impose an energy chirp on the bunch. Both of these facts mean that the merger could potentially be used as a bunch compressor. In this work as PERLE does not require particularly short bunches on injection and there is plenty of potential to compress the bunch elsewhere, either upstream using the buncher cavity or velocity bunching in the first cell of the booster or downstream in the recirculating arcs, the use of the merger as a bunch compressors will not be considered. However as the energy chirps at the exit of the booster are relatively small in the interest of simplicity in the lattice of the dispersive region specifically isochronous merger will also not be used.

In addition to the potential for bunch compressing another option for using the longitudinal dynamics of the merger is optical linearisation of the longitudinal phase space. The use of higher order multipoles in the dispersive region would allow for tuning the second and third order longitudinal dispersions. In these investigations like with using the merger as a compressor in the interest of simplicity of design in the space charge dominated region of the ERL this will not be considered. In terms of controlling the longitudinal phase space there is significant potential for optical linearisation downstream in the recirculating arcs of the ERL.

7.4 Merger optimisation

Optimisation process

Four merger schemes will be optimised and examined in detail. The specifics of these schemes will discussed in detail in the following sections. The optiminsation process for each scheme was done in two steps. Firstly space charge free settings for the quadrupoles were found using the matrix code Optim. These quadrupole settings were then used to to set the initial variable ranges for the second stage of the optimisation. This second stage was an NSGAII based optimisation of the merger using OPAL. The NSGAII implementation was from the python library JMetalPy [106]. The objectives of the optimisation were to minimise the average transverse emittance and the average mismatch factor between the two transverse planes both at the exit of the first main linac pass. The mismatch factor is a measure of the deviation of the beam phase space ellipse from the ideal ellipse [113]. It is defined as seen in equation 7.1.

$$MMF = \left[1 + \frac{\Delta + \sqrt{\Delta(\Delta+4)}}{2}\right]^{1/2} - 1 \tag{7.1}$$

Where $\Delta = \Delta\alpha^2 - \Delta\beta\Delta\gamma$ and $\Delta\alpha$, $\Delta\beta$ and $\Delta\gamma$ are the deviation of those Twiss parameters from the target values. Due to the fact the OPAL's default output mode is in terms of time rather than position the Twiss parameters of the bunch were calculated at a particular time rather than at a particular position. The optimisation also had the constraint that no particles should be lost.

The motivation for doing a two step optimisation process was that a large volume of the parameter space for quadrupole based mergers is occupied by

solutions where the beam becomes unrealistically large leading to the loss of all of the particles in the simulation. This means that if the initial population is generated with a wide range of parameters the majority of the individual produced will violate the constraints. This slows down the optimisation process as the initial stages will just be searching for the viable region of parameter space. It also reduces the effectiveness of the optimisation as the optimisation will be biased towards the areas of the parameter space which contained the initial viable solutions which were found by chance. These regions of parameter space may not contain the best solutions. To avoid this issue a zero space charge matrix code was used to find a region of the parameter space to explore that is know to contain good solutions. Rather than exploring the whole space.

The matrix code used for the first stage of the optimisation was Optim [74]. The Optim model of the merger extended from the exit flange of the booster linac to the entrance flange of the main linac. The input Twiss parameters at the start of the merger were found by calculating the Twiss parameters of the bunch at the exit of booster. The quadrupoles in the merger were set to cancel the dispersion and used to match to the entrance Twiss of the main linac. The target Twiss parameters at the entrance of the main linac were found by tracking a gaussian bunch through the main linac in OPAL with space charge and optimising the entrance Twiss to obtain the required exit Twiss at the end of the linac.

Once initial quadrupole settings for the merger were found using Optim the next stage of the optimisation process were performed. The variables ranges of the quadrupoles were set to be from 0.1 T/m less than the Optim quadrupole setting to 0.1 T/m greater than the Optim quadrupole setting unless the range would change sign in which case the limit in that direction was set to 0. The NSGAII optimisations used the default mutation and crossover rates. The population size used was 120 and the optimisation was run for 50 generations.

Overview of schemes

Four merger schemes have be optimised using the process discussed above. Sketches of the schemes can be seen in figure 7.3.

The first two schemes depicted at the top of the figure are the two possible two dipole schemes. The U-bend is of interest because it is the minimal scheme using the smallest possible number of magnets for an achromatic beamline. This has the advantage of having a short dispersive region which should mean

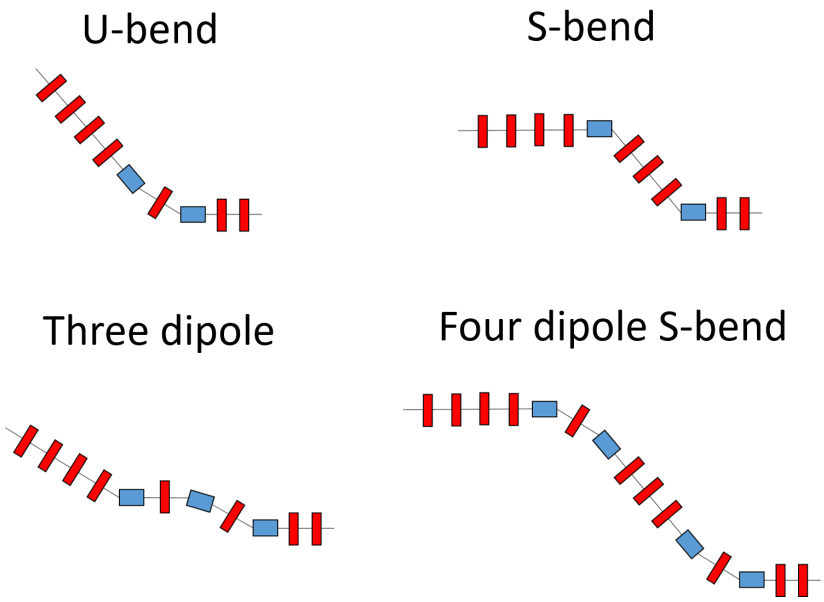

Figure 7.3: The layout of the four merger schemes. Dipoles are depicted in blue and quadrupoles in red.

that the particles don't have much time to change energy in the dispersive region. This should help with minimising the residual dispersion due to space charge and the associated emittance growth. The scheme does have a small R56 compared to some other schemes. This is good in the case of PERLE as there is no desire to compress in the merger and keeping the bunch chirp and bunch length as independent as possible may aid longitudinal matching through the merger. This would however be a disadvantage in the case of an ERL design where compression in the merger is desired. The scheme also requires a strong central quadrupole to cancel the dispersion.

The other two dipole scheme is the S-bend. This scheme is slightly more complicated than the U-bend with two extra quadrupoles in the dispersive region. However the central quadrupole is located at the point where the dispersion crosses the axis and is zero. So it can be used to control the Twiss parameters without affecting the dispersion. Which allows for more flexibility in the matching. This scheme does mean that the booster linac will be offset to the main linac but will not be angled. Depending on the amount of distance required between the main ERL loop and the booster linac this might mean

that this schemes either needs to be quite long or the dipole bending angles might need to be large. Which is not ideal and may lead to lower beam quality.

On the lower row of the figure the first scheme is the three dipole scheme. Variants of this scheme are widely used. Having been used for the JLab FELs, cERL and CBeta as well as proposed for BerlinPro. In the case of this version of the scheme quadrupoles between the dipoles are used to cancel the dispersion rather than using the dipole edge focusing. This scheme has the advantage of having been operationally proven. The scheme is not capable of cancelling the residual dispersion due to the logitudinal space charge affect. It does however have a fairly short dispersive region, doesn't require particularly strong quadrupoles to cancel the dispersion and has the largest R56 of the schemes considered. The R56 is however similar to a chicane-like compressor so the head of the bunch needs to be at lower energy than the tail to get compression otherwise decompression occurs. In the case of a space charge dominated bunch the space charge forces cause the head of the bunch to gain energy while the tail loses energy. So this acts against the necessary chirp for compression. A sufficiently large chirp would be able to overcome this issue though. Whether or not a significant R56 is desirable depends on whether or not the merger is going to be used as a bunch compressor. Approaches where the merger is used as a compressor have been proposed for other machine such as the short bunch operation mode of BerlinPro [62]. However in the case of PERLE the bunch length in the main ERL is not particularly short and can be achieved exclusively by the buncher cavity. Therefore having a relatively large R56 is considered a negative of this scheme.

The final scheme being examined is the four dipole S-bend or double U-bend. This is the most complicated of the four schemes. The motivation behind this scheme is to try and have a scheme which is capable of cancelling the space charge induced residual dispersion and hence prevent or minimise that emittance growth mechanism. The idea behind the scheme is to have two separate dispersive regions which have closed dispersion in the zero space charge case. Then in the space charge dominated case to use the residual dispersion from one to cancel the other. The three quadrupoles in between the two u-bends are used to control the residual dispersion so that it enters the second u-bend at the correct value to be cancelled. This could be done with a single quadrupole but three quadrupoles are used in this case to balance the focusing between the planes. This approach of cancelling the dispersion from one u-bend with a second is a similar to how the CSR kicks in a transfer line

can be used to cancel each other [111]. There are some similarities between the longitudinal space charge effect in a merger and CSR as both are mechanism by which particles change energy in a dispersive region leading to projected emittance growth due to slice misalignments at the end. This cancellation based approach to the residual dispersion relies on the energy change of the particles in each dispersive region being the same. For the two U-bends to cancel each other exactly this requires the merger to be isochoronous and to have symmetric optics from the entrance of the first dipole to the exit of the fourth. So that the space charge forces are the same in both U-bends. This may not be perfectly achievable in practice but benefit could be derived from even imperfect cancellation. Despite the benefit it has in terms of dispersion cancellation with space charge this scheme does have the disadvantage of being both long and complicated involving a larger number of magnets than other options. It also shares the problem with normal U-bends that it requires strong transverse focusing to cancel the dispersion. Which leads to unbalanced focusing between the planes and potentially chromatic effects that cause emittance degradation.

In all of the schemes discussed here the quadrupole magnets will be 15 cm long, the dipoles 20 cm long, the distances between the magnets in the pre-dispersive region matching section are 50 cm, in the post dispersive region matching section the distances are 32 cm, 31 cm and 32 cm for the three gaps respectively. The distances in that region are significantly more constrained by the main ERL loop. For the U-bend scheme the dipole angles are 20 degrees, the distances between the magnets in the dispersive region are 50 cm. The two dipole S-bend and four dipole S-bend both have 2 m transverse offsets between the booster and main linacs. The two dipole S-bend has 20 degree bends while the two dipole S-bend has 35 degree bends to reduce the length of the dispersive region required to achieve the offset. In the two dipole S-bend the distance between magnets in the two U-bends is 50 cm. The magnet spacings in the S-bend and between the two U-bends in the four dipole S-bend were set to achieve the required 2 m offset

Optimisation results

The Pareto fronts produced by the optimisation process discussed in the previous section can be seen in figure 7.4. One solution was picked from each of the Pareto fronts. The optimised parameters of each of these chosen solutions can be seen in table 7.3. During the optimisation process for the 4 dipole S-bend

scheme the third main linac cavity was placed 20 cm further away from the second main linac cavity than it should have been. After the optimisation the cavity position was corrected and the it was confirmed that moving the cavity changed the emittances by less than one percent, the Twiss parameters by less than one and half percent and the mismatch factor by around three percent. These are only small changes so the solution found by the optimisation was retained.

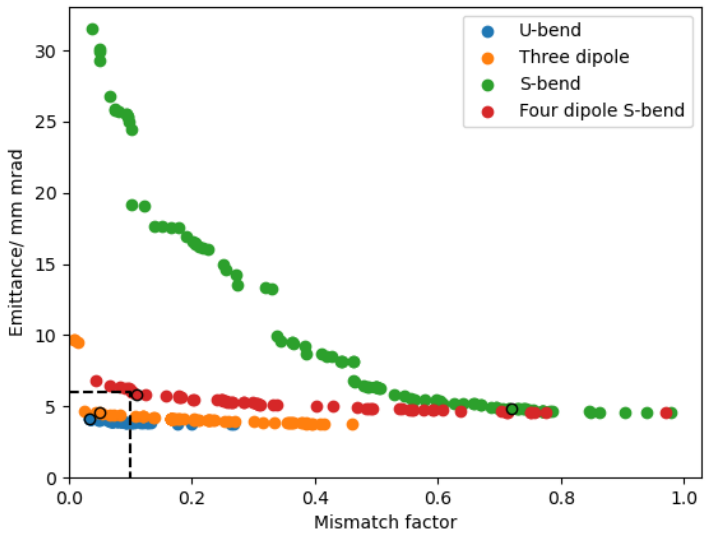

Figure 7.4: The Pareto fronts for the four different merger schemes. The four solutions which will be examined in more detail in the following sections are marked with black bordered points.

From this table it can be seen that two of the four selected solutions are capable of meeting the specification as could also be seen in the Pareto fronts in figure 4.3. The two schemes that are capable of meeting the specification are the U-bend and the three dipole scheme. From this table it can be seen that the two schemes differ in a number of important ways. Firstly and most obviously the final emittance values. The U-bend scheme shows similar emittance growth in both planes although slightly more in the vertical non-bending plane. While the three dipole scheme shows significant emittance growth in the horizontal bending plane to the point where it is nearly outside of the specification however

Table 7.1: The parameters of the chosen merger solution. The element positions indicate the location of the center of the element.

Parameter	**U-bend**	**S-bend**	**Three dipole**	**Four dipole S-bend**
		Dipoles		
Dipole length/ m	0.2	0.2	0.2	0.2
Dipole 1 positions/ m	3.2	3.2	3.2	3.2
Dipole 1 bending angle/ degrees	20	35	20	20
Dipole 1 entrance angle/ degrees	0	0	0	0
Dipole 1 exit angle/ degrees	20	35	20	20
Dipole 2 positions/ m	4.55	6.63	4.55	4.55
Dipole 2 bending angle/ degrees	20	-35	-20	20
Dipole 2 entrance angle/ degrees	20	35	10	20
Dipole 2 exit angle/ degrees	0	0	10	0
Dipole 3 positions/ m			5.9	6.24
Dipole 3 bending angle/ degrees			20	-20
Dipole 3 entrance angle/ degrees			20	0
Dipole 3 exit angle/ degrees			0	20
Dipole 4 positions/ m				7.59
Dipole 4 bending angle/ degrees				-20
Dipole 4 entrance angle/ degrees				20
Dipole 4 exit angle/ degrees				0
		Pre-dispersive region matching quadrupoles		
Quadrupole length/ m	0.15	0.15	0.15	0.15
Quadropole 1 position/ m	0.575	0.575	0.575	0.575
Quadrupole 1 gradient/ Tm^{-1}	-0.3668	0.1724	-0.08234	0.4164
Quadropole 2 position/ m	1.225	1.225	1.225	1.225
Quadrupole 2 gradient/ Tm^{-1}	0.3287	-0.2761	0.2293	-0.3324
Quadropole 3 position/ m	1.875	1.875	1.875	1.875
Quadrupole 3 gradient/ Tm^{-1}	-0.3684	0.2471	-0.2612	0.3527
Quadropole 4 position/ m	2.525	2.525	2.525	2.525
Quadrupole 4 gradient/ Tm^{-1}	0.1368	-0.1763	0.1418	-0.2342

Table 7.2: The parameters of the chosen merger solution. The element positions indicate the location of the center of the element.

Parameter	**U-bend**	**S-bend**	**Three dipole**	**Four dipole S-bend**
Dispersive region quadrupoles				
Quadrupole length/ m	0.15	0.15	0.15	0.15
Quadropole 1 position/ m	3.875	4.095	3.875	3.875
Quadrupole 1 gradient/ Tm^{-1}	-0.4482	-0.3830	-0.1064	-0.5018
Quadropole 2 position/ m		4.965	5.225	4.985
Quadrupole 2 gradient/ Tm^{-1}		0.2430	-0.1064	0.3023
Quadropole 3 position/ m		5.835		5.395
Quadrupole 3 gradient/ Tm^{-1}		-0.3830		-0.5019
Quadropole 4 position/ m				5.805
Quadrupole 4 gradient/ Tm^{-1}				0.3023
Quadropole 5 position/ m				6.915
Quadrupole 5 gradient/ Tm^{-1}				-0.5018
Post-dispersive region matching quadrupoles				
Quadrupole length/ m	0.15	0.15	0.15	0.15
Quadropole 1 position/ m	5.045	7.185	6.395	8.085
Quadrupole 1 gradient/ Tm^{-1}	0.2971	-0.4977	0.2150	0.3089
Quadropole 2 position/ m	5.505	4.645	6.855	8.545
Quadrupole 2 gradient/ Tm^{-1}	-0.3364	0.3095	-0.2545	-0.3475
Main linac				
Main linac cavity phase/ degrees	0	0	0	0
Main linac cavity amplitude/ MVm^{-1}	42.75	42.75	42.75	42.75
Main linac cavity 1 position/ m	8.018	10.158	9.368	11.058
Main linac cavity 2 position/ m	9.721	11.561	10.771	12.461
Main linac cavity 3 position/ m	10.823	12.963	12.173	13.863
Main linac cavity 4 position/ m	12.226	14.366	13.576	15.266
Main linac cryomodule end/ m	14.296	15.136	15.646	17.336

there is also emittance compensation down to 3.2 mm mrad in the y plane. The other significant difference is that the three dipole scheme has an order of magnitude larger R56 than the U-bend scheme. Whether or not this is an advantage depends on whether or not the design involves using the merger as a bunch compressor. In the case of PERLE there is no need to use the merger as a bunch compressor so a smaller R56 is preferable. Another important feature of the R56s of the two schemes is that the signs are different. The three dipole scheme has a chicane like R56 which means that bunch where the tail has higher energy than the head will be compressed while the U-bend has an arc like R56 which means that a bunch where the head has higher energy will be compressed. This is of particular significance at low energy as the space charge will cause the head of the bunch to gain energy and the tail to loose it. So the space charge forces will bias towards compression in arc like mergers and decompression in chicane like mergers. Although sufficient chirp imposed by the booster can overcome this. In the case of a compressive merger design however this might mean that arc like mergers are preferable.

Comparison of chosen merger schemes

The four different schemes will now be examined in more detail to further explore the emittance evolution and the sources of the emittance growth, the matching and the longitudinal dynamics. This is done so that the pros and cons of the two schemes which produced a viable solution can be examined and one of them selected as the preferred solution for PERLE. As well as so the reasons for why the other two schemes don't produce viable solutions can be found.

The first aspect of the bunch behaviour in the merger that will be compared between the four different schemes is the evolution of the transverse beam sizes. This can be seen in figure 7.5. The most obvious difference in behaviour compared to earlier in the injector is that the evolution of the beam size is no longer axially symmetric. This is a consequence of the change to quadrupole based focusing. The motivation for switching to quadrupoles rather than solenoid is that the merger is at a higher energy than earlier in the injector so solenoid focusing would now be less effective. Dipoles, which are unavoidable components in mergers as they required to bend the beam, also introduce asymmetry into the beam. This asymmetry appears in the form of the introduction of dispersion which is unavoidable and asymmetric focusing from the dipole which can

Table 7.3: The optimised parameters of the four merger schemes considered. The R56 value is of the Optim solution used as the initial guide for the optimisation not of the chosen solution.

Parameter	**U-bend**	**S-bend**	**Three dipole**	**four dipole S-bend**	Specifiation
ϵ_x/ mm·mrad	4.4	5.2	5.9	4.7	< 6
ϵ_y/ mm·mrad	3.9	4.5	3.2	7.0	< 6
Mismatch factor	0.034	0.72	0.05	0.11	0
Beta x/ m	9.53	13.51	9.13	10.5	8.6
Alpha x	-0.69	-3.4	-0.70	-0.71	-0.66
Beta y/ m	8.4	9.56	7.95	7.55	8.6
Alpha y	-0.65	-0.75	-0.71	-0.72	-0.66
Optim R56/ m	0.023	0.0185	-0.155	0.031	0

be avoided using special dipole designs with equal focusing in the both planes. Equal focusing dipoles are not necessary for this merger design and as a result in the interest of simplicity are not used in these mergers. This asymmetry in the beam size and focusing between the horizontal and vertical planes will have consequences for how the emittance changes due to the space charge forces. In the U-bend, three dipole and four dipole S-bend schemes there is a significant increase in the vertical beam size to a larger peak than found in the S-bend scheme. This is due to the horizontally focusing quadrupoles required to cancel the dispersion producing a strong vertical defocus. This is least significant in the three dipole scheme as the central dipole provides some vertical focusing abet weaker than the quadrupole's defocusing. Some information about the matching can be seen in these plots. The S-bend has a poor quality match. The largest deviation from the target value in the S-bend Twiss parameters was the horizontal alpha function as can be seen from the rate of change of horizontal beam size at the end of the beamline in figure 7.5. This can also clearly be seen in the figure where the horizontal beam size is strongly focused through the main linac leading to a significantly more diverging beam in the horizontal plane than desired by the specification. However the U-bend and three dipole schemes both have sufficiently good matches. The U-bend has a roughly symmetric transverse beam size between the two transverse planes as the emittance in both planes is similar. The three dipole has a noticeably larger horizontal beam size. This is because the horizontal emittance is larger than the vertical emittance and what has been matched to equal values is the β function not the beam sizes. So to get equal beta functions with asymmetric emittances asymmetric beam sizes are needed.

The evolution of the bunch length can be seen in figure 7.6. It should be noted that in all four schemes the initial bunch has a small initial chirp out of the booster as can be seen in the longitudinal phase space shown in figure 5.7. The bunch however develops a chirp along the merger as the longitudinal space charge forces accelerate the head of the bunch and decelerate the tail. From initially comparing the bunch length evolutions the fact that the three dipole merger has a significantly larger R56 than the other three schemes is clearly visible. This can be seen as bunch length changes by a much greater amount in the three dipole scheme than in all the others. The fact that the R56 has the opposite sign in the three dipole scheme than in the other three schemes is also apparent as all three of the other schemes exhibit some small amount of compression as opposed to the decompression seen in the three dipole merger.

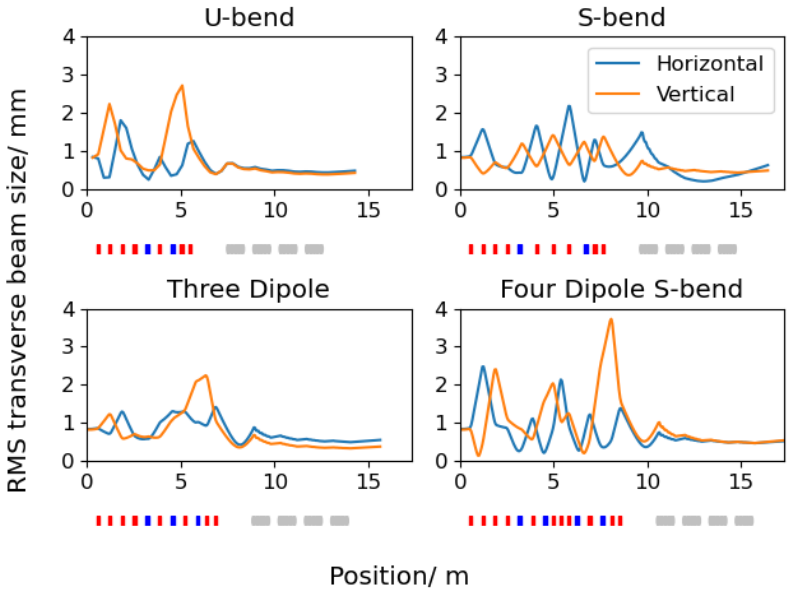

Figure 7.5: The transverse beam size of the bunch in the merger and first main linac pass. The locations of the beamline elements are marked below the plots. The dipoles are represented by blue rectangles, the quadrupoles by red rectangles and the SRF cavities by groups of grey ellipses.

In addition to the magnetic compression mentioned above there is also space charge induced debunching as the energy is still low enough that particles of different energies have meaningfully different speeds. This debunching can be seen in all four schemes and is the mechanism driving the debunching in all four schemes prior to the dispersive region. In the three schemes with the appropriate R56 for compression in the dispersive region this velocity based debunching is actually a more significant effect that the magnetic compression. So they all exhibit some net debunching. The four dipole S-bend exhibits the largest decompression of all the schemes that are not magnetically decompressing. This is simply because it is the longest so the space charge forces have more time to act and build up a larger chirp and the particles have more time for their velocity differences to have an effect on their final positions.

The evolution of the projected and slice emittances can be seen in figure 7.7. In this figure it can be clearly seen that the emittance evolutions differ between the two planes for all merger schemes. This is due to the asymmetric focusing applied on the beam and the consequent asymmetric space charge

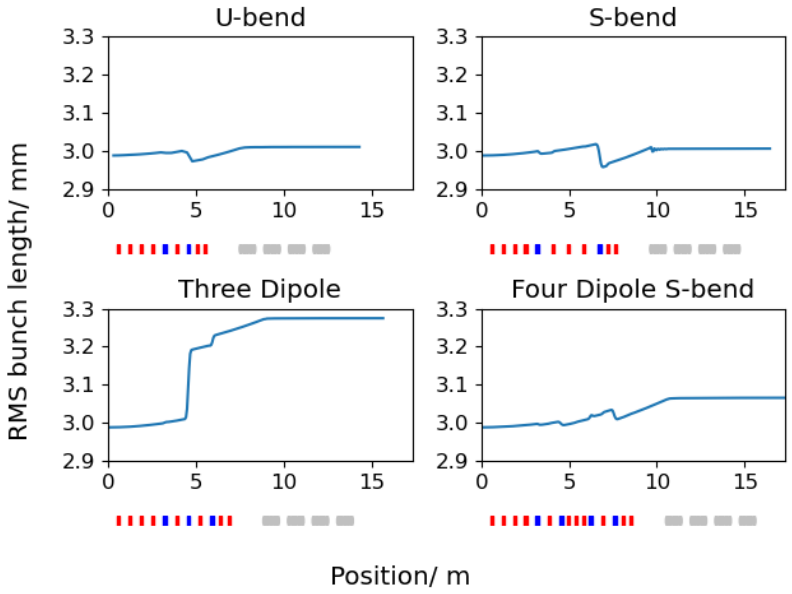

Figure 7.6: The bunch length in the merger and first main linac pass. The locations of the beamline elements are marked below the plot. The dipoles are represented by blue rectangles, the quadrupoles by red rectangles and the SRF cavities by groups of grey ellipses.

forces. Of the four solutions three of them have final emittance values that are within the specification. There is emittance growth through the merger in all four schemes and looking at how the slice emittance growth changes through the merger can help with determining some of the sources of this emittance growth.

For the U-bend scheme it can be seen that the emittances at the end of the beamline are roughly symmetric. However inspecting the evolution of the slice emittance in both planes shows that the mechanism of the emittance growth is different in both planes. In the case of the x plane the average slice emittance growth is very small. Although there is growth in the maximum slice emittance along the whole merger. The final maximum slice emittance is smaller than the final projected emittance value which indicates that either there are rotational slice misalignments in phase space due to imperfect compensation or residual dispersion. As this is the bending plane it is likely that residual dispersion contributes to the emittance growth. In the y plane there is significant average and maximum slice emittance growth. The final projected emittance is the same

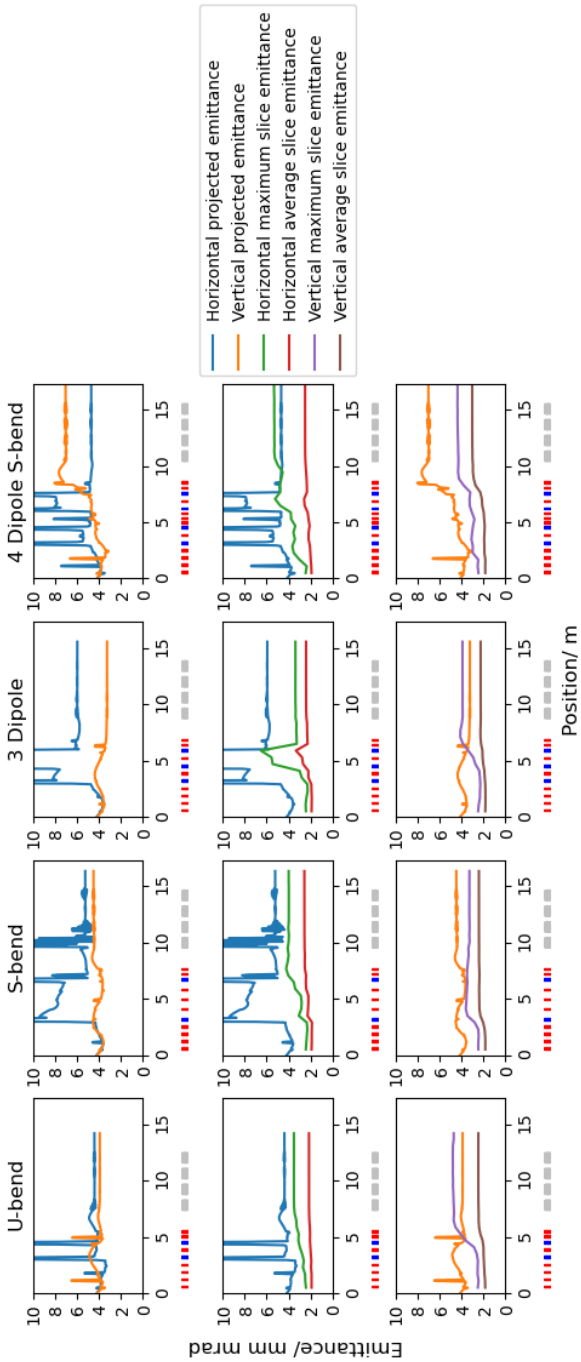

Figure 7.7: The evolution of the projected and slice emittances in the merger. In the row both the projected emittances are plotted together on one plot. In the middle row the horizontal projected emittance, average slice emittance and maximum slice emittance can be seen. On the bottom row the vertical projected emittance, average slice emittance and maximum slice emittance are plotted. The locations of the beamline elements are marked below the plots. The dipoles are represented by blue rectangles, the quadrupoles by red rectangles and the SRF cavities by groups of grey ellipses.

as the final maximum slice emittance suggesting that slice emittance growth is the dominant emittance growth mechanism. The emittance growth mostly occurs between the dispersion cancelling quadrupole and the final quadrupole of the matching section in the main ERL loop which is where the beam size grows to its largest extent and is then focused down.

For the S-bend it can be seen that there is emittance growth in both planes but the largest emittance growth is in the horizontal bending plane. In both planes the projected emittance decreases then increases again in the matching section prior to the dispersive region without any slice emittance growth. Indicating that this emittance change is due to emittance compensation and then decompensation. Once the beam reaches the first dipole the emittance behaviour becomes different in each plane. In the horizontal bending plane the emittance increases after the first dipole and then sharply decreases after the second dipole. There is some slice emittance growth after the first dipole in the dispersive region. The final projected emittance value is larger than the slice emittance values indicating that the slice emittance isn't the limiting factor on the projected emittance. Some amount of the emittance growth is likely due to the residual dispersion although there may also be some imperfect emittance compensation. In the vertical plane slice emittance growth can be seen around the first dipole. The projected emittance compensates down to the value of the maximum slice emittance suggesting good emittance compensation at that point. It then however grows again without slice emittance growth suggesting that there is poor emittance compensation at the exit of the main linac in vertical plane.

In the case of the three dipole solution the emittance in the x plane has a significant increase and is much larger than the y emittance at the main linac exit. Looking at figure 7.7 the contribution of the slice emittance to the projected emittance can be seen. In the x plane it can be seen that there is a significant increase in the slice emittance in the dispersive region which followed by a significant decrease. Although there is still net maximum slice emittance growth. The final projected emittance is larger than the slice emittances suggesting a slice misalignment related emittance growth mechanism. Which could be residual dispersion or poor emittance compensation or a combination of the two. In the y plane there is slight average slice emittance growth and more substantial maximum slice emittance growth starting in the center of the dispersive region. The projected emittance noticeable compensates down to a value smaller than the maximum slice emittance which indicates good slice

alignment and emittance compensation. So the slice emittance is the limiting factor on the emittance in the y plane.

The final merger scheme is the four dipole S-bend. This scheme is intended to minimise the emittance growth due to the residual dispersion. From looking at the projected emittance it can be seen that in the horizontal plane there is some emittance growth but after the two U-bend dispersive sections there is not significant emittance growth due to the residual dispersion. In the vertical plane there is however significant emittance growth starting at the final dipole of the dispersive region. Looking at the evolution of the slice emittance in the horizontal plane. It can be seen that the growth in the average slice emittance is small but there is significant growth in the maximum slice emittance to a value larger than the final projected emittance. Which implies that the slice emittance growth is the limiting factor on the final emittance. So the residual dispersion related emittance growth is mostly eliminated. The looking at the vertical plane it can be seen that there is some slice emittance growth most noticeably just before the main linac. However at the end there the projected emittance is much larger than the slice emittance so slice misalignments and poor emittance compensation are the source of majority the emittance growth.

Inspecting the transverse phase space distributions can give some insight about the slice alignment and level of distortion. The transverse phase space distributions can be seen in figure 7.8. Emittance growth due to slice emittance growth, rotational misalignments due to poor emittance compensation and misalignments in the central location of the slices due to residual dispersion all have different appearances in the phase space.

Looking first at the U-bend scheme in the both planes some distortion to the phase spaces can be seen indicating slice emittance growth. In the horizontal plane an offset the slices can be seen however the rotational slice alignment appears to be good. This suggests that most of the difference between the projected and slice emittance is due to the residual dispersion. In the vertical plane there is, as expected, no offset in the slice centers as there should be no dispersion in the non-bending plane. The rotational slice alignment also appears to be as good as expected from figure 7.7 which suggested that the limiting factor on the projected emittance was the slice emittance.

Next looking at the S-bend solution. In the horizontal plane the rotational slice alignment is good indicating good emittance compensation. The offset in the slices due to the residual dispersion is clearly seem indicating that as for the U-bend the residual dispersion is the dominant emittance growth mechanism

in the bending plane. In the vertical plane distortion to the slices can be seen indicating slice emittance growth which is the dominant emittance growth mechanism in the vertical plane as the slice aligment is good.

For the three dipole solution the horizontal phase space shows both that there is slice emittance growth as there is distortion of the slice phase spaces as well as transverse offsets to the slice which will be due to the residual dispersion. This scheme seems to exhibit the largest projected emittance growth due to the residual dispersion which can be seen in way the slices have offset from each other in a way which maximises the area of the phase space occupied by the slices for a given offset. The vertical phase space shows transverse phase space distribution distortion so there is slice emittance growth. The slice alignment is however good. Which shows that the limiting factor on the projected emittance in the vertical plane is the slice emittance. Which matches with what is shown in figure 7.7.

The final phase spaces to be examined are those of the four dipole S-bend. In the horizontal phase space there is not a significant offset in the slice centers compared to the other three schemes showing that the residual dispersion is not a major source of emittance growth in this scheme. Indicating this scheme is capable of mitigating that emittance growth mechanism as it is intended to. The rotational slice alignment is good but there is some distortion to the phase space so the slice emittance is limiting factor on the horizontal projected emittance for this scheme. In the vertical plane some slice emittance growth is apparent in the form of phase space distortions but the main factor in the emittance growth is the clearly apparent rotational slice misalignment due to poor emittance compensation.

Analysis of the transverse phase spaces shows clear distortion and hence slice emittance grow for many of the schemes. In the specific case of the vertical plane of the U-bend and three dipole mergers the evolution of the projected emittance and slice emittance suggests that the slice emittance is the limiting factor on the projected emittance. Looking at the slice emittance values for the bunch can provide additional insight as to where in the bunch that growth occurs. The slice emittances for both planes at the exit of the main linac for all solutions can be seen in figure 7.9. Generally looking at all the schemes the slice emittances for both planes show the same rough pattern as the slice emittances at the exit of the booster with the highest slice emittance towards the head of the bunch. In many of the cases there has however been slice emittance growth at the front of the bunch. Sometimes even with noticeably

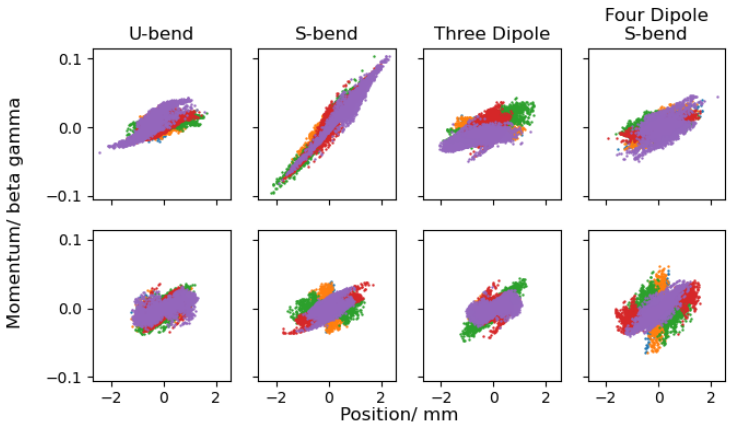

Figure 7.8: The transverse phase space distributions at the main linac exit. The horizontal (bending plane) phase space is on the top row and the vertical phase space is on the bottom row.

spikes of increased slice emittance in front of the core of the bunch as in for example the vertical plane of the U-bend scheme or in the horizontal plane of the four dipole S-bend. The four dipole S-bend is the scheme which has the most different slice emittance distributions with the tail and center of the bunch both exhibiting slice emittance growth in the horizontal plane. In the vertical plane the slice emittance growth is more centrally focused within the bunch then is usual compared to the other schemes.

Apart from the slice emittance growth and rotational slice misalignments due to space charge there is another major source of projected emittance growth in the merger due to space charge. This is the space charge induced residual dispersion in the dispersive region of the merger. This leads to relative transverse offsets of the slices in phase space and then consequently projected emittance growth. This mechanism will only affect the emittance in the x plane. However from looking at the phase spaces in figure 7.8 the offsets between the centers of the slices can be seen. The offsets in physical space should also be apparent in the physical shape of the bunch in space. Looking at the distribution in the bunch should also show where in the bunch these offsets occur which may be significant. The distribution of the bunch seen from the side and from above can be seen in figure 7.10. For the all the schemes the bunch can be seen in both planes to have a core where the majority of the charge in the bunch is distributed and then a head and tail which are more diffuse and have different

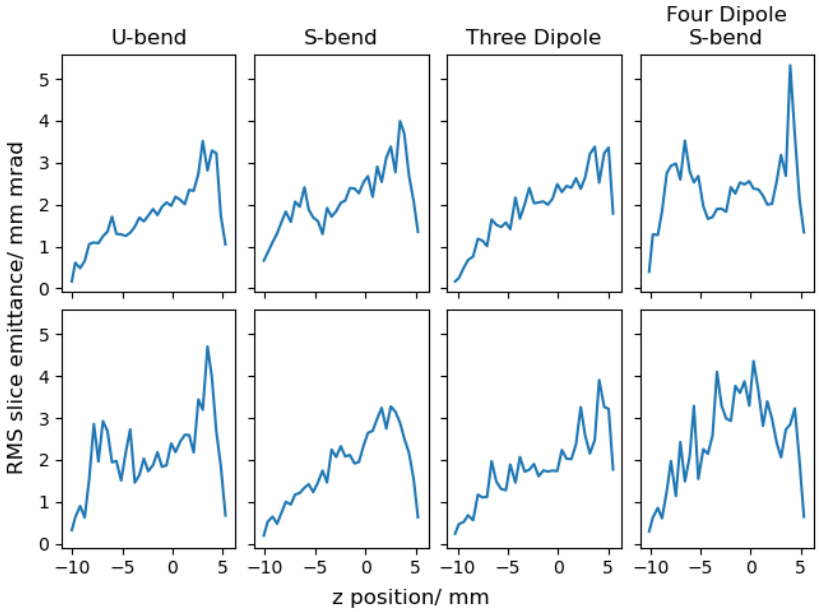

Figure 7.9: The slice emittances at the main linac exit. The horizontal slice emittances are on the top row and the vertical slice emittances are' on the bottom row.

size. This is a characteristic of the bunch which has been preserved from the injector. A more even distribution of charge along the bunch at the end of the injection line could be obtained using one of the variant injectors designs with the addition of the normal conducting higher harmonic cavity. Looking at the top down z-x plane which shows the bunch distribution in space in the bending plane it can be seen that the bunches are asymmetric around the reference orbit. This is because of the residual dispersion at the end of the merger. It can be seen in the first three schemes the U-bend, S-bend and three dipole merger that the front of the bunch is angled. This suggests that the front of the bunch is where the residual dispersion is located. This makes sense as the front of the bunch is where the majority of the charge is concentrated. Hence it is where the space charge forces are strongest and where the particles will change energy in the merger the most leading to the dispersion error. The fourth and final merger scheme, the four dipole S-bend, does show asymmetry around the reference orbit. However it doesn't show as significant a tilt at the front of the bunch indicating that this scheme is successful in mitigating the dispersion error due to the space charge. Even if it isn't capable of completely

eliminating it. In contrast to the z-x plane looking at the bunch side on in the z-y plane it can be seen that there is no transverse offset along length of the bunch. This is as expected as there is no dispersion in the non-bending vertical direction.

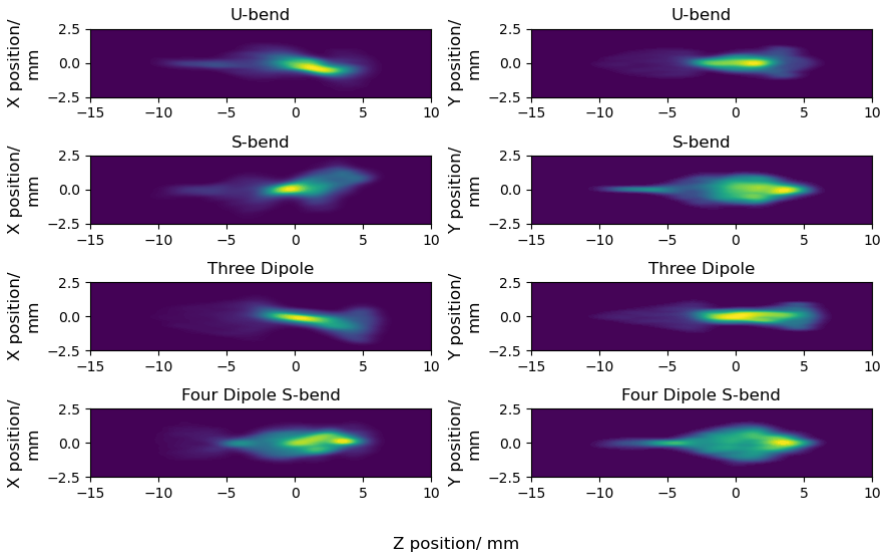

Figure 7.10: The particle density of the bunch in space at the exit of the main linac. The z-x distribution is in the left hand column and the z-y in the right hand column.

The bunch density distributions show the fact that there is an angle to the bunch with parts of it offset to the axis in the x plane to be clearly seen. In the presence of residual dispersion it would also be expected that there would be a similar offset in Z-P_x space. To visualise the offset more clearly the average slice value in both space and momentum for both the transverse planes was calculated and plotted against position in the bunch for all the schemes. This can be seen in figure 7.12. From the bottom half of this figure it can be seen that the there are no significant offsets in Z-Y and Z-P_y. Which is what would be expected as there is no dispersion in the y plane. In the x plane offsets can be seen although the offsets vary depending on the scheme. The U-bend, S-bend and three dipole scheme all show offsets which are concentrated at the front of the bunch where the space charge forces are strongest. Which is where the residual dispersion effects due to space charge would occur. In terms of these three schemes noticeably the U-bend scheme doesn't have a significant

offset in z-px. The four dipole S-bend, the fourth and final scheme, has much smaller offsets in z-x and z-px indicating as in earlier results that it has been successful in mitigating the space charge induced residual dispersion.

In addition to the transverse emittance preservation and transverse matching another important consideration is the matching of the longitudinal phase space to what is required in the main ERL loop. For this it is important to know what effect the merger has on the longitudinal phase space. The longitudinal phase space at the entrance to the main linac can be seen in figure 7.11. The phase space distributions at the main linac entrance were plotted because after the main linac the majority of the non-linearities in the bunch come from the RF distortion caused by the main linac. Which means that the extent to which the merger preserves the non-linearities out of the booster and introduces its own cannot be seen. The bunch entering the merger had the characteristic "M" shape of the baseline injector design. In figure 7.11 it can be seen that for all mergers the "M" shape is roughly preserved but the front of the bunch has gained energy. This can be thought of as a linear chirp developing in the core of the bunch due to the space charge forces while the tail of the bunch continues through the merger without this significant change due to space charge. As it is much more diffuse and has less charge present. This behaviour in the longitudinal phase space aligns with what is seen in figure 7.10 and figure 7.12 where the offsets in the bunch that are due to the energy change within the bunch and the consequent residual dispersion are most apparent in the core of the bunch where the majority of the charge is localised. Despite the similarities between the longitudinal phase spaces there are a number of differences between the schemes. Firstly the S-bend and four dipole S-bend exhibit larger chirps in the core of the bunch. This is because they are longer than the other two schemes so there is more time for the space charge induced chirp to build up. Secondly the three dipole scheme shows debunching in the core. This is due to magnetic debunching and is expected as the three dipole scheme has an order of magnitude larger R56 than the other schemes. The debunching is mostly localised to the core where the space charge induced chirp is mostly located.

Conclusion and merger scheme selection

From looking at the performance of the four merger schemes it can be seen that two of them meet the required specification for PERLE. The two viable

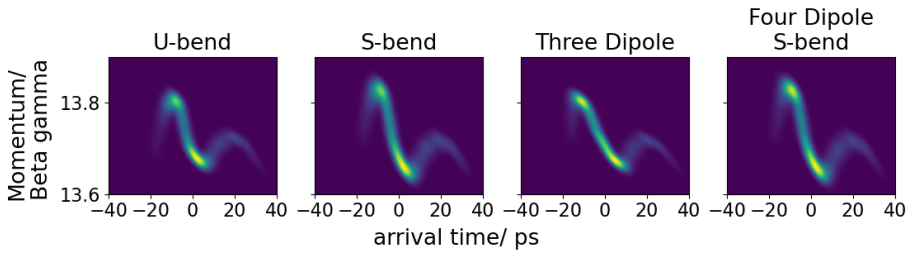

Figure 7.11: The longitudinal phase spaces of the bunch at the entrance flange of the main linac.

schemes are the U-bend and the three dipole scheme. When deciding which scheme is preferred for PERLE both the final transverse emittances and the R56 values of the mergers need to be considered. Looking first at the transverse emittances the U-bend has emittance growth in both planes to 4.4 mm mrad in horizontal plane and 3.9 mm mrad in the vertical plane. In contrast the three dipole scheme has an emittance reduction due to emittance compensation in the vertical plane down to 3.2 mm mrad but significant emittance growth in the horizontal plane to 5.9 mm mrad. The emittance growth in the horizontal plane for the three dipole scheme is to a value close to the upper bound of the emittance specification of < 6 mm mrad. While the largest transverse emittance for the U-bend 4.4 mm mrad comfortably within the specification. The other factor that needs to be considered when deciding which scheme is preferred is the R56 of the merger and its longitudinal dynamics. In the case of PERLE it is not considered desirable to be able to use the merger as a bunch compressor although in other ERL designs that may be desirable. As compression is not desired lower R56 merger are preferred. The U-bend has a smaller R56 of 0.023 m compared to the three dipole scheme's R56 of -0.155 m. Taking account of both the transverse emittance values and the R56s of the mergers the U-bend is the preferred scheme for both factors and as a result it will be recommended as the preferred scheme.

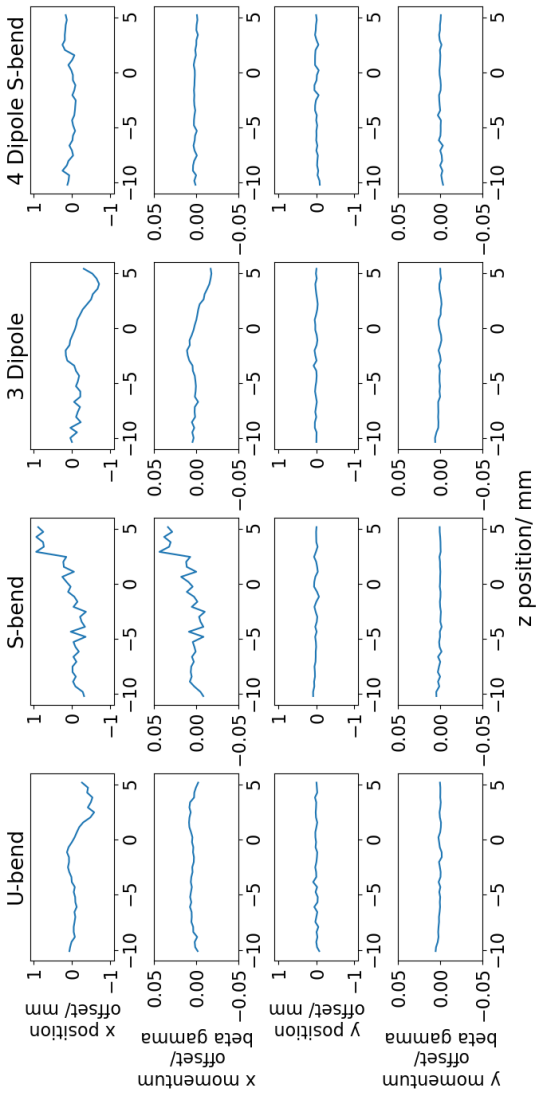

Figure 7.12: The z-x, z-px, z-y and z-py slice offsets for all four merger schemes.

Chapter 8

Conclusion

8.1 Summary

In this thesis a conceptual design for the PERLE injector has been considered which meets the required specification for PERLE. First a hybrid voltage electron photocathode gun was optimised which is capable of functioning at 220 kV and 350 kV to allow for the potential of upgrading the injector so that can deliver both unpolarised and polarised beams. Then four different designs from the electron gun cathode to the booster exit were compared. The designs examined were: a design without any higher harmonic cavities and hence no longitudinal phase space linearisation, a design with a normal conducting higher harmonic cavity before the booster, a design with an SRF higher harmonic cavity in the booster and a design with both higher harmonic cavities. It was shown that all four designs were capable of achieving transverse emittances within the specification. The normal conducting cavity could linearise the ballistic bunching due to the buncher. It removed the central dip caused in the longitudinal phase space and reduced the size of the bunch tail formed. The SRF higher harmonic cavity could linearise the longitudinal phase space by removing the 2nd order RF non-linearity introduced by the accelerating cavities of the booster. However the solutions with the SRF higher harmonic cavity did also have a crossover in the bunch due to the strong RF focusing in the booster cavity after the higher harmonic cavity. Despite the fact that the higher harmonic cavities were capable of linearising the longitudinal phase space and reducing the longitudinal tail it was decided that the design without higher harmonic cavities should be selected as the baseline. This decision was

motivated by the fact higher harmonic cavities would add significant cost to the injector and it is not currently clear that the non-linearities at the exit of the baseline injector need to be removed. As there is potential for linearisation in arcs or the non-linearities may simply be acceptable for PERLE's applications. At present it is also not clear that the tail that is formed during the ballistic bunching process will cause problems for the operation of PERLE. Finally four different merger schemes were compared. These schemes were a U-bend, a Dogleg, a three dipole scheme and a four dipole dogleg. Of these two schemes the U-bend and the three dipole scheme both met the specification. The U-bend was selected as the baseline over the three dipole scheme due to its smaller maximum emittance and lower R56. A lower R56 was considered desirable as the PERLE merger is not going to be used as a bunch compressor and instead the ability to adjust the injection chirp with as small an effect on the bunch length as possible is considered a beneficial feature.

8.2 Start to end performance of the conceptual design of the injector

The final design consisting of the hybrid electron gun, an injector without higher harmonic cavities and a U-bend merger was run start to end from the cathode to the exit of the main linac. This simulation was done at higher particle count and with smaller timesteps to increase the accuracy of the results. The particle count used was 90000 with space charge grid settings of 30x30x50 and a time step size of 1 ps. The results of this higher accuracy start to end simulation can be seen in table 8.1.

Table 8.1: The optimised parameters of the chosen injector scheme.

Parameter	**Achieved values**	**Specification**
x emittance/ mm·mrad	4.3	< 6
y emittance/ mm·mrad	3.8	< 6
Bunch length/ mm	2.9	3
Beta x/ m	11.5	8.6
Alpha x	-0.86	-0.66
Beta y/ m	8.67	8.6
Alpha y	-0.35	-0.66

It can be seen from this table that the emittances remain within specification although some fine tuning of bunch length and Twiss parameters is

needed.

The calculated start to end RMS beam sizes can be seen in figure 8.1. From this plot it can be seen that the beam is never larger than the maximum permitted value of 6 mm. It is also largest in the low energy section of the machine before the booster as would be expected. It can also be seen that the Twiss parameters are not matched correctly from the evolution of the beam size in the main linac. This will need to be fine tuned.

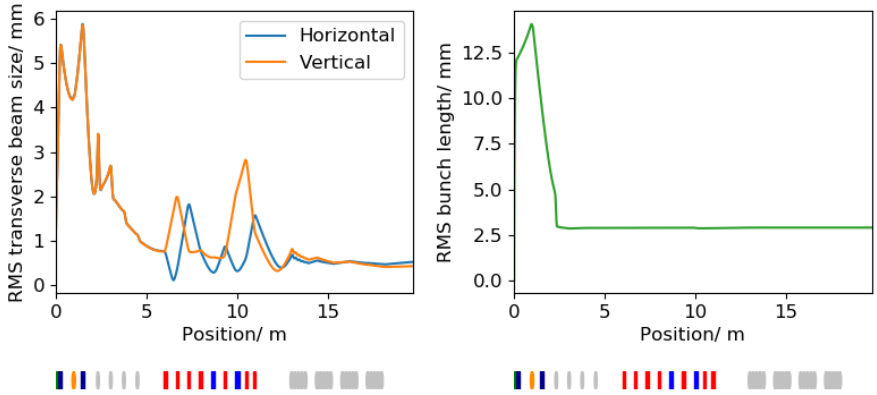

Figure 8.1: The evolution of the transverse beam size on the left and the bunch length on the right along the injector to the exit of the first main linac pass. The positions of the beamline elements are indicated below the plots. The electron gun is indicated by a green box, the solenoids by dark blue boxes, the buncher cavity by the orange ellipse, the accelerating cavities by the grey ellipses, quadrupoles by red rectangles and dipoles by blue rectangles.

The evolution of the emittances along the injector to the main linac exit can be seen in figure 8.2. There is clear emittance growth in both planes in the merger. Though the emittance growth is more significant in the horizontal plane. The longitudinal emittance grows a small amount up to the exit of the booster before showing a steady growth through the merger. There is then significant longitudinal emittance growth in the main linac due to the RF distortion from being on crest in the main linac.

The transverse phase spaces at the exit of the main linac can be seen in figure 8.3. The general shape of the phase spaces are the same as in the lower particle count simulations. In particular the asymmetry of the transverse phase space due to residual dispersion is still apparent. The higher particle count does

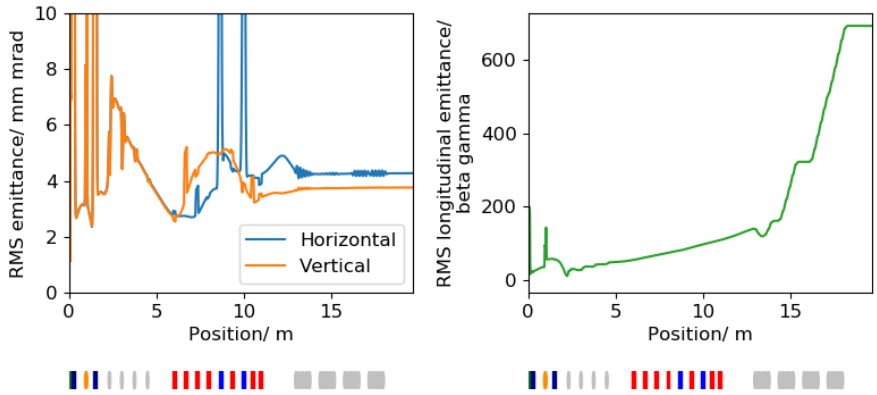

Figure 8.2: The evolution of the transverse emittances on the left and the longitudinal emittance on the right along the injector to the exit of the first main linac pass. The positions of the beamline elements are indicated below the plots. The electron gun is indicated by a green box, the solenoids by dark blue boxes, the buncher cavity by the orange ellipse, the accelerating cavities by the grey ellipses, quadrupoles by red rectangles and dipoles by blue rectangles.

however mean that the more diffuse parts of the bunch have more particles in them and that low density tails which would not have previously be captured by the lower particle count simulations are now apparent in the simulations and the more diffuse parts of the bunch can be seen.

8.3 Future work

The conceptual design of the PERLE injector has been performed and it has been shown that the design specification can be achieved. However there are still a couple of areas where there are effects that have not yet been modelled. The phase slippage in the main linac is not current modelled correctly. Additionally CSR is also not currently modelled in the merger simulations. OPAL is however not currently an appropriate tool for doing this as its CSR model makes the ultrarelativistic assumption which is not valid at 7 MeV. The simulations should be improved to account for these effects or analytical calculations should be performed to show that the effects are negligible.

It should also be confirmed that the design decisions made in this thesis are the best options for PERLE. Both in case there have been changes in the design

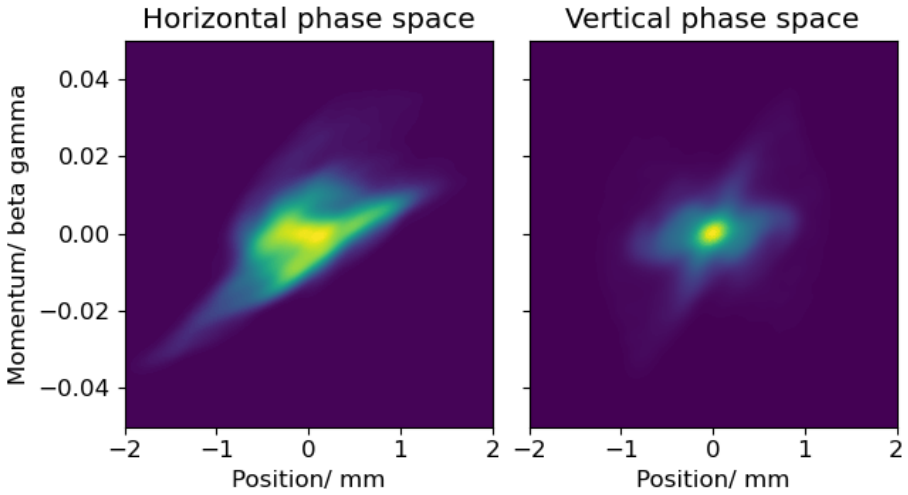

Figure 8.3: The horizontal phase space at the main linac exit on the left and the vertical phase space at the same location on the right.

requirements as well as by confirming the performance of the conceptual design based on start to end simulations of the whole machine from the cathode to the dump. This means firstly deciding if the hybrid gun is appropriate for PERLE. If pursing a polarised upgrade is no longer considered likely the gun should be redesigned for purely 350 kV operation as there is likely to be a performance improvement from using a specialised gun. Even if there is still an interest in developing a polarised upgrade it may still be more appropriate to initially use a 350 kV electron gun and then replace the cathode electrode with a hybrid electrode as part of the polarised upgrade. If the decision is made to switch to a purely 350 kV electron gun the beam dynamics optimisations of the injector will need to be redone for that new electron gun geometry. Once the decision about the gun has been made the decision to not use any higher harmonic cavities in the injector and to use a U-bend merger should be evaluated by doing a start to end simulation of the whole machine from the cathode to the dump. It should be confirmed that beam meets the requirements through the beam transport, at the interaction point and at the dump. There are a number of aspects of the beam behaviour in the main ERL loop that should be looked at in particular. These are the longitudinal match, the effects of the residual dispersion and the evolution of the diffuse tail of the electron bunch.

The longitudinal match between the injector and the main ERL loop is an

important aspect of the PERLE design which has not yet been completed. The baseline injector design exhibits an "M" shaped non-linearity at the entrance of the main linac. The effect of this non-linearity on the performance of the rest of the machine needs to be explored. It should then be decided whether the non-linearity is tolerable in which case nothing further needs to be done. However it isn't tolerable linearisation will be required. If this is the case it should be decided where that linearisation should be performed. It could be done in the arcs by control of the second and third order longitudinal dispersions. If that approach is not viable then one of the higher harmonic cavity containing injector options explored in chapter 6 could be used. The possibility of optical linearisation in the merger could also be explored although the presence of significant space charge forces and the desire to keep the merger short and simple may mean that option is not preferred.

The majority of the merger schemes investigated in this thesis exhibit residual dispersion at the exit of the merger. The effects of this on the beam quality at the IP and on the ability to decelerate the beam and transport it to the dump should be investigated. If the residual dispersion presents an issue for the operation of the machine there are a couple of options which could be explored. Firstly merger schemes which cancel this dispersion could be further explored. The scheme capable of cancelling the residual dispersion shown in chapter 7 wasn't capable of meeting the specification for PERLE however with further development in this direction it may be possible to obtain a merger design which meets the specification. Another possible approach which could be used with a merger scheme which still has residual dispersion would be to tune one of the ERL arcs away from achromaticity so that it takes the beam with residual dispersion at the start of the arc and produces a dispersion free beam at the end. This would be easier in a separate transport machine as having a non-achromatic arc would have implications for the decelerating beam in a common transport machine. As an arc which takes a beam with dispersion and produces a beam without dispersion will introduce dispersion if there was no dispersion to begin with. Which might make transporting a beam to the dump challenging. Although as beam quality is not a major consideration during the deceleration perhaps introducing dispersion at this point is not an issue. If this approach was considered as a serious option for the machine studies would need to be done to assess its feasibility and effectiveness.

The tail of the electron bunch is much more diffuse than the core and consequently has much lower charge density. This means that in the injector

where the bunch is space charge dominated the evolution of the tail can be quite different than the rest of the bunch. With appropriate emittance compensation and matching the tail should have similar Twiss parameters to rest of the bunch however both the emittance compensation and matching will inevitably be somewhat imperfect. This might mean that the evolution of the tail in the main ERL loop could be quite different than the evolution of the core of the bunch. As PERLE will have a high average beam power of 10 MW at its top energy even losing a small portion of the beam may cause problems with heating and activation of the accelerator components. It should be checked that the tail with its potentially different evolution through the main ERL loop does not cause significant beam losses and is fully transmitted. If there are issues with beam losses from the tail options involving the use of a NC higher harmonic cavity in the injector to reduce the size of tail formed, which are discussed in chapter 6 could be considered. Alternatively, or in combination with the use of a higher harmonic cavity, options involving collimation could be considered as well. Collimation in the merger might be of particular interest in this specific case as it is a dispersive section of the machine. So depending on the chirp different longitudinal sections of the bunch may end up at different transverse offsets allowing the tail to be collimated without affecting the core of the bunch. The merger is also at fairly low energy and it is preferable to collimate at as low an energy as possible to minimise heating and activation.

Once this process of evaluating the design decision made in this thesis has been completed and either the baseline presented in this thesis has been accepted or an alternative has been developed the design should then progress to the next stage. This next stage would involve doing tolerance studies for the injector to confirm that a real machine with errors in the placement and settings of the components is still capable of meeting the design specification. The designs of the magnetic and RF components of the beamline should also be progressed and the accurate fieldmaps used for beam dynamics simulations. This may require iteration between the beam dynamics and the magnetic and RF designs to get the best results. The locations and types of diagnostics in the merger should also be decided upon. It is important to ensure that there are sufficient diagnostics to measure all of the beam properties required to match the beam in terms of the Twiss parameters and in terms of the longitudinal match, to ensure that emittance compensation process is working and to cancel the dispersion out of the merger as much as is possible. The mechanical design of the whole beamline should also be performed. The combination of

the physical layout requirements of the beamline, the design of the magnetic and RF components and the placement of the diagnostics and vacuum systems may be require modifications to the layout of the injector. This work should be iterated with the beam dynamics until a solution is found which satisfies all of the potentially competing requirements.

Outside of design of PERLE there are a number of open questions and possible future routes for development in ERL injectors. Firstly technical developments in DC gun technology to reliable obtain higher operating voltages will lead to improvements in beam performance. Secondly further exploration of non-DC gun based injectors may lead to improvement in performance. As both VHF and SRF guns are promising lines of development. Thirdly from a beam dynamics perspective there is still improvement to made in merger design. The cancellation of the residual dispersion being an area of particular significance as many current merger schemes do not cancel the residual dispersion. In conclusion a conceptual design for the beam dynamics of the PERLE injector has been developed which meets the specification but there is still a lot of potential for interesting work to be done to push the performance of ERL injectors towards brighter beams.

Bibliography

[1] G. A. Krafft. "Energy recovered linacs". In: *Proc. LINAC2008*. Victoria, BA, Canada, 2008, pp. 688–692.

[2] E. Bloom et al. "High-Energy Inelastic e-p Scattering at 6° and 10°". In: *Physical Review Letters* 23 (1969), p. 930. DOI: 10.1103/PhysRevLett.23.930.

[3] C. W. Leemann et al. "The continuous electron beam accelerator facility: CEBAF at the Jefferson Laboratory". In: *Annual Review of Nuclear and Particle Science* 51.1 (2001), pp. 413–450. DOI: 10.1146/annurev.nucl.51.101701.132327.

[4] M. Tigner. "A possible apparatus for electron clashing-beam experiments". In: *Il Nuovo Cimento* 37 (1965), pp. 1228–1231. DOI: 10.1007/BF02773204.

[5] S. O. Schriber et al. "Experimental Measurements on a 25 Mev Reflexotron". In: *IEEE Transactions on Nuclear Science* 24.3 (1977), pp. 1061–1063. DOI: 10.1109/TNS.1977.4328851.

[6] J. L. Abelleira Fernandez et al. "A Large Hadron Electron Collider at CERN Report on the Physics and Design Concepts for Machine and Detector". In: *Journal of Physics G: Nuclear and Particle Physics* 39.7 (2012). DOI: 10.1088/0954-3899/39/7/075001.

[7] I. Ben-Zvi. "The ERL high energy cooler for RHIC". In: *Proc. EPAC06*. Edinburgh, Scotland, 2006, pp. 940–944.

[8] S. Benson et al. "High power operation of the JLab IR FEL driver accelerator". In: *Proc. PAC07*. Albuquerque, USA, 2007, pp. 79–81.

[9] G. Priebe et al. "Inverse Compton backscattering source driven by the multi-10 TW laser installed at Daresbury". In: *Laser and Particle Beams* 26.4 (2008), pp. 649–660. DOI: 10.1017/S0263034608000700.

[10] European Strategy Group. *2020 Update of the European Strategy for Particle Physics*. Geneva, 2020. DOI: 10.17181/ESU2020. URL: https://cds.cern.ch/record/2720129.

[11] M. Klein et al, Energy Recovery Linacs, in: European Strategy for Particle Physics - Accelerator RD Roadmap, N. Mounet (ed.), CERN Yellow Reports: Monographs, CERN-2022-001, DOI: 10.23731/CYRM-2022-001, p. 185.

[12] P. Agostini et al. "The Large Hadron–Electron Collider at the HL-LHC". In: *Journal of Physics G: Nuclear and Particle Physics* 48.11 (2021). DOI: 10.1088/1361-6471/abf3ba.

[13] M. Klein and R. Yoshida. "Collider Physics at HERA". In: *Prog. Part. Nucl. Phys.* 61 (2008), pp. 343–393. DOI: 10.1016/j.ppnp.2008.05.002.

[14] D. Angal-Kalinin et al. "PERLE: Powerful Energy Recovery Linac for Experiments - Conceptual Design Report". In: *Journal of Physics G: Nuclear and Particle Physics* 45.6 (2018). DOI: 10.1088/1361-6471/aaa171.

[15] W. Kaabi et al. "PERLE: A high power energy recovery facility". In: *Proc. IPAC2019*. Melbourne, Australia, 2019, pp. 1396–1399. DOI: 10.18429/JACoW-IPAC2019-TUPGW008.

[16] M. Klein and A. Stocchi. "PERLE: A High Power Energy Recovery Facility for Europe A contribution to the Update of the European Strategy on Particle Physics". In: (2018). URL: https://cds.cern.ch/record/2652336.

[17] S. A. Bogacz. *Baseline lattice for PERLE*. Talk presented at the PERLE collaboration meeting 3-5 June 2020.

[18] B. Militsyn. *Electron injector for PERLE on the basis of the ALICE photocathode gun*. Talk presented at the PERLE meeting 15-16 January 2018.

[19] F. Hannon and R. Rimmer. *Booster Design Adaptation*. Talk presented at the PERLE collaboration meeting 11-12 January 2022.

[20] S. A. Bogacz. *ERL Lattices for the LHeC/FCC-eh and PERLE*. Talk presented at the electrons for the LHeC: Workshop on the LHeC, FCC-eh and PERLE in Chavannes de Bogis. 2019.

[21] W. Kaabi. *PERLE: Status and Prospects*. Talk presented at the electrons for the LHeC: Workshop on the LHeC, FCC-eh and PERLE in Chavannes de Bogis. 2019.

[22] V. N. Litvinenko, R. Hajima, and D. Kayran. "Merger designs for ERLs". In: *Nuclear Instruments and Methods in Physics Research Section A: Accelerators, Spectrometers, Detectors and Associated Equipment* 557.1 (2006), pp. 165–175.

[23] T. Rao and D. H. Dowell. *An Engineering Guide To Photoinjectors*. ISBN: 978-1481943222. 2013.

[24] *ERL facility summary*. ERL19. URL: https://www.helmholtz-berlin.de/events/erl19/index_en.html.

[25] R. Hajima et al. "First demonstration of energy-recovery operation in the JAERI superconducting linac for a high-power free-electron laser". In: *Nuclear Instruments and Methods in Physics Research Section A: Accelerators, Spectrometers, Detectors and Associated Equipment* 507.1 (2003), pp. 115–119. DOI: 10.1016/S0168-9002(03)00849-0.

[26] O. A. Shevchenko at al. "The Novosibirsk free electron laser facility". In: *AIP Conference Proceedings* 2299.1 (2020), p. 020001. DOI: 10.1063/5.0031513.

[27] V. N. Volkov et al. "New RF gun for Novosibirsk ERL FEL". In: *Physics Procedia* 84 (2016), pp. 86–89.

[28] T. Rao et al. "Design, construction and performance of all niobium superconducting radio frequency electron gun". In: *Nuclear Instruments and Methods in Physics Research Section A: Accelerators, Spectrometers, Detectors and Associated Equipment* 562.1 (2006), pp. 22–33. ISSN: 0168-9002. DOI: https://doi.org/10.1016/j.nima.2006.02.172.

[29] J. Sekutowicz et al. "Nb-Pb superconducting RF-gun". In: *Proc. EPAC2006*. Edinburgh, Scotland, 2006, pp. 3493–3495.

[30] L. Cultrera et al. "Photocathode behavior during high current running in the Cornell energy recovery linac photoinjector". In: *Phys. Rev. ST Accel. Beams* 14 (12 Dec. 2011), p. 120101. DOI: 10.1103/PhysRevSTAB.14.120101.

[31] E. Wang et al. "Long lifetime of bialkali photocathodes operating in high gradient superconducting radio frequency gun". In: *Sci. Rep.* 11.1 (2021), p. 4477. DOI: 10.1038/s41598-021-83997-1.

[32] C. Hernandez-Garcia et al. “A high average current DC GaAs photocathode gun for ERLs and FELs”. In: *Proc. PAC2005*. Knoxville, USA, 2005, pp. 3117–3119.

[33] M. W. Poole and E. A. Seddon. “4GLS and the Prototype Energy Recovery Linac Project at Daresbury”. In: *Proc. EPAC 2004*. Lucerne, Switzerland, 2004, pp. 456–457.

[34] N. Nishimori et al. “Development of a 500-kV photocathode DC gun for the ERL light sources in Japan”. In: *Proc. FEL2009* (2009), pp. 277–280.

[35] T. Omori et al. “Large enhancement of polarization observed by extracted electrons from the AlGaAs-GaAs superlattice”. In: *Phys. Rev. Lett.* 67 (23 Dec. 1991), pp. 3294–3297. DOI: 10.1103/PhysRevLett.67.3294.

[36] S. Friederich, K. Aulenbacher, and C. Matejcek. “Vacuum lifetime and surface charge limit investigations concerning high intensity spin-polarized photoinjectors”. In: *Proc. IPAC2019*. Melbourne, Australia, 2019, pp. 1954–1957.

[37] S. Friederich and K. Aulenbacher. “The Small Thermalized Electron Source at Mainz (STEAM)”. In: *Proc. ERl2017*. Geneva, Switzerland, 2018, pp. 9–12. DOI: 10.18429/JACoW-ERL2017-MOPSPP005.

[38] N. Nishimori et al. “Generation of a 500-keV electron beam from a high voltage photoemission gun”. In: *Applied Physics Letters* 102.23 (2013), p. 234103.

[39] “A 500 kV photoemission electron gun for the CEBAF FEL”. In: *Nuclear Instruments and Methods in Physics Research Section A: Accelerators, Spectrometers, Detectors and Associated Equipment* 318.1 (1992), pp. 410–414. DOI: https://doi.org/10.1016/0168-9002(92)91090-V.

[40] D. J. Holder. “First results from the ERL prototype (ALICE) at Daresbury”. In: *Proc. LINAC08*. Victoria, Canada, 2008, pp. 694–698.

[41] R. Nagai et al. “High-voltage testing of a 500-kV dc photocathode electron gun”. In: *Review of Scientific Instruments* 81.3 (2010), p. 033304.

[42] C. K. Sinclair. “Very high voltage photoemission electron guns”. In: *Proc. PAC2003*. Vol. 1. Portland, USA, 2003, pp. 76–80.

[43] A. Neumann et al. "Towards a 100mA superconducting RF photoinjector for bERLinPro". In: *Proc. SRF2013*. Paris, France, 2013, pp. 42–49.

[44] T. Xin et al. "Performance of 112 MHz SRF Gun at BNL". In: *Proc. SRF2019)*. Dresden, Germany, 2019, pp. 1225–1229. DOI: 10.18429/JACoW-SRF2019-FRCAB5.

[45] F. Sannibale et al. "Advanced photoinjector experiment photogun commissioning results". In: *Phys. Rev. ST Accel. Beams* 15 (10 Oct. 2012), p. 103501. DOI: 10.1103/PhysRevSTAB.15.103501. URL: https://link.aps.org/doi/10.1103/PhysRevSTAB.15.103501.

[46] F. Sannibale et al. "Upgrade possibilities for continuous wave rf electron guns based on room-temperature very high frequency technology". In: *Phys. Rev. Accel. Beams* 20 (11 Nov. 2017), p. 113402. DOI: 10.1103/PhysRevAccelBeams.20.113402.

[47] B. Kuske et al. "The injector layout of BERLinPro". In: *Proc. IPAC 2013*. Shanghai, China, 2013, pp. 288–290.

[48] F. Hannon. "A high average-current electron source for the Jefferson Laboratory free electron laser". PhD thesis. 2008.

[49] C. F. Papadopoulos et al. "RF injector beam dynamics optimization for LCLS-II". In: *Proc. IPAC14*. Dresden, Germany, 2014, pp. 1974–1976. DOI: 10.18429/JACoW-IPAC2014-WEPRO015.

[50] C. Gerth and F. Hannon. "Injector design for the 4GLS energy recovery linac prototype". In: *Proc. EPAC2004*. Lucerne, Switzerland, 2004, pp. 437–439.

[51] I. V. Bazarov and C. K. Sinclair. "High brightness, high current injector design for the Cornell ERL prototype". In: *Proc. PAC2003*. Portland, USA, 2003, pp. 2062–2064.

[52] T. Miyajima et al. "Beam Simulations of High Brightness Photocathode DC Gun and Injector for High Repetition FEL Light Source". In: *Proc. FEL2014* (2014), pp. 980–984.

[53] H. Liu et al. "Modeling of space charge dominated performance of the CEBAF FEL injector". In: *Nuclear Instruments and Methods in Physics Research Section A: Accelerators, Spectrometers, Detectors and Associated Equipment* 358.1-3 (1995), pp. 475–478.

[54] S. H. Shaker et al. “Beam Dynamics Optimization of a Normal-Conducting Gun Based CW Injector for the European XFEL”. In: *Proc. FEL2019*. Hamburg, Germany, 2019, pp. 452–455. DOI: 10.18429/JACoW-FEL2019-WEP054.

[55] C. Matejcek, K. Aulenbacher, and S. Friederich. “Low Energy Beam Transport System for MESA”. In: *Proc. IPAC2019*. Melbourne, Australia, 2019, pp. 1461–1464. DOI: 10.18429/JACoW-IPAC2019-TUPGW028.

[56] J. Rathke et al. “Design and fabrication of an FEL injector cryomodule”. In: *Proc. PAC05* (2005), pp. 2292–2294.

[57] A. M. M. Todd et al. “State-of-the-art electron guns and injector designs for energy recovery linacs (ERLs)”. In: *Proc. PAC05* (2005), pp. 3724–3726.

[58] R. Heine and K. Aulenbacher. “Injector linac for the MESA facility”. In: *Proc. IPAC2013*. Shanghai, China, 2013, pp. 2150–2152.

[59] C. Hernandez-Garcia et al. “Performance and modeling of the JLab IR FEL Upgrade Injector”. In: *Proc. FEL2004*. Trieste, Italy, 2004, pp. 558–561.

[60] G. Hoffstaetter, D. Trbojevic, and C. Mayes. “CBETA Design Report”. In: (June 2017). DOI: 10.2172/1412724. URL: https://www.osti.gov/biblio/1412724.

[61] J. Hwang, E. Kim, and T. Miyajima. “Investigation of the Effect of Space Charge in the compact-Energy Recovery Linac”. In: *Proc. ERL2011*. Tsukuba, Japan, 2011, pp. 78–82.

[62] M. Abo-Bakir et Al. *Conceptual Design Report BERLinPro*. 2012.

[63] A. Khan, O. Boine-Frankenheim, and K. Aulenbacher. “Dispersion Matching With Space Charge in MESA”. In: *Proc. ERL2019*. Berlin, Germany, 2019, pp. 74–79.

[64] B. Muratori, H. L. Owen, and J. A Varley. “Optics Layout for the ERL Prototype at Daresbury Laboratory”. In: *Proc. EPAC2004*. Lucerne, Switzerland, 2004.

[65] R. Hajima et al. “Recent Results of the JAERI Energy-Recovery Linac FEL”. In: (2004), pp. 301–303.

[66] D. Kayran and V. N. Litvinenko. "Novel Method of Emittance Preservation in ERL Merging System in Presence of Strong Space Charge Forces". In: *Proc. EPAC2005*. Knoxville, USA, 2005, pp. 2512–2514.

[67] B. Kuske, M. Abo-Bakr, and A. Matveenko. "Merger Considerations For BERLinPro". In: *Proc. IPAC2010*. Kyoto, Japan, 2010, pp. 2138–2140.

[68] E. Wang et al. "The accelerator design progress for EIC strong hadron cooling". In: *Proc. IPAC2021*. Campinas, Brazil, 2021, pp. 1424–1427. DOI: 10.18429/JACoW-IPAC2021-TUPAB036.

[69] K. E. Deitrick et al. "Novel Straight Merger for Energy Recovery Linacs". In: *Proc LINAC2018*. Beijing, China, 2018, pp. 702–705. DOI: 10.18429/JACoW-LINAC2018-THPO010.

[70] C. Wang, J. Noonan, and J. W. Lewellens. "Dual-axis energy-recovery linac". In: *Proc. ERL2007* (2007), pp. 122–125.

[71] K. Floettmann. "Some basic features of the beam emittance". In: *Phys. Rev. ST Accel. Beams* 6 (3 Mar. 2003), p. 034202. DOI: 10.1103/PhysRevSTAB.6.034202.

[72] C. K. Allen and T. P. Wangler. "Parameters for quantifying beam halo". In: *Proc. PAC2001*. Chicago, USA, 2001, pp. 1732–1734. DOI: 10.1109/PAC.2001.987164.

[73] L. Deniau et al. "The mad-x program". In: *User's Reference Manual* (2017).

[74] *Optimx: A Program For Accelerator Optics[online], Available at: https://home.fnal.gov/£\sim£ostiguy/OptiM [Accessed 11 December 2020].*

[75] K. Floettmann (1997), *ASTRA: A Space Charge Tracking Algorithm* [Online], Avaliable: http://www.desy.de/ mpyflo/.

[76] A. Adelmann et al. "OPAL a Versatile Tool for Charged Particle Accelerator Simulations". In: *arXiv e-prints*, arXiv:1905.06654 (May 2019), arXiv:1905.06654. arXiv: 1905.06654 [physics.acc-ph].

[77] M. J. De Loos and S. B. Van der Geer. "General Particle Tracer: A new 3D code for accelerator and beamline design". In: *Proc. EPAC1996*. Barcelona, Spain, 1996, pp. 1241–1243.

[78] *Poisson Superfish* [Online], Avaliable: https://laacg.lanl.gov/laacg/services/download_sf.phtml.

[79] M. Mitchell. *An introduction to genetic algorithms*. MIT press, 1998.

[80] I. V. Bazarov and C. K. Sinclair. "Multivariate optimization of a high brightness dc gun photoinjector". In: *Physical Review Special Topics-Accelerators and Beams* 8.3 (2005), p. 034202.

[81] K. Deb. *Multi-Objective Optimization using Evolutionary Algorithms*. Wiley, 2001.

[82] K. Deb et al. "A fast and elitist multiobjective genetic algorithm: NSGA-II". In: *IEEE transactions on evolutionary computation* 6.2 (2002), pp. 182–197.

[83] K. Deb and R. B. Agrawal. "Simulated binary crossover for continuous search space". In: *Complex systems* 9.2 (1995), pp. 115–148.

[84] K. Deb and H. Jain. "An evolutionary many-objective optimization algorithm using reference-point-based nondominated sorting approach, part I: solving problems with box constraints". In: *IEEE transactions on evolutionary computation* 18.4 (2013), pp. 577–601.

[85] H. Jain and K. Deb. "An evolutionary many-objective optimization algorithm using reference-point based nondominated sorting approach, part II: Handling constraints and extending to an adaptive approach". In: *IEEE Transactions on evolutionary computation* 18.4 (2013), pp. 602–622.

[86] I. Das and J. E. Dennis. "Normal-boundary intersection: A new method for generating the Pareto surface in nonlinear multicriteria optimization problems". In: *SIAM journal on optimization* 8.3 (1998), pp. 631–657.

[87] B. L. Militsyn et al. "Design of an Upgrade to the ALICE Photocathode Electron Gun". In: Genoa, Italy, 2008, pp. 235–237.

[88] B. L. Militsyn. Private communication. 2019.

[89] J. Grames et al. "A Biased Anode to Suppress Ion Back-Bombardment in a DC High Voltage Photoelectron Gun". In: *AIP Conference Proceedings*. Vol. 980. 1. American Institute of Physics. 2008, pp. 110–117.

[90] K. Aulenbacher et al. "Operational experience with the MAMI polarized source". In: *Proc. Workshop on Photocathodes for Polarized Electron Sources for Accelerators*. Stanford, USA, 1993, pp. 1–12.

[91] H. Fisher et al. "Thermal Stability of Cs on NEA III-V-Cathodes and its Effect on Quantum Efficiency". In: *Proc. Workshop on Photocathodes for Polarized Electron Sources for Accelerators*. Stanford, USA, 1993, pp. 249–260.

[92] B. Dunham et al. "Advances in DC photocathode electron guns". In: *AIP Conference Proceedings* 472 (July 1999), pp. 813–822. DOI: 10.1063/1.58933.

[93] J. Mckenzie and B. Militsyn. "3D simulations of a non-axisymmetric high average current DC photocathode electron gun". In: *Proc. EPAC2008* (2008), pp. 238–240.

[94] J. R. Pierce. "Rectilinear electron flow in beams". In: *Journal of applied physics* 11.8 (1940), pp. 548–554.

[95] F. A. Fortin et al. "DEAP: Evolutionary Algorithms Made Easy". In: *Journal of Machine Learning Research* 13 (2012), pp. 2171–2175.

[96] P. Bézier. "How Renault Uses Numerical Control for Car Body Design and Tooling". In: *SAE Technical Paper 680010* (1968).

[97] A. R. Forrest. "Interactive Interpolation and Approximation by Bézier Polynomials". In: *The Computer Journal* 15.1 (Feb. 1972), pp. 71–79. ISSN: 0010-4620. DOI: 10.1093/comjnl/15.1.71.

[98] J. M. Garland et al. "Characterisation of the ALICE Accelerator as an Injector for the EMMA ns-FFAG". In: *Proc. IPAC10*. Kyoto, Japan, 2010, pp. 4343–4345.

[99] C. Gulliford et al. "Demonstration of low emittance in the Cornell energy recovery linac injector prototype". In: *Phys. Rev. ST Accel. Beams* 16 (7 2013), p. 073401. DOI: 10.1103/PhysRevSTAB.16.073401.

[100] W. E. Spicer. "Photoemissive, Photoconductive, and Optical Absorption Studies of Alkali-Antimony Compounds". In: *Phys. Rev.* 112 (1 Oct. 1958), pp. 114–122. DOI: 10.1103/PhysRev.112.114.

[101] L. Cultrera et al. "Thermal emittance and response time of a cesium antimonide photocathode". In: *Applied Physics Letters* 99.15 (2011), p. 152110.

[102] P. Denham and P. Musumeci. *Analytical Scaling Laws for Radiofrequency Based Pulse Compression in Ultrafast Electron Diffraction Beamlines*. 2021. DOI: 10.48550/ARXIV.2106.02102. URL: https://arxiv.org/abs/2106.02102.

[103] B.E. Carlsten. "New photoelectric injector design for the Los Alamos National Laboratory XUV FEL accelerator". In: *Nuclear Instruments and Methods in Physics Research Section A: Accelerators, Spectrometers, Detectors and Associated Equipment* 285.1 (1989), pp. 313–319. ISSN: 0168-9002. DOI: https://doi.org/10.1016/0168-9002(89)90472-5.

[104] O. J. Luiten et al. "How to Realize Uniform Three-Dimensional Ellipsoidal Electron Bunches". In: *Phys. Rev. Lett.* 93 (9 Aug. 2004), p. 094802. DOI: 10.1103/PhysRevLett.93.094802.

[105] Y. Li, S. Chemerisov, and J. Lewellen. "Laser pulse shaping for generating uniform three-dimensional ellipsoidal electron beams". In: *Phys. Rev. ST Accel. Beams* 12 (2 Feb. 2009), p. 020702. DOI: 10.1103/PhysRevSTAB.12.020702.

[106] A. Benítez-Hidalgo et al. "jMetalPy: A Python framework for multi-objective optimization with metaheuristics". In: *Swarm and Evolutionary Computation* 51 (2019), p. 100598. ISSN: 2210-6502. DOI: https://doi.org/10.1016/j.swevo.2019.100598.

[107] K. Floettmann. "Emittance compensation in split photoinjectors". In: *Phys. Rev. Accel. Beams* 20 (1 Jan. 2017), p. 013401. DOI: 10.1103/PhysRevAccelBeams.20.013401.

[108] L. Serafini and J. B. Rosenzweig. "Envelope analysis of intense relativistic quasilaminar beams in rf photoinjectors:mA theory of emittance compensation". In: *Phys. Rev. E* 55 (6 1997), pp. 7565–7590. DOI: 10.1103/PhysRevE.55.7565.

[109] G. Pérez Segurana, I. R. Bailey, and P. H. Williams. "Construction of self-consistent longitudinal matches in multipass energy recovery linacs". In: *Phys. Rev. Accel. Beams* 25 (2 Feb. 2022), p. 021003. DOI: 10.1103/PhysRevAccelBeams.25.021003.

[110] R. Hajima. "A First-Order Matrix Approach to the Analysis of Electron Beam Emittance Growth Caused by Coherent Synchrotron Radiation". In: *Japanese Journal of Applied Physics* 42.Part 2, No. 8A (Aug. 2003), pp. 974–976. DOI: 10.1143/jjap.42.1974.

[111] D. Douglas. *Suppression & Enhancement of CSR-driven Emittance Degradation in the IR-FEL Driver*. JLAB-TN-98-012. 1998.

[112] N. Neveu et al. "Benchmark of rf photoinjector and dipole using ASTRA, GPT, and OPAL". In: *Proc. NAPAC2016* (2016), pp. 1194–1196.

[113] T. P. Wangler. *RF Linear Accelerators*. Germany: Wiley, 2008.